# **NOTE TO USERS**

This reproduction is the best copy available.



# Effect of Applied Hydrostatic Pressure on the Structure and Rheological Properties of Whey Proteins

by Pedro Alvarez

Department of Food Science and Agricultural Chemistry

Macdonald Campus, McGill University

Montreal, Quebec

Canada

A Thesis Submitted to the Graduate and Post-Doctoral Studies Office in Partial Fulfillment of the Requirements of the Degree of Master of Science

August 2004

© Pedro Alvarez, 2004



Library and Archives Canada

rchives Canada Archives Canada

Published Heritage Branch

395 Wellington Street Ottawa ON K1A 0N4 Canada Direction du Patrimoine de l'édition

395, rue Wellington Ottawa ON K1A 0N4 Canada

Bibliothèque et

Your file Votre référence ISBN: 0-494-12389-3 Our file Notre référence ISBN: 0-494-12389-3

#### NOTICE:

The author has granted a non-exclusive license allowing Library and Archives Canada to reproduce, publish, archive, preserve, conserve, communicate to the public by telecommunication or on the Internet, loan, distribute and sell theses worldwide, for commercial or non-commercial purposes, in microform, paper, electronic and/or any other formats.

#### AVIS:

L'auteur a accordé une licence non exclusive permettant à la Bibliothèque et Archives Canada de reproduire, publier, archiver, sauvegarder, conserver, transmettre au public par télécommunication ou par l'Internet, prêter, distribuer et vendre des thèses partout dans le monde, à des fins commerciales ou autres, sur support microforme, papier, électronique et/ou autres formats.

The author retains copyright ownership and moral rights in this thesis. Neither the thesis nor substantial extracts from it may be printed or otherwise reproduced without the author's permission.

L'auteur conserve la propriété du droit d'auteur et des droits moraux qui protège cette thèse. Ni la thèse ni des extraits substantiels de celle-ci ne doivent être imprimés ou autrement reproduits sans son autorisation.

In compliance with the Canadian Privacy Act some supporting forms may have been removed from this thesis.

While these forms may be included in the document page count, their removal does not represent any loss of content from the thesis.

Conformément à la loi canadienne sur la protection de la vie privée, quelques formulaires secondaires ont été enlevés de cette thèse.

Bien que ces formulaires aient inclus dans la pagination, il n'y aura aucun contenu manquant.



Suggested short title:

Structure and Rheological Properties of Pressure Treated Proteins

#### Abstract

Recent studies have demonstrated that applied hydrostatic pressure can affect the functional properties of whey protein isolate (WPI). In this work, the effects of applied hydrostatic pressure on the tertiary and secondary structure of whey proteins were investigated by spectroscopic and rheological techniques to elucidate the molecular basis of such pressure-induced changes in protein functionality. The individual protein components of WPI and various samples of WPI obtained from different sources were subjected to different single-cycle pressure treatments of up to 400 MPa in 100 MPa increments with 30-min holding time as well as to pressures ranging from 450 to 650 MPa without a holding time. Electrospray ionization-mass spectrometry, circular dichroism, and Fourier transform Raman spectroscopic studies of pressure-treated samples of  $\beta$ -lactoglobulin, the major protein component of WPI, revealed significant changes in tertiary structure. Fourier transform infrared spectroscopic studies revealed that the secondary structure of  $\beta$ -lactoglobulin was also sensitive to applied pressure and holding time. The secondary and tertiary structure of  $\alpha$ -lactalbumin, the second most prevalent protein in WPI, was unaffected by applied hydrostatic pressure. The spectroscopic behaviour of the various samples of WPI subjected to pressure treatment was variable and indicated that the response of WPI to applied hydrostatic pressure is dependent on the method used to isolate the WPI from whey. The rheological profiles of β-lactoglobulin, α-lactalbumin, and WPI samples after various pressure treatments were also recorded. Both β-lactoglobulin and WPI exhibited marked increases in viscosity with increasing pressure, whereas α-lactalbumin remained solutions exhibited no significant change in viscosity. These studies have furthered the understanding of the effects of applied hydrostatic pressure on the molecular structure and rheological properties of WPI proteins.

#### Résumé

De récentes études ont démontré que la pression hydrostatique appliquée peut affecter les propriétés fonctionnelles des isolats protéiques de lactosérum (WPI). Dans cette étude, les effets de la pression hydrostatique appliquée sur les structures tertiaire et secondaire des protéines de lactosérum ont été observés grâce à des techniques spectroscopiques et rhéologiques afin d'élucider les bases moléculaires de ces types de changements causés par la pression dans la fonctionnalité de la protéine. Les protéines individuelles composant le WPI et plusieurs échantillons de WPI provenant de différentes sources ont été soumis à différents traitements de pression à cycle unique allant de 100 MPa à 400 MPa avec un temps d'attente de 30 minutes ainsi qu'à une échelle de pression allant de 450 à 650 MPa sans temps d'attente. La spectrométrie de masse à ionisation electrospray, le dichroïsme circulaire et les études spectroscopiques « Fourier transform Raman » d'échantillons traités à la pression de β-lactoglobuline, la composante protéique principale du WPI, ont révélé des changements significatifs dans la structure tertiaire. Les études spectroscopiques infrarouges « Fourier transform » ont révélé que la structure secondaire de la β-lactoglobuline était autant sensible à la pression appliquée qu'au temps d'attente. Les structures secondaire et tertiaire de l'a-lactoalbumine, la seconde protéine en importance dans le WPI, n'étaient pas affectées par la pression hydrostatique appliquée. Le comportement spectroscopique des différents échantillons de WPI soumis aux traitements de pression était variable et indiquait que la réponse du WPI à la pression hydrostatique appliquée dépend de la méthode utilisée afin d'isoler le WPI du lactosérum. Les profils rhéologiques de la β-lactoglobuline, de l'α-lactoalbumine et des échantillons de WPI suite à divers traitements de pression ont également été mesurés. La βlactoglobuline et le WPI ont présenté des augmentations marquées de viscosité lorsque la pression augmentait, tandis que l'a-lactoalbumine, demeurée en solution, n'a démontré aucun changement significatif de viscosité. Ces présentes études ont fait progresser la compréhension des effets de la pression hydrostatique appliquée sur la structure moléculaire et sur les propriétés rhéologiques des protéines de WPI.

to my newborn son Marco Andrés, great source of inspiration

# Acknowledgments

My most sincere thanks to Dr. Ashraf A. Ismail for his excellent guidance and for being a real friend trough this journey. Thanks to Dr. Hosahalli S. Ramaswamy for all the support and motivation.

I would like to express my gratitude to Dr. Jacqueline Sedman for her valuable advice and help in the editing of the manuscript.

Thanks to the Department of Food Science for awarding me twice with the "international fee waiver". Thanks also to Lise and Barbara.

I would like to thank my colleagues and friends Nasser, Ziad, Ahmed, Sarah and Robert. Thanks to the rest of the guys in the McGill IR group.

Thanks to my wife Laura for encourage me to pursue my dreams and for her infinite moral support.

# **Table of Contents**

Résumé	iv
Acknowledgments	vi
Table of Contents	vii
List of Figures	xi
Index of Tables	xiii
Chapter 1	1
General Introduction	1
Chapter 2	2
Literature Review	2
2.1. Infrared and Raman Spectroscopy in Food Science	2
2.1.1. Introduction	2
2.1.2. Fundamental Principles of IR and Raman Spectroscopy	3
2.1.3. Instrumentation	8
2.1.3.1. Infrared Spectroscopy	8
2.1.3.2. Raman Spectroscopy	10
2.1.4. Sampling Methods	
2.1.4.1. Infrared Spectroscopy	12
2.1.4.1.1.Transmission Mode	12
2.1.4.2. Raman Spectroscopy	13
2.1.5. IR and Raman Spectroscopy of Food Components and Foods	12
2.1.5.1. IR and Raman Spectroscopy of Food Proteins	20
2.1.5.2. Analysis of Milk and Dairy Products by FTIR and Raman Spec	troscopy .32
2.2. Electrospray Ionization Mass Spectrometry (ESI-MS) in the Study of	Protein
Structure	34
2.2.1. Introduction	34
2.2.2. Background	34
2.2.3. The Modern Mass Spectrometer	36
2.2.4. Fundamental Principles of Mass Spectrometry	30
2.2.5 Instrumentation	36

2.2.5.1. Ionization Techniques	36
2.2.5.1.1. Hard Methods	38
2.2.5.1.1.1. Electron Impact	t (EI)38
2.2.5.1.1.2. Fast Atom Bom	abardment (FAB)38
2.2.5.1.2. Soft Methods	38
2.2.5.1.3. Desorption Techniq	ues38
2.2.5.1.3.1. Laser Desorption	on38
2.2.5.1.3.2. Matrix Assisted	Laser Desorption Ionization (MALDI)39
2.2.5.1.3.3. ElectroSpray Io	onization (ESI)39
2.2.6. ESI-MS and Protein Struc	ture39
2.2.6.2. Application of ESI-MS	in the Study of Protein structure43
2.3. References	45
Chapter 3	49
Structure-Functionality Relationship o	f Ultra High Hydrostatic Pressure Processed Whey
Proteins	49
3.1. Abstract	49
3.2. Introduction	50
3.3. Materials and Methods	50
3.3.1. Series A	51
3.3.2. Series B	51
3.3.3. Rheology	52
3.3.4. FTIR spectroscopy	52
3.4. Results and Discussion	52
3.4.1. Series A	52
3.4.2. Series B	54
3.4.3. Rheology	59
3.5. Conclusion	61
3.6. References	62
Chapter 4	65
Effect of Ultra High Hydrostatic Press	sure on the Electrospray Ionization Mass
Spectroscopy (ESI-MS) Profile of Wh	ey Proteins65

4.1.	Abs	stract	.65
4.2.	Intr	oduction	.66
4.3.	Ma	terials and Methods	.66
4.3.	.1.	Experiment A	.68
4.3.	.2.	Experiment B	.69
4.3.	.3.	ESI Mass Spectrometer	.69
4.4.	Res	sults and Discussion	69
4.4.	.1.	Effect of UHP on the conformation of $\beta$ -lg and $\alpha$ -lac	70
4.4.	.2.	Effect of UHP on the conformation of $\beta$ -lg and $\alpha$ -lac in WPI	74
4.4	.2.1.	Bipro®	74
4.4	.2.2.	Inpro®	75
4.5.	Co	nclusion	76
4.6.	Ref	ferences	76
Chapte	r 5		78
Tertiary	y Str	ructure Changes of Whey Proteins after Ultra High Hydrostatic Pressure	
Process	s		78
5.1.	Ab	stract	78
5.2.	Int	roduction	79
5.3.	Ma	terials and Methods	79
5.3	3.1.	Series A	80
5.3	3.2.	Series B	80
5.3	3.3.	Fluorescence spectroscopy using ANS as probe	80
5.3	3.4.	Near UV circular dichroism spectroscopy	80
5.3	3.5.	FT-Raman spectroscopy	81
5.4.	Re	sults and Discussion	81
5	5.4.1	.1. Fluorescence spectroscopy using ANS as probe	81
		.2. Near UV circular dichroism spectroscopy	
		.3. FT-Raman spectroscopy	
5.4	4.2.	Series B	86
5.5.		mmary	
5.6.	Re	ferences	91

Chapter 6	92
General Conclusion	92

# List of Figures

Figure 1. The symmetric stretch of the CO <sub>2</sub> molecule5
Figure 2. Schematic representation of a Raman spectrum7
Figure 3. Schematic diagram of a Michelson interferometer9
Figure 4. (A) Interferogram recorded with no sample (B) interferogram recorded with a thin film of polyethylene and (C) Absorbance spectrum of PE obtained by the mathematical transformation shown on the figure
Figure 5. FTIR spectra of (A) water, (B) milk and (C) difference spectrum15
Figure 6. ATR/FTIR spectra of (A) water, (B) milk and (C) difference spectrum16
Figure 7. ATR/FTIR spectra of (A) powdered $\beta$ -lg and (B) $\alpha$ -lac
Figure 8. FT-Raman spectra of (A) powdered $\beta$ -lg and (B) $\alpha$ -lac
Figure 9. (A) Raw FTIR spectrum, (B) spectrum after Fourier self-deconvolution (FSD),
and (C) "overdeconvolved" spectrum of $\beta$ -lg
Figure 10. FT-Raman spectra of (A) L-cysteine and (B) L-cystine29
Figure 11. Spectral overlay plot of the deconvolved amide I' band in the FTIR spectrum
of $\beta$ -lg as a function of increasing temperature
Figure 12. The parabola spectrograph35
Figure 13. Schematic representation of a mass spectrometer37
Figure 14. Schematic representation of the MALDI desorption technique40
Figure 15. Schematic representation of the electrospray ionization technique41
Figure 16. Different modes of creating the sample aerosol for ESI

Figure 17. Non-reversible effect of pressure on the amide I' region of the FSD-FTIR
spectra of β-lg. 30 minutes holding time
Figure 18. Difference spectra from figure 1756
Figure 19. Non-reversible effect of pressure on the amide I' region of the FSD-FTIR
spectra of β-lg. Instant pressure57
Figure 20. Difference spectra from figure 19
Figure 21. Rheological data for whey proteins with different pressure treatments60
Figure 22. Electrospray ionization mass spectrometry (ESI-MS) relative charge-state-
distribution (CSD) of β-lg A and B genetic variants without pressure treatment67
Figure 23. ESI-MS absolute CSD of the pure whey proteins after pressure71
Figure 24. ESI-MS absolute CSD of the protein components in WPI Bipro® after
pressure
Figure 25. ESI-MS absolute CSD of the protein components in WPI Inpro® after pressure
Figure 26. Fluorescence spectra of ANS bind to pure $\beta$ -lg protein subjected to increasing
pressure
Figure 27. Near-UV CD spectra of pure β-lg protein subjected to different pressure
treatments84
Figure 28. FT-Raman spectrum of β-lg powder not pressure treated85
Figure 29. The third dimensional orientation of some amino acids groups in $\beta$ -lg solutions
after different pressure treatments, obtained from its FT-Raman spectrum
Figure 30. Fluorescence of ANS bind to two brand-names of WPI exposed to different
pressure treatments89

# **Index of Tables**

Table 1. Selected vibrational bands of major food components	17
Table 2. Amide bands of proteins	21
Table 3. Approximate positions (cm <sup>-1</sup> ) of amide I' band components in I proteins	_
Table 4. Band assignment of the amide I' spectral region of β-lg	53
Table 5. FT-Raman ratios of intesities for amino acids	87

# Chapter 1

#### **General Introduction**

Ultra high pressure (UHP) processing technology is a growing alternative to the classical thermal food processing techniques. Applying ultra high hydrostatic pressures ranging from 100 to 1000 mega-Pascals (MPa) has been shown to make foods safer and extends their shelf life, while allowing the product to retain many of its organoleptic and nutritional attributes. This technique meets consumer demands for freshness without the disapproval related to other methods such as irradiation.

UHP has been used on many products to achieve: inactivation of food-borne pathogens, inactivation of bacterial spores, enhancing or inhibiting selected enzymes, tenderization of meat, shuck oysters, extend shelf life, promote ripening of cheeses, and minimizing oxidative browning. Ultra high pressure in conjunction with elevated temperatures has been also employed for the sterilization of many food products.

Recent studies have revealed that pressurization of a protein solution causes partial protein unfolding that can lead to the irreversible process of gelation. Pressure induced gels have superior texture and viscoelastic properties in comparison to temperature-induced gels. Pressure-induced gel formation is dependent on a multitude of parameters including the nature of the protein, protein concentration, level of the pressure applied and holding time, number of pressure cycles, temperature, pH, and ionic strength. The relationship between pressure-induced structural changes that lead to gelation is still under investigation.

The purpose of this thesis work is to examine the effect of applied ultra high hydrostatic pressure on the structure of whey proteins and whey protein isolates (WPI) using Fourier transform infrared (FTIR) spectroscopy, electrospray ionization mass spectrometry (ESI-MS), near-ultraviolet circular dichroism (near-UV CD), fluorescence and FT-Raman spectroscopy. And ultimately relate the viscoelastic properties of the proteins, observed by dynamic rheology techniques, to the changes observed at the structural level.

# Chapter 2

### Literature Review

#### 2.1. Infrared and Raman Spectroscopy in Food Science

#### 2.1.1. Introduction

Infrared (IR) and Raman spectroscopy provide detailed information about both the composition of foods and the molecular structure and the functionality of the components in food systems. Both techniques are based on molecular interactions with electromagnetic radiation that result in transitions between the vibrational energy levels of the ground electronic energy state of the molecule, corresponding to the excitation of various stretching and bending vibrations. However, the nature of these interactions is fundamentally different in these two types of vibrational spectroscopy, and hence they are regarded as complementary techniques. In general terms, as well as specifically in regard to applications to food systems, IR spectroscopy has found much more extensive use than Raman spectroscopy owing to the greater simplicity and lower cost of the instrumentation as well as the greater utility of IR spectroscopy as a quantitative analysis tool. On the other hand, Raman spectroscopy offers certain advantages in relation to sample handling, the study of aqueous systems, and possibilities for on-line process monitoring. Thus, the selection of IR or Raman spectroscopy, or the combined use of both techniques, depends on the nature of the application. Near-infrared (NIR) spectroscopy combines the samplehandling advantages of Raman spectroscopy with the powerful multicomponent analysis capabilities of IR spectroscopy and thus has found widespread application for quality control and process monitoring in the food industry for several decades. However, by comparison with (mid-) IR and Raman spectra, NIR spectra are fairly uninformative, and NIR analysis is largely based on statistical treatment of the spectral data. Entire books have been devoted to NIR analysis of foods (46, 37) and NIR spectroscopy will not be considered in this chapter.

In the following sections, the principles of IR and Raman spectroscopy and the instrumentation and sample-handling techniques employed to acquire spectra will be briefly described. The utility of these two techniques for investigations of the individual components of food systems will then be illustrated by considering the information that

can be extracted from the IR and Raman spectra of food proteins. Finally, a survey of the applications of IR and Raman spectroscopy in the analysis of foods will be presented.

### 2.1.2. Fundamental Principles of IR and Raman Spectroscopy

IR and Raman spectroscopy are both based on the excitation of molecular vibrations by interaction with electromagnetic radiation. A nonlinear molecule made up of N atoms possesses 3N-6 vibrational modes, each of which has a discrete frequency; the number of vibrational modes is reduced by one in the case of linear molecules. The factors determining the frequencies of molecular vibrations can be illustrated by considering the simplest case, a diatomic molecule AB, which has a single vibrational mode involving the stretching of the bond linking atoms A and B. The frequency at which this bond vibrates can be calculated from the model of a harmonic oscillator, whereby the restoring force (F) on the bond is given by Hooke's law:

$$F = -kx$$
 [1]

where k is the force constant of the bond and x is the displacement from the equilibrium internuclear distance. Under this approximation, the vibrational frequency, v, is given by

$$v = (1/2\pi)(k/\mu)^{1/2}$$
 [2]

where  $\mu$  is the reduced mass of the system, as defined by the following equation:

$$\mu = m_{\text{A}} \bullet m_{\text{B}} / (m_{\text{A}} + m_{\text{B}})$$
 [3]

where  $m_A$  and  $m_B$  are the individual atomic masses of A and B. By convention, vibrational frequencies are given in wavenumbers ( $\bar{v} = v/c$ , where c is the speed of light), expressed in units of reciprocal centimeters (cm<sup>-1</sup>), rather than in units of frequency (s<sup>-1</sup>), although in older literature, band positions are often reported in units of wavelength ( $\lambda$ ), i.e., microns ( $\mu$ ). The frequencies of molecular vibrations fall primarily in the mid-IR region of the electromagnetic spectrum (4000-400 cm<sup>-1</sup>; 2.5-25  $\mu$ m).

The quantum-mechanical treatment of molecular vibrations leads to modifications of the harmonic oscillator model as the vibrational energy levels are quantized:

$$E = (v + 1/2)hv$$
 [4]

where v is the vibrational quantum number, h is Planck's constant, and v is the fundamental vibrational frequency. The quantum-mechanical theory predicts that at room

temperature, only transitions from the ground-state vibrational level (v = 0) to the first excited vibrational level (v = 1) will occur; however, experimentally this is not the case as weak overtone bands, corresponding to transitions to higher energy levels, can be observed, especially in the NIR spectral region.

IR spectroscopy is based on the measurement of molecular absorption of IR radiation of frequencies that match those of the molecular vibrations. However, all of a molecule's vibrational modes do not give rise to IR absorption bands because a vibration will only be IR-active if it results in a change in the dipole moment of the molecule. For example, the stretching vibration of a homonuclear diatomic molecule, such as N<sub>2</sub> or O<sub>2</sub>, is not IR-active because the equal displacement of the two atoms from the center of mass does not change the dipole moment of the molecule. However, this is no longer the case when the two atoms in the diatomic molecule have different masses, and hence the stretching vibrations of molecules such as CO are IR-active. Similarly, the symmetric stretching vibration of the CO<sub>2</sub> molecule illustrated in Figure 1 is IR-inactive because of the molecule's linear geometry while the corresponding vibration of a nonlinear triatomic molecule such as H<sub>2</sub>O is IR-active, as are the asymmetric stretching vibrations of both linear and nonlinear triatomics.

Raman spectroscopy is based on the inelastic scattering of light by the molecules in a sample rather than their absorption of IR radiation. When a sample is irradiated with light, most of the photons are elastically scattered; that is, the wavelength of the scattered photons is unchanged. However, a small fraction (~1 in 10<sup>6</sup> photons) will show a shift in wavelength from that of the incident light. This phenomenon was theoretically predicted by Adolf G. Smekal in 1923 but was first observed experimentally by Sir Chandrasekhara V. Raman in 1928 and hence is called the Raman effect. Detection of the inelastically scattered photons requires that the sample be irradiated with monochromatic (i.e., single-wavelength) light. Furthermore, since the Raman effect is very weak, an intense monochromatic light source is required. For these reasons, Raman spectroscopy only became practicable in the 1960s with the development of lasers and highly sensitive photon-counting devices, such as photomultiplier tubes.

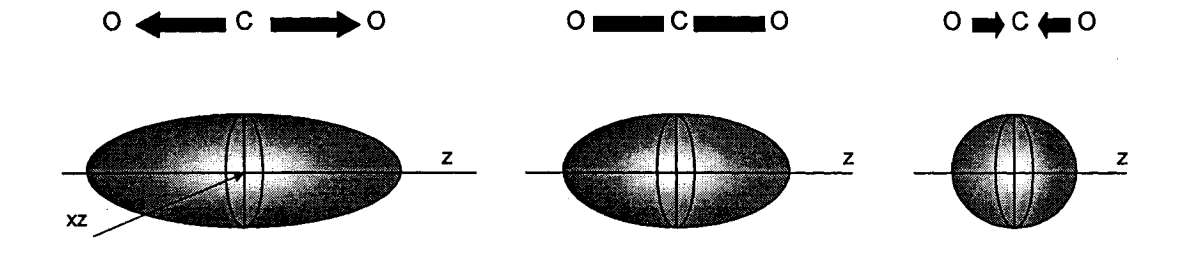


Figure 1. The symmetric stretch of the CO<sub>2</sub> molecule is a Raman-active but not an IR-active vibration because it results in a change in the molecule's polarizability but does not involve a change in its dipole moment.

In Raman spectroscopy, a sample is irradiated with a laser line of frequency  $v_0$ , and the intensity of the scattered light as a function of frequency is then measured, yielding a Raman spectrum (see Figure 2). Although most of the elastically scattered light is filtered out prior to reaching the detector, the spectrum is still predominated by a broad signal centered at the frequency of the incident light (referred to as the Rayleigh line). The remainder of the spectrum is composed of much weaker bands at lower frequencies,  $\overline{v}_0 - \overline{v}_i$  (referred to as Stokes lines). The frequency shifts  $\overline{v}_0 - \overline{v}_i$  (referred to as Raman shifts) are independent of  $\overline{v}_0$ , the frequency emitted by the excitation source, and correspond to the vibrational frequencies of the molecules in the sample. Even weaker bands occur at higher frequency,  $\overline{v}_0 + \overline{v}_i$  (referred to as anti-Stokes lines). The Stokes and anti-Stokes lines are equally displaced from the Rayleigh line; however, the anti-Stokes lines are rarely observed owing to their very low intensity.

For a molecular vibration to be Raman active (i.e., show a Raman effect), it must result in a change in the polarizability of the molecule, which is represented by an ellipsoid, and therefore must result in a change in the shape of the electron density cloud around the molecule. For example, as illustrated in Figure 1, in the symmetric stretching vibration of CO<sub>2</sub> the shape of the electron cloud is different between the minimum and maximum internuclear distances. Therefore, the polarizability of the molecule changes during the vibration and this vibrational mode is Raman-active. In the asymmetric stretch, the change in the polarizability ellipsoid as one of the bonds extends is cancelled by the opposite change due to the compression of the other bond, and hence there is no overall change in polarizability and the asymmetric stretch is Raman-inactive.

It is important to note that the criteria (referred to as "selection rules") for an IR-active vibration (i.e., a change in the dipole moment of the molecule) and a Raman-active vibration (i.e., a change in the polarizability of the molecule) are different. In fact, for any molecule that possesses a center of symmetry (such as the CO<sub>2</sub> molecule considered above), vibrations that are IR-active are Raman-inactive, and vice versa. In general, vibrations that give rise to weak IR bands often produce intense Raman bands, and vice versa. Hence, IR and Raman spectroscopy are complementary techniques, and it is usually necessary to apply both these types of vibrational spectroscopy to obtain the full spectral profile of a sample.

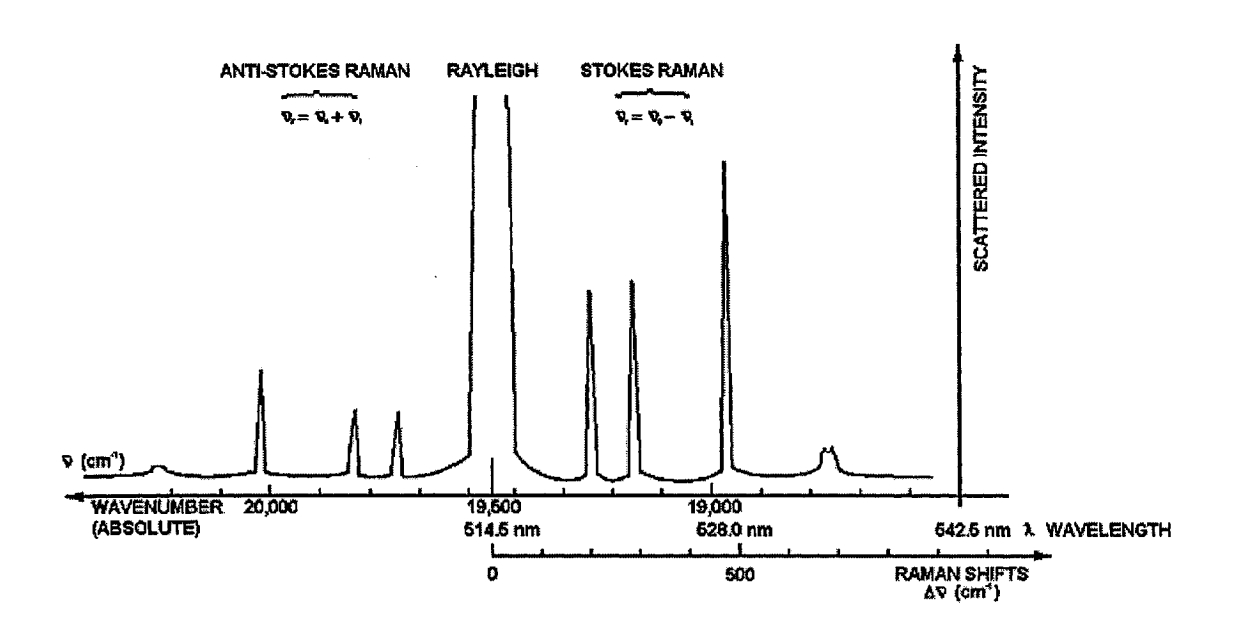


Figure 2. Schematic representation of a Raman spectrum excited with the 514-nm line of an argon ion laser. Most of the laser light is elastically scattered with the same frequency  $(v_0)$  as the incident light. However, a small proportion is inelastically scattered with frequencies of  $\overline{v_0} + \overline{v_i}$  and  $\overline{v_0} - \overline{v_i}$ , where  $\overline{v_i}$  is the frequency of one of the fundamental vibrations of the molecules in the sample.

#### 2.1.3. Instrumentation

### 2.1.3.1. Infrared Spectroscopy

IR spectrometers essentially consist of a broad-band source of IR radiation, a means for resolving the IR radiation into its component wavelengths, and a detector. Generally speaking, an IR spectrum of a sample can be represented mathematically by the following equation:

$$T(\overline{v}) = I(\overline{v})/I_0(\overline{v})$$
 [5]

where T is defined as transmittance, I is the intensity of IR radiation reaching the detector when it passes through the sample,  $I_0$  is the intensity of IR radiation reaching the detector with no sample in the beam, and  $\overline{v}$  is the wavenumber of the radiation. Usually, transmittance is converted to absorbance (A) using the following relationship:

$$A = -\log T \tag{6}$$

In the early years of IR spectroscopy, prisms were used to resolve IR radiation from the source into its component wavelengths but they were subsequently replaced by diffraction gratings. In the 1970s, the field of IR spectroscopy was revolutionized when these dispersive IR spectrometers began to be replaced by Fourier transform infrared (FTIR) spectrometers. FTIR spectroscopy is based on interferometry and makes use of a beamsplitter to divide the IR radiation into two beams, with one beam being directed to a fixed mirror and the other to a moving mirror (Figure 3). When these two beams are reflected back to the beamsplitter and recombine, they undergo constructive and destructive interference due to the path difference between the two mirrors, yielding an interferogram. The path difference, known as the retardation  $\delta$ , is proportional to time t because the moving mirror travels at a constant velocity, v, i.e.  $\delta = 2vt$ . Through the use of a fast Fourier transform (FFT) algorithm, the time domain interferogram,  $I(\delta)$ , is converted into the frequency domain,  $I(\overline{v})$ , according to the following relationship:

$$I(\delta) = 0.5H(\overline{v})I(\overline{v})\cos 2\pi \overline{v}\delta$$
 [7]

where H(v) is a single wavenumber-dependent correction factor that accounts for instrumental characteristics. The interferogram decoded into the frequency domain is in the form of an energy curve called a single-beam spectrum (Figure 4). The ratio of the single-beam spectrum of the sample against a background single-beam spectrum recorded

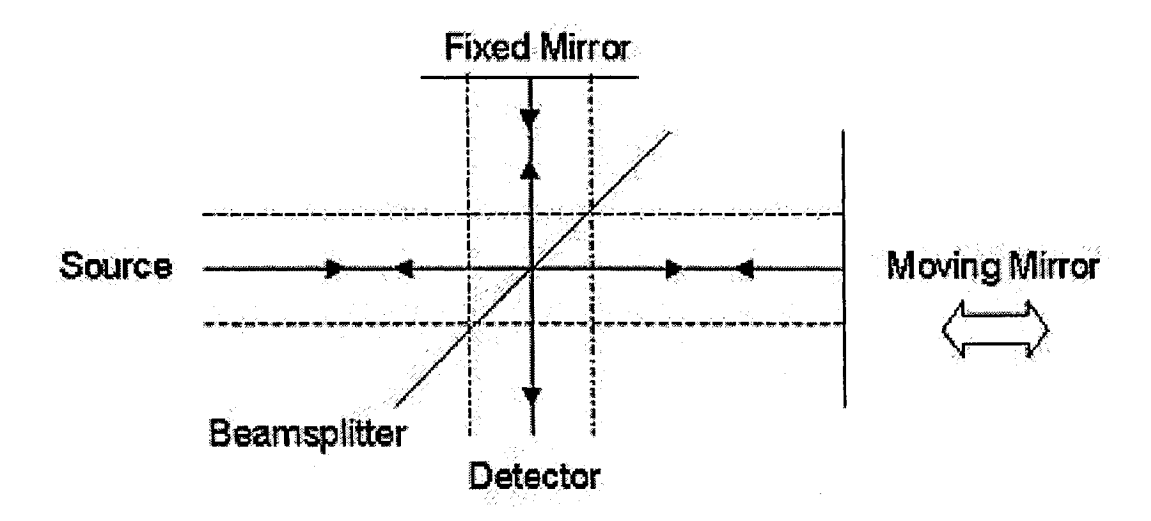


**Figure 3**. Schematic diagram of a Michelson interferometer. The IR radiation from the source is split into two beams by a beamsplitter and directed to the fixed and moving mirrors. The two IR beams recombine at the beamsplitter and are directed to the sample and the detector.

with no sample in the optical path results in a transmittance spectrum, in accordance with Eq. [5], which is then normally converted into an absorbance spectrum by carrying out the mathematical transformation represented by Eq. [6]. FTIR spectrometers have several advantages over conventional dispersive IR instruments, including a dramatic improvement in the signal-to-noise ratio (S/N) obtained by multiplexing (simultaneous detection of all frequencies), reduction in scan time, and higher energy throughput. Another important advantage is the excellent wavelength reproducibility of FTIR spectrometers, owing to the use of an internal reference laser, which allows spectral data manipulations such as spectral subtraction, addition, and ratioing to be performed with a very high degree of accuracy. The advancement of FTIR spectroscopy has been greatly assisted by the availability of increasingly powerful personal computers, which have facilitated the use of sophisticated software packages for both qualitative and quantitative applications.

#### 2.1.3.2. Raman Spectroscopy

The design of traditional dispersive Raman spectrometers differs markedly from that of IR instruments. However, FT-Raman spectrometers, which have become increasingly common in recent years, are similar in design to FTIR spectrometers, and combined FTIR/FT-Raman systems are available from most major FTIR vendors. In dispersive Raman spectroscopy, the source is a high-power laser emitting visible radiation at several discrete frequencies, with filters being employed to select a single laser line; commonly employed laser lines are the 488.0-nm (blue) and 514.5-nm (green) lines of an argon-ion laser. After this monochromatic radiation impinges on the sample, a portion of the scattered radiation is directed to a monochromator to resolve it into its component wavelengths and then to a photomultiplier tube. The resulting signal as a function of frequency is plotted as intensity versus Raman shift, yielding a Raman spectrum.

The major drawbacks of traditional Raman spectrometers originate with the use of high-power visible lasers as excitation sources. Samples that are susceptible to either thermal or photochemical degradation may be destroyed by the laser radiation, although

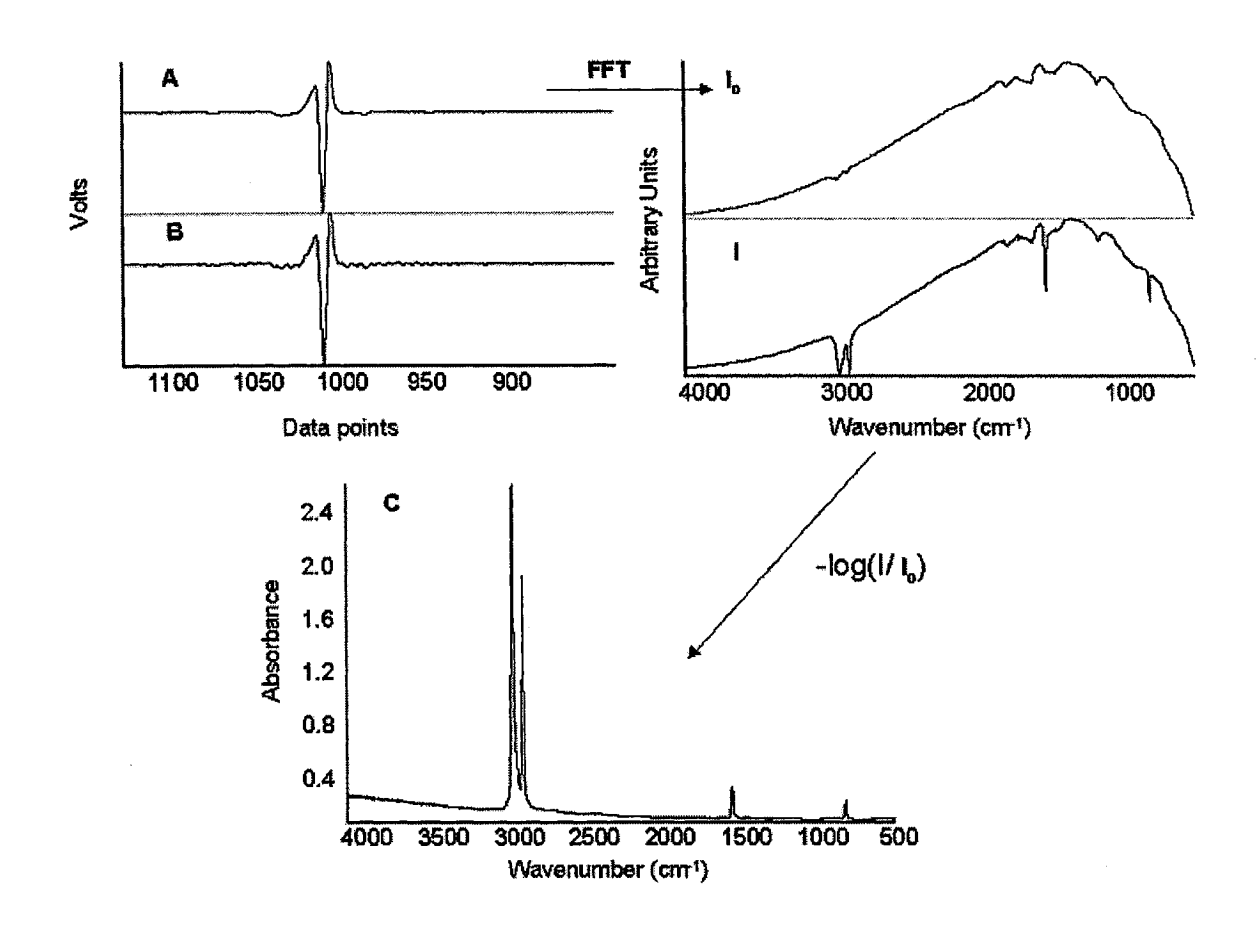


Figure 4. (A) Interferogram recorded with no sample in the path of the IR beam; (B) interferogram recorded with a thin film of polyethylene (PE) placed in the path of the IR beam. Fourier transformation of interferograms A and B by a fast Fourier transform (FFT) algorithm yields, respectively, the open-beam spectrum ( $I_0$ ) and the single-beam spectrum ( $I_0$ ) of PE. (C) Absorbance spectrum of PE obtained by the mathematical transformation shown on the figure.

various experimental approaches can be taken to minimize such damage. However, a more pervasive problem is the fluorescence that results when species present in the sample are electronically excited by the visible laser radiation. Because the Raman effect is weaker than fluorescence by many orders of magnitude, even the fluorescence from a trace impurity can completely mask the Raman spectrum of the sample. In the past, this phenomenon severely restricted the scope of Raman spectroscopy, particularly in relation to samples of biological origin. However, it has been substantially alleviated by the use of laser excitation lines in the NIR instead of the visible region of the electromagnetic spectrum, such as the 1064-nm line emitted by neodymium-doped yttrium aluminum garnet (Nd:YAG) lasers. Because the use of NIR lasers as excitation sources in conventional dispersive Raman spectrometers is not technically feasible, this option only became practicable with the development of FT-Raman spectrometers (17), which, like FTIR spectrometers, are based on interferometry. In fact, FTIR spectrometers can be modified to acquire Raman spectra by incorporating a Nd:YAG laser and using beamsplitters and detectors appropriate for the NIR region. The availability of these dualpurpose instruments has greatly facilitated comprehensive vibrational spectroscopic studies, although their high cost remains a disadvantage.

#### 2.1.4. Sampling Methods

#### 2.1.4.1. Infrared Spectroscopy

Infrared sample-handling accessories include transmission cells, attenuated total reflectance (ATR) accessories (both multiple- and single-bounce crystals and fiber-optic probes), as well as diffuse reflectance infrared Fourier transform (DRIFT) and photoacoustic spectroscopy (PAS). The latter two techniques are discussed in Ref. 13, they have had limited application in mid-IR food analysis, although DRIFT is widely used in NIR food analysis.

# 2.1.4.1.1. Transmission Mode

The transmission mode is the most common and oldest mode of IR sample analysis. The sample is placed in the optical path of the IR beam, and the amount of light transmitted through the sample is inversely proportional to the sample thickness, which can vary from meters for gas samples to microns for condensed-phase samples. The spectra of liquids and solutions are recorded in a transmission cell, composed of two optical windows separated by a spacer that determines the pathlength. The optical windows commonly employed are polished salt crystals (e.g., NaCl or KBr), because all materials containing covalent bonds, including glass, do not transmit IR radiation. There are also severe restrictions on the pathlength that can be employed because of the limited energy available from IR sources. For instance, aqueous solutions are typically measured in cells having pathlengths of 0.015-0.040 mm (15-40 µm), owing to the intense absorption of IR radiation by water; beyond this thickness, virtually no IR radiation reaches the detector.

In the case of solid samples, light scattering effects are a problem when particle dimensions are comparable to or exceed the wavelengths of mid-IR radiation and, as such, particles must be ground to <3 µm prior to analysis. The sample can then be diluted with KBr, KCl, or NaCl and pressed to form a pellet. An alternative procedure for analyzing solid samples is to make a liquid dispersion using oils, such as mineral oil (Nujol) or paraffin oil. Both the pellet and the dispersion method have the disadvantage of destroying the sample.

#### 2.1.4.2. Raman Spectroscopy

In terms of sample handling, Raman spectroscopy is a much more versatile and flexible method than IR spectroscopy because it does not suffer from restrictions on sample thickness (or pathlength), the need for specialized sample-handling accessories, or problems caused by light scattering. Thus, Raman spectra can be recorded directly from solid samples, even if opaque, with no sample preparation, and samples can be contained in ordinary glass vials. Thin glass capillaries are ideal for recording Raman spectra of solids or liquids because the laser is a highly focused energy source, allowing spectra to be obtained from samples as small as 100 µm in diameter. The main sample-handling difficulty encountered in Raman spectroscopy is excessive heating of the sample if an intense visible laser is employed as an excitation source. To alleviate this problem, the laser beam may be defocused, or various accessories that are available to prevent heating of the sample may be employed; these range from devices that continuously rotate the

sample, which can effectively reduce sample heating in the case of fluid samples, to expensive helium-cooled cryostats, which can be required to prevent burning in the case of thermally unstable solids. The need for such measures has been reduced, however, with the use of NIR lasers in FT-Raman spectroscopy.

#### 2.1.5. IR and Raman Spectroscopy of Food Components and Foods

The vibrational spectra of foods are the superposition of the spectra of all the individual components present and are thus generally very complex. The IR spectra of aqueous systems are dominated by the intense absorptions of water (Figure 5A), which can obscure the spectral features of other components in broad regions of the spectrum, as illustrated by the transmission spectrum of milk in Figure 5B. Although the spectral contributions of water can be removed digitally by spectral subtraction (Figure 5C), information cannot be obtained from regions of intense IR absorption by water except when very short pathlengths are employed; this limitation is often addressed by taking advantage of the inherently short effective pathlengths of ATR accessories (Figure 6). This difficulty is absent in Raman spectroscopy because water is a weak Raman scatterer.

The other major components of foods -fats, proteins, and carbohydrates- give rise to strong bands in both IR and Raman spectra. Although many of the bands due to these individual components overlap with each other, fats, proteins, and carbohydrates each have certain characteristic bands that arise from particular functional groups. The band positions and assignments of some of the major bands of these components are summarized in Table 1. However, it should be noted that vibrational frequencies are sensitive to electrical effects, steric effects, the nature, size, and electronegativity of neighboring atoms, phase changes, hydrogen bonding, and solvent polarity. Although this sensitivity may complicate spectral interpretation, it also contributes to the high information content of vibrational spectra. Thus, IR and Raman spectroscopy are valuable techniques for the characterization of materials in terms of their chemical composition, detailed investigations of molecular structure and bonding, and studies of the interactions of molecules with their environment. Furthermore, the IR and Raman spectra of substances serve as their "fingerprints", allowing for the identification of substances with

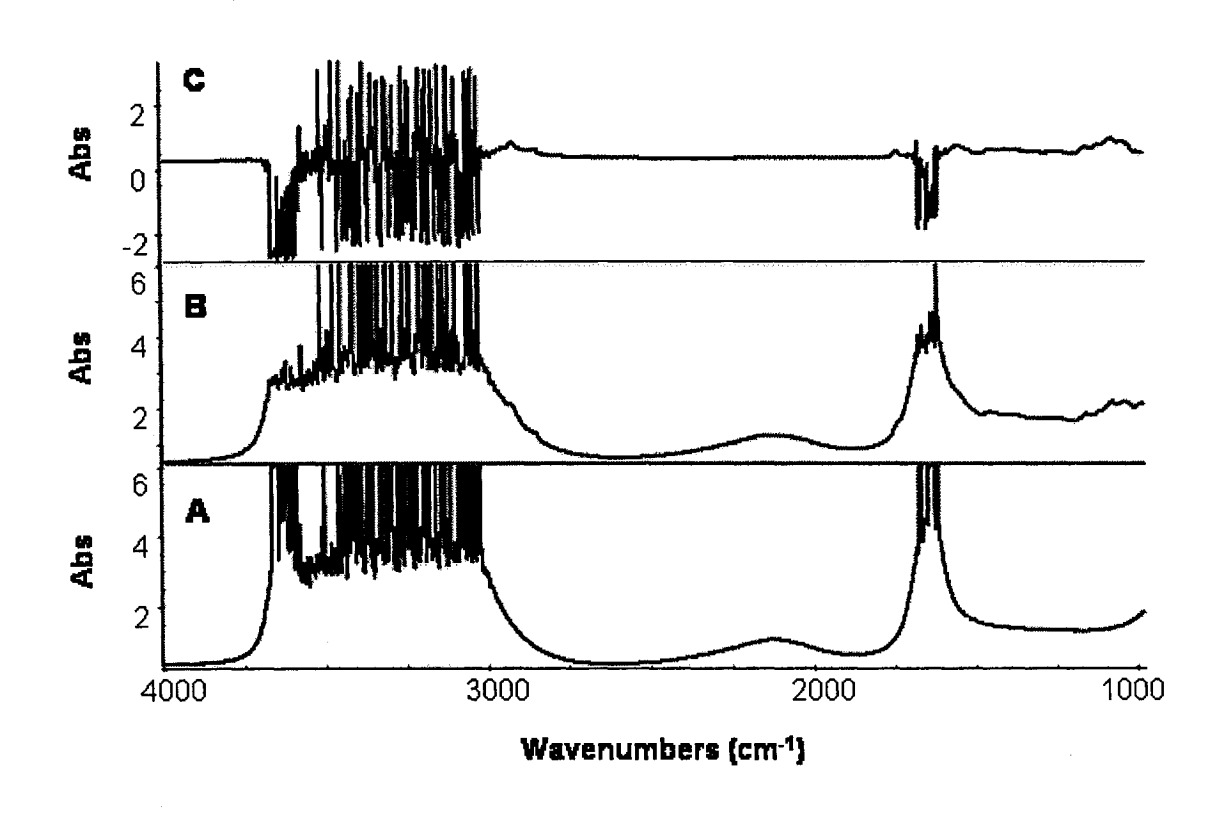


Figure 5. FTIR spectra of (A) water and (B) milk recorded using a 50- $\mu$ m transmission cell and (C) difference spectrum, obtained by subtraction of spectrum A from spectrum B.

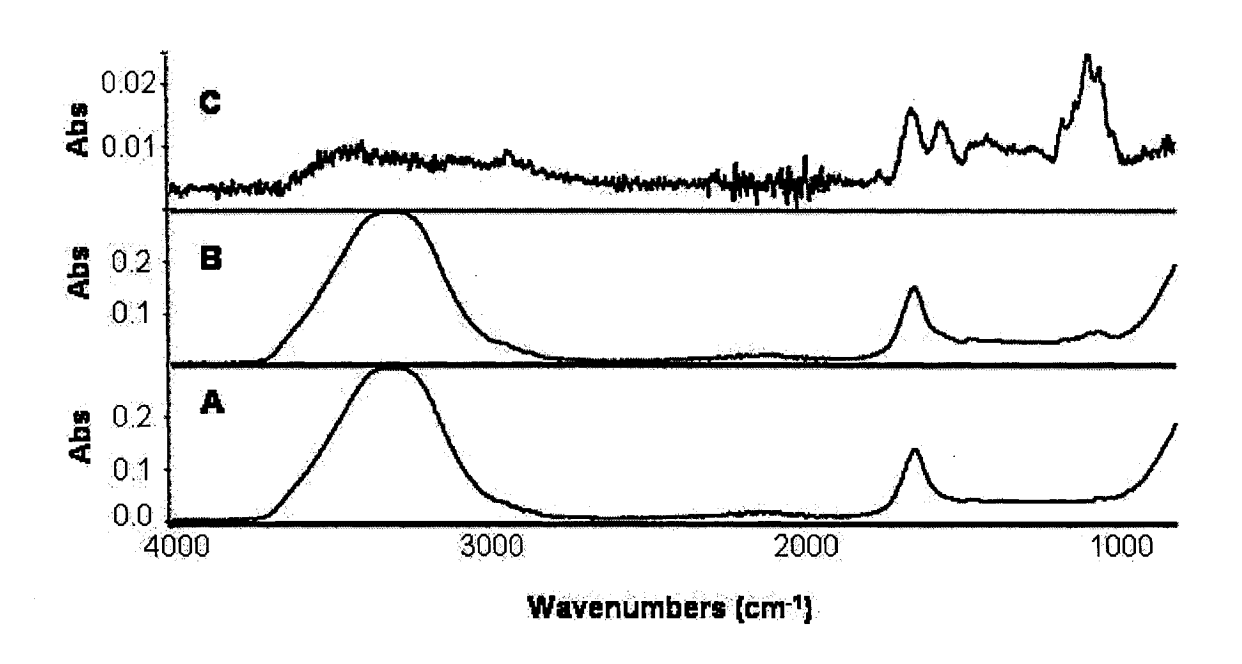


Figure 6. ATR/FTIR spectra of (A) water and (B) milk recorded using an SB-ATR accessory and (C) difference spectrum, obtained by subtraction of spectrum A from spectrum B.

Table 1. Selected vibrational bands of major food components<sup>a</sup>

Food component(s)	Frequency (cm <sup>-1</sup> )	Band assignment(s)
Water, carbohydrates	3600-3200	O-H stretching vibration; strong water IR absorption band.
Fats	3012-3004	C-H stretching of <i>cis</i> double bonds
Fats, carbohydrates, and proteins	3000-2800	C-H stretching of CH <sub>2</sub> and CH <sub>3</sub> groups
Fats	1745-1725	C=O stretching, ester linkages in triacylglycerols
Proteins	1700-1600	Amide I band, peptide linkages of proteins
Fats <sup>b</sup>	1678-1665	C=C stretching of <i>trans</i> double bonds
Fats	1662-1648	C=C stretching of <i>cis</i> double bonds
Water	1650	H-O-H bending vibration; strong IR absorption band.
Proteins	1560-1520	Amide II band, peptide linkages of proteins
Proteins	1300-1190	Amide III band, peptide linkages of proteins
Carbohydrates	1250-800	C-O stretching and C-O-H bending vibrations
Fats <sup>b</sup>	971-965	C=C-H bending of isolated <i>trans</i> double bonds

<sup>&</sup>lt;sup>a</sup>Compiled from a review of the literature. <sup>b</sup>Predominantly hydrogenated fats and oils.

a high degree of specificity by comparison of their spectra with those in a spectral database or "library".

The powerful qualitative analysis capabilities of vibrational spectroscopy can be applied to complex samples, such as foods, for purposes of classification and authentication. For such applications, multivariate analysis techniques such as principal component analysis (PCA) are commonly used to reduce the dimensionality of the spectral data (22). Because an FTIR or FT-Raman spectrum is produced by Fourier transformation of an interferogram, as described in Section 2.1.3.1, the spectra inherently consist of digital data. The dimensionality of the data depends on the spacing between data points, which is a function of the instrument resolution at which the spectra were collected and the level of zero filling employed in the calculation of the Fourier transform. For example, the FTIR spectra of condensed-phase samples are typically collected at 4-cm<sup>-1</sup> resolution between 4000 and 400 cm<sup>-1</sup> and thus, with one level of zero filling, each spectrum contains ~1800 data points. Each of these data points is a variable that contains the absorbance at a particular wavenumber, but many of these variables are highly correlated since (a) the inherent widths of the bands are usually much greater than the resolution so that a given band contributes to several contiguous data points and (b) any given species present in the sample usually has multiple bands and the intensities of these bands thus change collinearly as a function of change in concentration. By using PCA, most of the variation in the data can be described by a few orthogonal principal components (PCs), or latent variables, which are linear combinations of the original variables. The data are characterized by (a) scores, which are projections of the spectra onto each PC, and (b) loadings, which represent the contributions of the variables to each PC. Cluster analysis based on PCA scores may then be performed to group samples according to their degree of spectral similarity, which in turn reflects their degree of compositional similarity. Alternatively, with the application of supervised pattern recognition techniques (e.g., discriminant analysis), the PCA scores may be employed to assign samples to particular classes for purposes of authentication. The capability of distinguishing between different classes of samples on the basis of differences in their vibrational spectra has led to investigations of the potential utility of IR and Raman

spectroscopy as a means of detecting adulteration of foods, as will be illustrated in Section 2.1.5.2.

Both IR and Raman spectroscopy can also be employed for quantitative analysis. However, although Raman scattering intensity is directly related to concentration, quantitative analysis by Raman spectroscopy has generally been regarded as problematic, and relatively few applications in the area of food analysis have been reported. On the other hand, the scope of reported applications of quantitative IR spectroscopy in food analysis has increased substantially in recent years owing to the advantages of FTIR spectrometers and the new sample handling technologies available combined with the development of a range of sophisticated multivariate analysis methods. As in other types of absorption spectroscopy, IR quantitative analysis is based on the linear relationship between absorbance and concentration, as expressed by the Bouguer-Beer-Lambert law, commonly known as Beer's law:

$$A_{v} = \varepsilon_{v}bc \tag{9}$$

where  $A_v$  is the absorbance measured at frequency v,  $\varepsilon_v$  is the absorption coefficient of the absorbing species at the same frequency, b is the pathlength of the cell, and c is the concentration of the absorbing species. Therefore, a calibration curve can be developed by relating changes in absorbance to changes in concentration of a species at a fixed pathlength. It is important to note that IR spectroscopy is a secondary method of analysis, so the development of a calibration requires a set of standards of known composition, prepared gravimetrically or analyzed by a primary reference method. Once a calibration has been developed, it can be used to predict the concentrations of unknowns, provided that the spectra of the unknowns are recorded under the same conditions as those of the calibration standards and the spectra of the standards are representative of those of the unknowns in the spectral region(s) employed for quantitation. IR spectroscopy can also be employed to directly predict various physical properties and quality attributes of samples, provided that they are dependent on the chemical composition of the substance.

Although simple in theory, implementation of quantitative IR spectroscopy can be complicated by underlying absorptions due to other components as well as inter- and intramolecular interactions. However, these effects can usually be modeled by the application of multivariate analysis methods, such as multiple linear regression (MLR),

partial-least-squares regression (PLS), or principal component regression (PCR). A full discussion of the mathematical basis of these multivariate analysis methods is available elsewhere (29) and is beyond the scope of this chapter.

A detailed review of IR and Raman spectroscopic studies of the major components of foods has recently been published (26). Thus, in the following section, the information that can be extracted from the IR and Raman spectra of individual food components will be illustrated by considering only a single class of food components, namely, proteins. In the subsequent section, reported applications of IR and Raman spectroscopy in the qualitative and quantitative analysis of various types of foods will be surveyed. This section will highlight the most significant research findings and practical applications and will focus mainly on IR spectroscopy, owing to its more widespread use in food analysis as well as the much larger amount of research activity in this area. However, certain specific applications for which Raman spectroscopy is particularly well suited will also be discussed.

### 2.1.5.1. IR and Raman Spectroscopy of Food Proteins

IR and Raman spectroscopy have found extensive application in the study of proteins and are particularly useful techniques for the elucidation of protein secondary structure. The spectra of polypeptides and proteins exhibit nine amide bands that represent different vibrations of the peptide linkage. The wavenumber positions of these bands and their vibrational assignments are listed in Table 2. Obtaining information pertaining to protein secondary structure from IR and Raman spectra is based on empirical correlations between the wavenumbers of certain of these bands and the various conformations adopted by the polypeptide chain. The amide I band (in the range of 1700-1600 cm<sup>-1</sup>) is the most frequently employed in IR spectroscopy, and characteristic amide I band positions have been identified for  $\alpha$ -helices,  $3_{10}$ -helices, parallel or antiparallel  $\beta$ -sheets, turns, and unordered or irregular structures (Table 3). Using these band assignments, secondary structures of proteins can be deduced, although it is generally advisable to confirm the results with a second technique such as circular dichroism. The amide III band (in the range of 1300-1190 cm<sup>-1</sup>) can similarly be employed for the estimation of the relative proportions of the secondary-structure components. However, in

Table 2. Amide bands of proteins<sup>a</sup>

Designation	Nature of vibration		
A	N-H stretching		
В	N-H stretching		
I	80% C=O stretching; 10% C-N stretching; 10% N-H bending		
II	60% N-H bending; 40% C-N stretching		
III	30% C-N stretching; 30% N-H bending; 10% C=O stretching; 10% O=C-N bending; 20% other		
IV	60% O=C-N bending; 40% other		
V	N-H bending		
VI	C=O bending		
VII	C-N torsion		

<sup>&</sup>lt;sup>a</sup>Adapted from Ref. 42.

Table 3. Approximate positions (cm<sup>-1</sup>) of amide I' band components in IR spectra of proteins<sup>a</sup>

Secondary-structure component	Frequency (cm <sup>-1</sup> )
Antiparallel β-sheet (intra- or intermolecular)	1695-1675
Loops and turns	1674-1662
α-Helix	1659-1646
Unordered structure (random coil)	1645-1641
3 <sub>10</sub> -Helix	1639-1637
Intramolecular parallel or antiparallel β-sheet <sup>b</sup>	1636-1625
Intermolecular antiparallel β-sheet <sup>c</sup>	1624-1614

 $<sup>^{</sup>a}$ Compiled from a review of the literature. The band positions are for proteins in  $D_{2}O$  solution (by convention, termed amide I' band components).

<sup>&</sup>lt;sup>b</sup>Assigned to antiparallel β-sheet structure when it is accompanied by a high-wavenumber component (1695-1675 cm<sup>-1</sup>); otherwise, assigned to parallel (or extended) β-sheet structure.

<sup>&</sup>lt;sup>c</sup>Indicative of protein aggregation.

some cases, the amide III band can be overlapped by bands due to side-chain vibrations of particular amino acid residues--or absorptions from other biomolecules present, for example, in a food matrix--and consequently one must be cautious when assigning bands in this region. In IR spectra, the amide III band is much weaker than the amide I band and hence is much less frequently employed in secondary-structure investigations. However, both the amide I and amide III bands are commonly employed in Raman spectroscopy (Table 4), as their Raman intensities are comparable.

The IR spectra of proteins are most commonly recorded in aqueous solution in a transmission cell, although ATR accessories have also been employed to study the spectra of protein films and powdered samples (Figure 7). The Raman spectra of proteins can also be recorded in aqueous solution but the spectra obtained from solid samples are generally of much higher quality and exhibit sharper bands (Figure 8). For IR studies involving examination of the secondary-structure-sensitive amide I band, proteins are commonly dissolved in D<sub>2</sub>O because H<sub>2</sub>O has a strong band in the amide I region. Since D<sub>2</sub>O has no absorptions that overlap with the amide I band (which, by convention, is termed the amide I' band when D<sub>2</sub>O is the solvent), the use of D<sub>2</sub>O solutions allows the protein absorptions to be observed without the need for subtraction of the spectrum of the solvent. More importantly, it also makes it permissible to use much longer pathlengths (40-80 μm vs. 10 μm for aqueous solutions), thereby yielding a higher signal-to-noise ratio. An additional advantage of dissolving proteins in D<sub>2</sub>O is the resulting ability to study the rate at which the hydrogens of the amide groups exchange with the D<sub>2</sub>O solvent due to the ~100-cm<sup>-1</sup> shift of the amide II band (from 1560-1520 to 1460-1420 cm<sup>-1</sup>) that occurs upon H-D exchange. This rate is indicative of the compactness of the protein since amide groups exposed to the solvent undergo H-D exchange faster than those in the interior of the protein. Thus, increases in the rate of H-D exchange as a result of variations in physicochemical parameters such as pH, temperature, and pressure can be interpreted in terms of the extent of protein unfolding.

Because of the inherent overlap between the amide I' band components of the various conformations of the polypeptide backbone, computational band-narrowing techniques such as Fourier self-deconvolution (FSD) and derivative spectroscopy are routinely employed. It should be noted that caution must be exercised in applying these

Table 4. Approximate positions (cm<sup>-1</sup>) of amide I and amide III band components in Raman spectra of proteins<sup>a</sup>

Secondary structure component	Amide I (cm <sup>-1</sup> )	Amide III (cm <sup>-1</sup> )
α-Helix	1660-1645	1300-1265
β-Sheet	1680-1665	1240-1230
Unordered structure (random coil)	1670-1660	1260-1240

<sup>&</sup>lt;sup>a</sup>Adapted from Ref. 9.

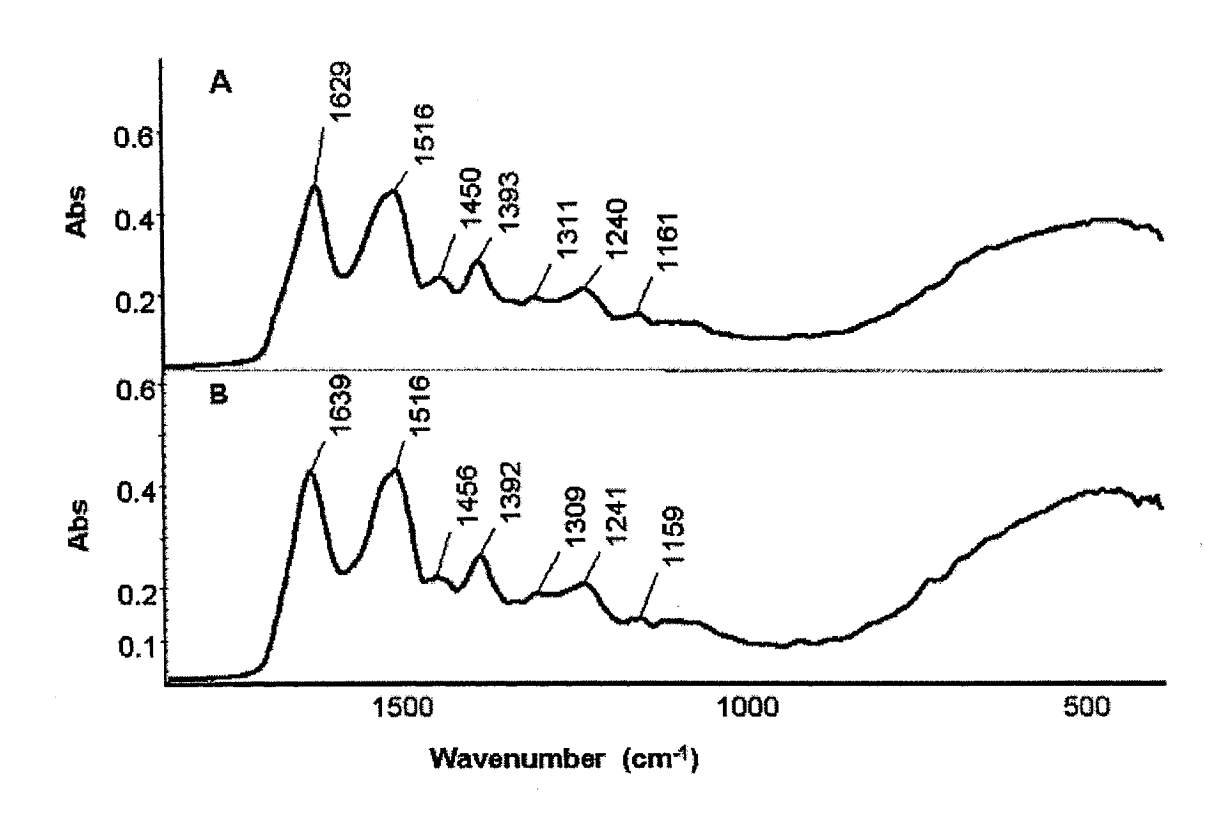
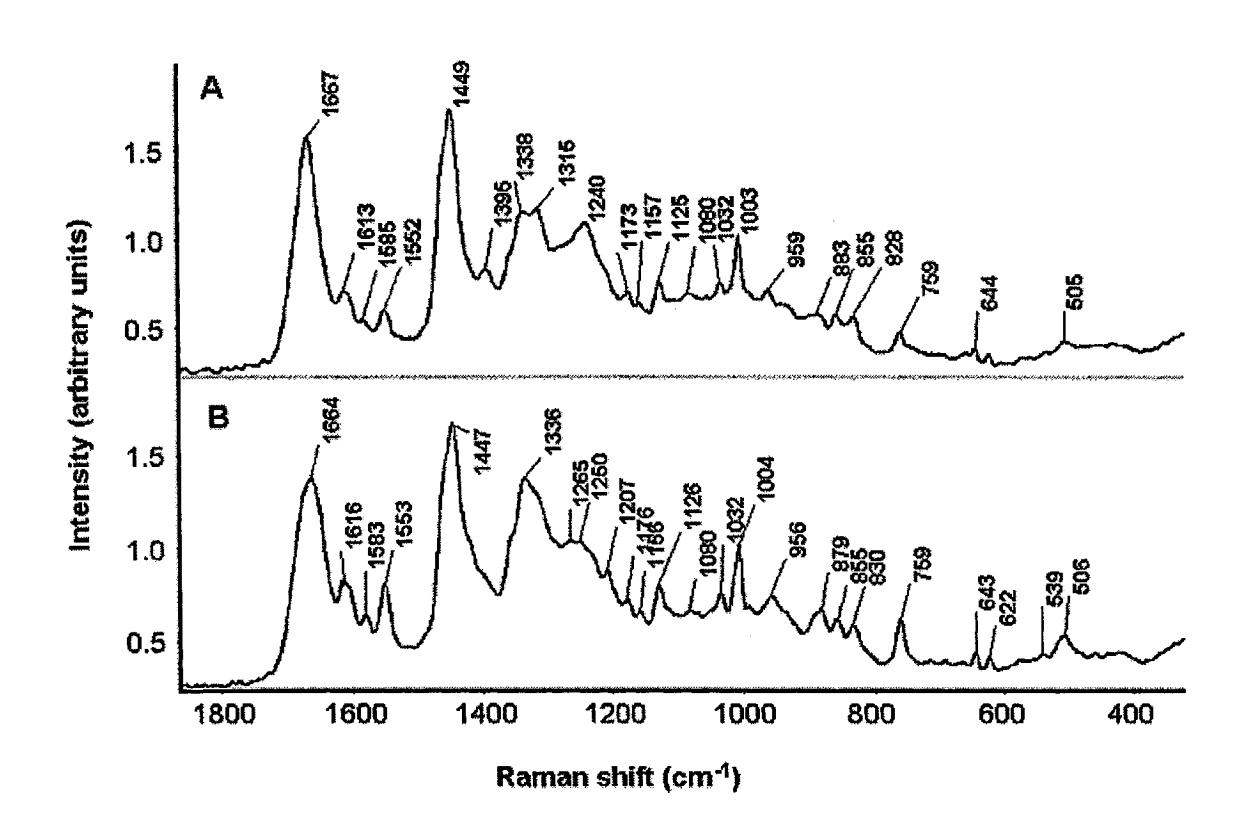


Figure 7. ATR/FTIR spectra of (A) powdered  $\beta$ -lactoglobulin and (B)  $\alpha$ -lactalbumin recorded using an SB-ATR accessory. A pressure device was employed to ensure optical contact between the sample and the ATR crystal.



**Figure 8.** FT-Raman spectra of (A) powdered  $\beta$ -lactoglobulin and (B)  $\alpha$ -lactalbumin in 1-mm glass capillaries recorded with 1064-nm excitation. (Nd:YAG laser). For band assignments, see Ref. 36.

techniques because they can distort the shapes of the bands and can also decrease the signal-to-noise ratio (43). Furthermore, the relative band intensities in derivative spectra are affected by the inherent widths of the bands, whereas deconvolution has the advantage of preserving the true relative band intensities (43). On the other hand, the results of deconvolution depend strongly on the values of the adjustable deconvolution parameters and are thus more subject to artifacts. For example, as illustrated in Figure 9, the selection of inappropriate deconvolution parameters that result in "overdeconvolution" amplifies the spectral noise, which may lead to spurious peaks. Similarly, atmospheric water vapor gives rise to very weak narrow peaks in the amide I region of IR spectra that can also be misinterpreted as amide I' band components in deconvolved spectra. The latter pitfall is best avoided by thoroughly purging the spectrometer, including the optical compartment, with dry air or nitrogen. Other possible sources of artifacts are absorptions of buffers or contaminants in the protein solution (44).

Additional information about protein structure can be obtained from bands due to side-chain vibrations of amino acid residues, such as aspartic acid, glutamic acid, tyrosine, and tryptophan. For example, the ratio of the intensities of the Raman bands of tyrosine at 850 and 830 cm<sup>-1</sup>, attributed to ring-breathing and out-of-plane bending vibrations, respectively, provides the following information about the polarity of the microenvironment of tyrosine residues (39):

- High  $I_{850}/I_{830}$  (>2.5): Tyr acts as H-bond acceptor.
- Low  $I_{850}/I_{830}$  (<0.5): Tyr acts as H-bond donor.
- $I_{850}/I_{830} \sim 1$ : Tyr is exposed to an aqueous environment (i.e., Tyr near or at the protein surface)

Raman spectroscopy is also a very useful tool for probing the formation and rupture of disulfide linkages because the S-S and S-H stretching vibrations can be clearly discerned in the Raman spectra of proteins. The FT-Raman spectra of the amino acids L-cysteine and L-cystine are presented in Figure 10 and show, respectively, a band at 2552 cm<sup>-1</sup> assigned to the S-H stretching vibration and a band at 498 cm<sup>-1</sup> assigned to the S-S stretching vibration. In the Raman spectra of proteins, these bands are shifted to 2580-2550 and 550-500 cm<sup>-1</sup>, respectively (25). The corresponding IR bands are not readily discernible, making Raman spectroscopy the technique of choice for the observation of

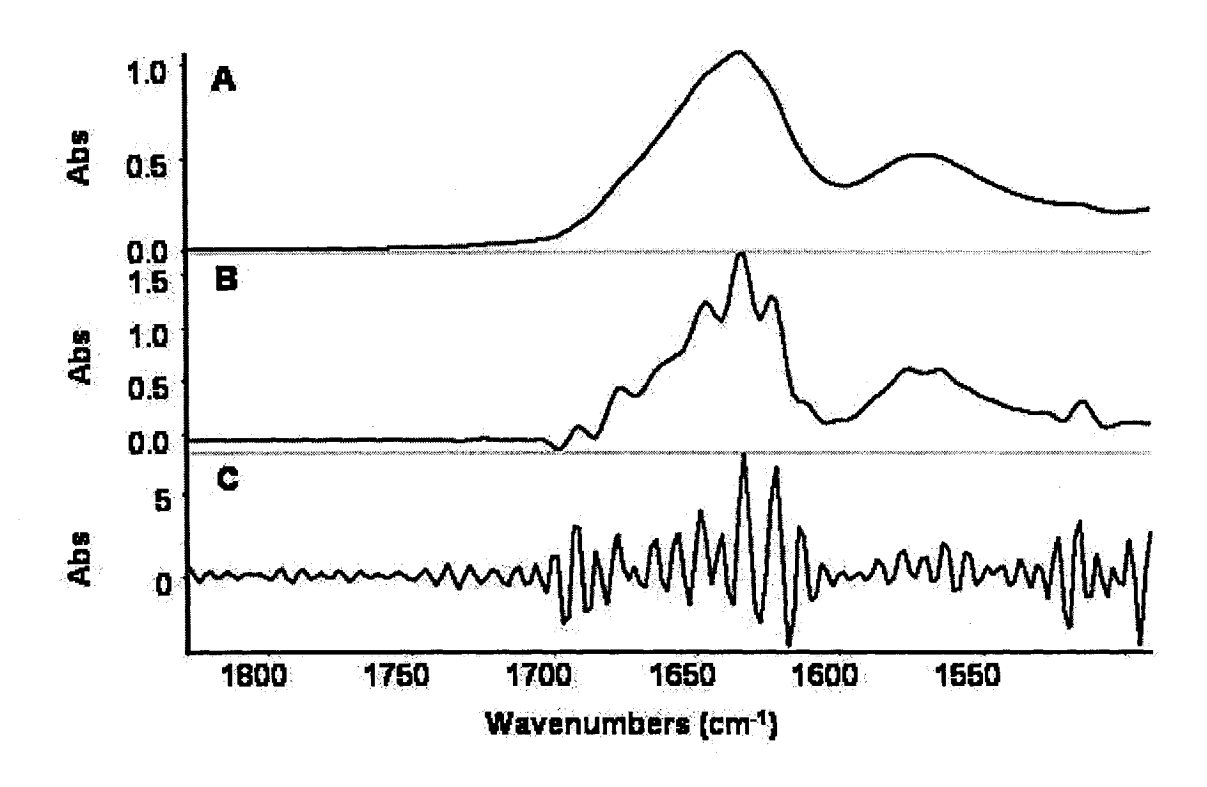
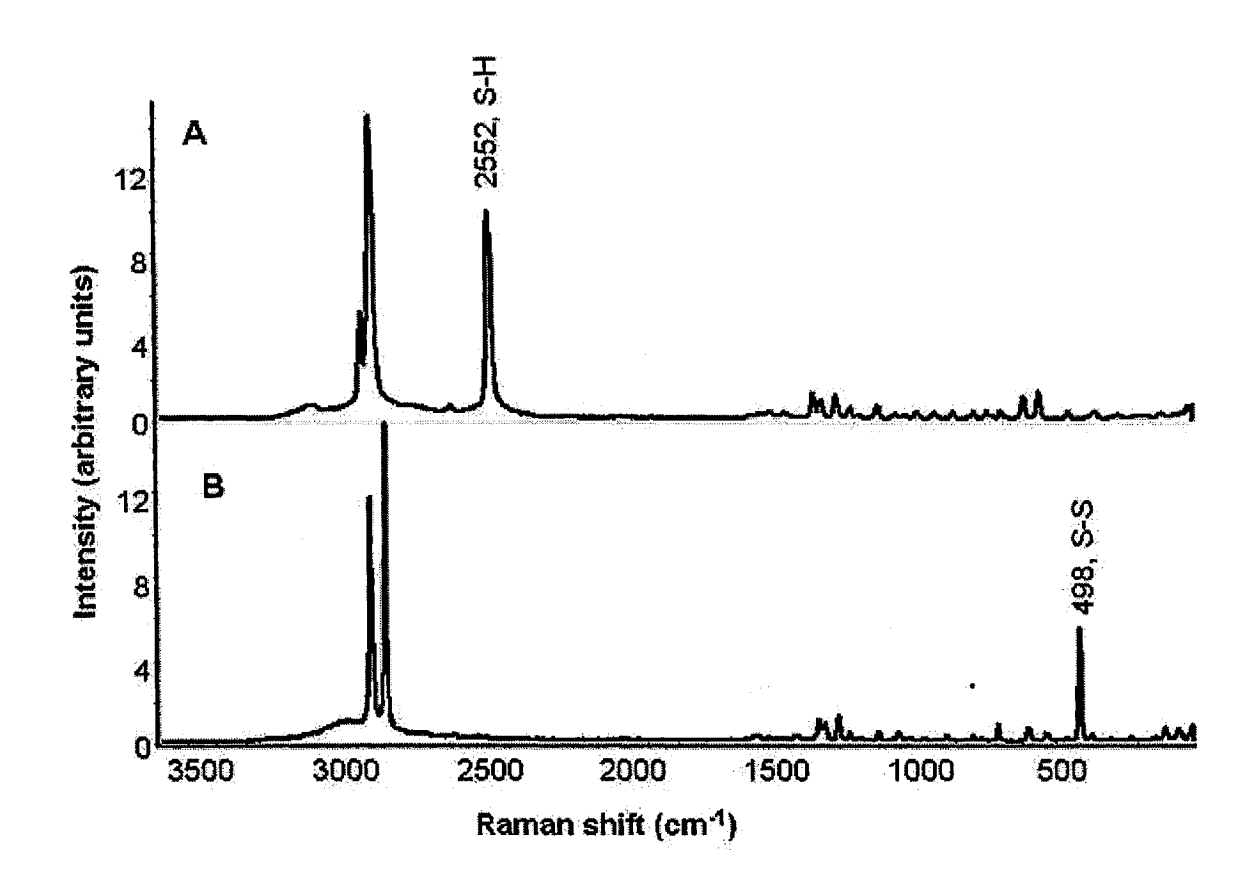


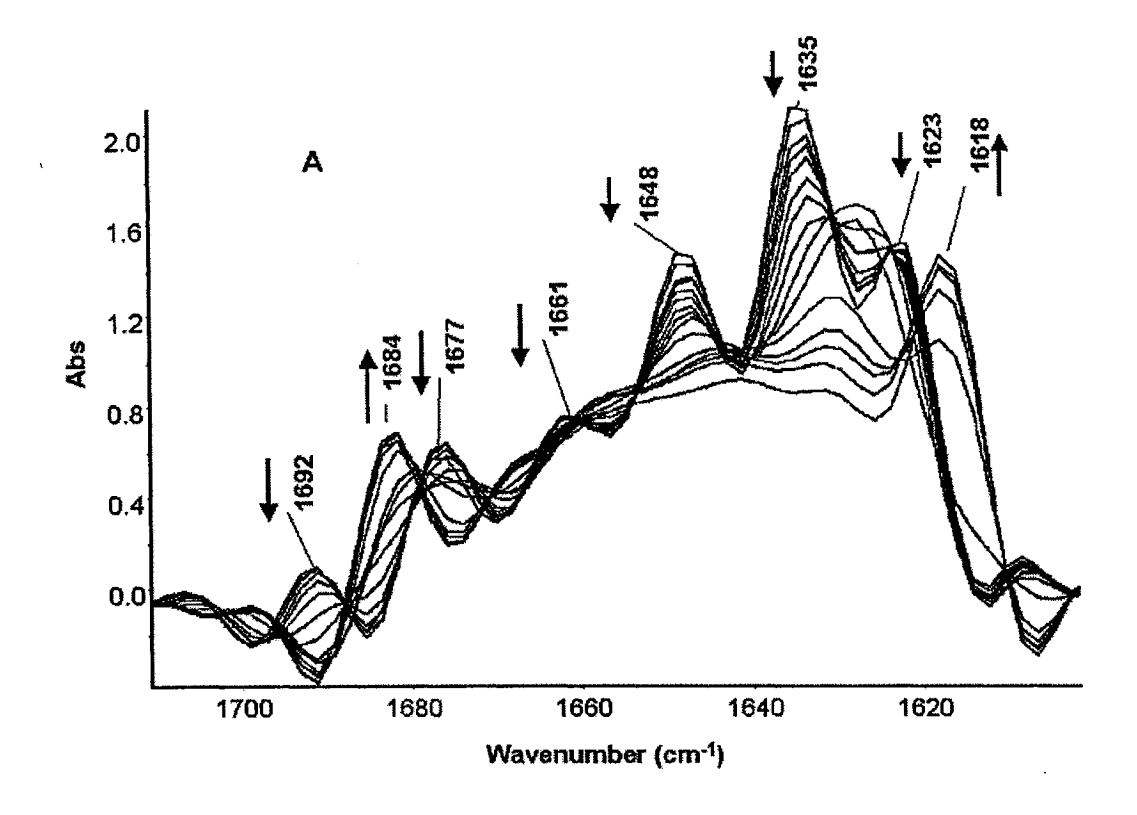
Figure 9. (A) Raw FTIR spectrum, (B) spectrum after Fourier self-deconvolution (FSD), and (C) "overdeconvolved" spectrum of  $\beta$ -lactoglobulin in  $D_2O$  (5% w/v). FSD parameters: (B) bandwidth factor of w=27 and resolution enhancement factor of k=2.4; (C) w=27 and k=4.



**Figure 10**. FT-Raman spectra of (A) L-cysteine and (B) L-cystine. The spectra were recorded from solid samples in 1-mm glass capillaries, with 1064-nm excitation (Nd:YAG laser). Laser power was 500 mW; 1024 co-added scans were collected at 8-cm<sup>-1</sup> spectral resolution.

disulfide linkages and examination of thiol-disulfide exchange. For example, in Figure 8, the higher content of disulfide linkages in  $\alpha$ -lactalbumin as compared to  $\beta$ -lactoglobulin is evident from the stronger intensity of the v(S-S) band at  $\sim 505$  cm<sup>-1</sup>.

Although many of the proteins that have been studied by FTIR and Raman spectroscopy may be categorized as food proteins, such as whey, soy, and egg proteins, the majority of these studies have not been specifically concerned with the behavior of the proteins as food components. However, as reviewed in Ref. 26, some detailed investigations of food proteins have been conducted to gain a better understanding of protein stability and structure-functionality relationships, with the overall objective of obtaining information that can assist the food industry in making more effective use of food proteins. Figure 11 shows an example from our studies on the thermal denaturation of whey proteins by variable-temperature FTIR spectroscopy (5-8). The spectra in the amide I region in Figure 11A were recorded during heating of a 7% (w/v) solution of \u03b3lactoglobulin in D<sub>2</sub>O in a temperature-controlled transmission cell from 25 to 95°C and have been deconvolved by Fourier self-deconvolution. A plot of the changes in intensity of several of the amide I' band components as a function of temperature is shown in Figure 11B. The decreases in band intensity at 1648 (A) and 1635 cm<sup>-1</sup> (•), assigned to α-helical and intramolecular β-sheet structures, respectively, are indicative of protein denaturation and occur prior to a sharp increase in the band intensity at 1618 cm<sup>-1</sup> (■), assigned to intermolecular β-sheet formation and characteristic of protein aggregation. Similar experiments have been performed with the use of a diamond-anvil high-pressure IR cell to monitor denaturation of whey proteins under conditions of applied hydrostatic pressure, similar to those to which they are subjected during high-pressure processing, and have provided information on the nature of the differences between thermal and pressure-induced denaturation (19, 20). In addition, multivariate analysis techniques have been employed to correlate FTIR spectral changes observed as a function of changes in physicochemical parameters, such as pH, ionic strength, temperature, and pressure, with rheological data collected under the same conditions (26). Such studies provide a unique means of gaining a better understanding of the structural changes at the molecular level that govern rheological behavior.



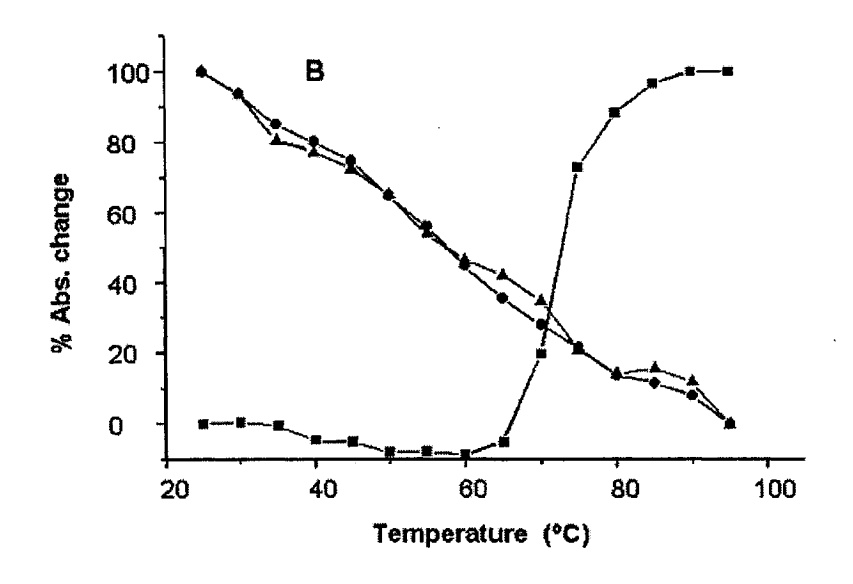


Figure 11. (A) Spectral overlay plot of the deconvolved amide I' band in the FTIR spectrum of  $\beta$ -lactoglobulin (7% w/v) as a function of increasing temperature (25-95°C). FSD parameters: w = 27 and k = 2.4. (B) Plot of changes in intensity at 1648 ( $\blacktriangle$ ), 1635 ( $\bullet$ ), and 1618 cm<sup>-1</sup> ( $\blacksquare$ ) as a function of increasing temperature.

# 2.1.5.2. Analysis of Milk and Dairy Products by FTIR and Raman Spectroscopy

To date, the utility of IR spectroscopy in the quantitative analysis of foods has been most clearly exemplified by milk analysis. The determination of fat, protein, and lactose in milk by IR spectroscopy is an official method of the Association of Official Analytical Chemists (AOAC) and is used extensively as a basis for milk payment, dairy herd recording, and routine quality control in the dairy industry. High-volume automated instruments allow for the analysis of 100-500 samples per hour. Dispersive spectrometers and subsequently filter-based instruments were originally employed in commercial IR milk analyzers, but FTIR milk analyzers are now on the market (3). The accepted IR milk analysis methodology employs a 37-µm CaF<sub>2</sub> transmission flow cell, which is kept at a constant temperature (40±0.1°C) to obtain reliable, stable, and accurate measurements. Typically, IR milk analyzers incorporate a high-pressure (150-200 kPa) homogenizer to reduce the size of the fat globules to <1 μm in order to avoid light scattering effects. The pressure is maintained in the system throughout the analysis to avoid formation of air bubbles in the cell, and the cell is flushed with the next sample at extremely high velocity (30 m/s), eliminating the need for rinsing of the cell. Whereas filter-based IR milk analyzers were restricted to the analysis of fat, protein, and lactose, because the filters employed were specifically selected for the measurement of these components, commercial FTIR milk analyzers can be calibrated to measure other components in a wide range of dairy products, such as infant formula, ice cream, yogurt, and whey and whey concentrates (3).

In transmission measurements of dairy products, light scattering by fat globules must be eliminated in order to obtain quantitative analytical results. In the case of fluid products, this requirement can be addressed, albeit at some cost, by the use of high-pressure homogenizers, as described above. Because ATR measurements are not affected by light scattering, ATR accessories would appear ideal for the analysis of dairy products, including non-fluid products such as butter and cheese. However, the presence of fat globules in dairy products is, in fact, highly problematic because it results in sample inhomogeneity on the scale of the depth of penetration, which is on the order of a few microns or less, and thus the spectrum obtained is not truly representative of the sample

composition. In a study of the effect of fat globule size in cream on ATR/FTIR measurements, a nonlinear relationship was found between absorbance at 1744 cm<sup>-1</sup> (commonly used as a measurement peak for fat) and fat content over the range of 0-48% (by volume) (23). The authors of this study proposed the use of a nonlinear calibration curve for samples having fat globules > 1 \text{ \text{µm}}. In a study of the feasibility of employing ATR/FTIR spectroscopy for fat, protein, and moisture determination in cheese (30), large variations in the ATR/FTIR spectra of replicate samples taken from the center of a cheese were observed owing to both variations in the diameter of the fat globules and inhomogeneous distribution of fat within the cheese. Based on the fairly poor accuracy of PLS calibrations that were developed for the determination of fat, protein, and moisture contents, the authors concluded that the utility of the ATR/FTIR method for the analysis of cheese was quite limited but might be improved by homogenization of the samples prior to analysis; however, this requirement would significantly complicate the procedure. Another approach to overcoming the problem was employed in the development of a rapid FTIR quality control method for fat and moisture determination in butter employing an ATR sample-handling accessory (45). Samples were dissolved in 1-propanol and warmed to 40°C, thereby solubilizing the fat without causing separation of an aqueous phase, and applied to a heated ATR crystal (40°C) for spectral recording. A calibration was developed by employing gravimetrically prepared mixtures of anhydrous butterfat and water in 1-propanol as calibration standards. Analysis of 20 butter samples by this ATR/FTIR method yielded good agreement with reference values obtained by the Mojonnier method (45).

The speed of FTIR analysis (typically, <2 min/sample) is particularly advantageous in a processing environment since it allows the manufacturing process to be monitored and adjusted as it proceeds. A method for the simultaneous determination of sucrose, lactose, total solids, and fat in chocolate milk by FTIR spectroscopy for use in a production environment has been described (11). An ATR/FTIR method for fat and solids determination was developed for quality control purposes during manufacture of sweetened condensed milk (34). The ATR sample-handling technique is highly suitable for this type of viscous product, which would be very difficult to handle if a transmission cell were used, and highly reproducible results were obtained when samples were

homogenized at 65°C using a polytron mixer prior to ATR/FTIR analysis. More recently, an SB-ATR/FTIR method has been developed for monitoring enzymatic hydrolysis of lactose during the production of lactose-reduced milk (10).

# 2.2. Electrospray Ionization Mass Spectrometry (ESI-MS) in the Study of Protein Structure

#### 2.2.1. Introduction

The mass spectrometry (MS) has undergone a series of modifications and improvements in the last decade to enable the study of high molecular weight molecules such as proteins and to examine the non-covalent interactions between different moieties present in the molecule (15). These include electrostatic, hydrophobic protein-ligand, protein-DNA and protein subunits interactions.

## 2.2.2. Background

The history of MS began with Sir Joseph John Thomson (1856-1940) at the Cavendish Laboratory of the University of Cambridge, where the studies on electrical discharges of gases led to the discovery of the electron in 1897. In the first decade of the 20<sup>th</sup> century, Thomson went on to construct the first mass spectrometer (then called a parabola spectrograph) for the determination of mass-to-charge ratios of ions. Figure 12 shows a representation of this instrument where ions generated in the discharge tubes were passed into electric and magnetic fields which made the ions move through parabolic trajectories. The ion impacts formed spots that were detected and recorded on a fluorescent screen or a photographic plate. Sir Thomson received the 1906 Nobel Prize in physics "in recognition of the great merits of his theoretical and experimental investigations on the conduction of electricity by gases" (21).

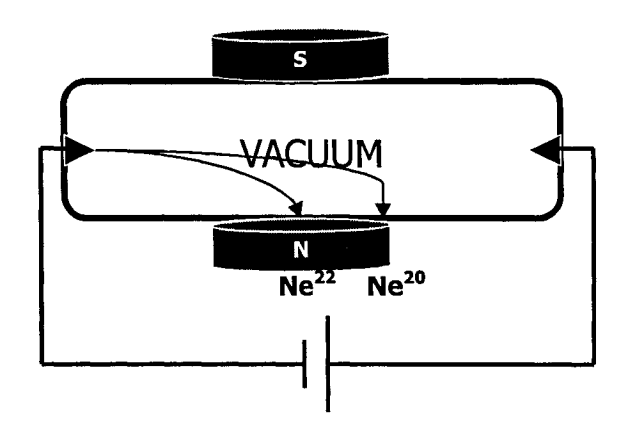


Figure 12. The parabola spectrograph. This set up allowed Thomson to separate stable isotopes of an element such as neon. The ions of different mass, velocity, and charge are moved differently by the electric and magnetic fields, permitting their separation.

# 2.2.3. The Modern Mass Spectrometer

The modern mass spectrometer can be separated in the following components: the ionization source, the analyzer and the detector. There are several different types of this components and each array has its own capabilities and applicability. Figure 13 show an oversimplified representation of a mass spectrometer, where the sample is first ionized, the positive or negative ions separated one from each other; ultimately the ions of the charge of choice are resolved by their different masses by the time they reach the detector (12).

# 2.2.4. Fundamental Principles of Mass Spectrometry

Mass spectrometry uses the differences in weight of the molecules to identify them by comparison with a standard or the theoretical weight of that specific molecule; all the calculations are relative to the carbon molecule being exactly 12.000 g/mol. The primary interests in MS studies can be catalogued in 3 areas: a) to determine the precise mass of a specie which can be achieved with an accuracy of 0.1% of the actual mass; b) to determine the relative abundance of the different types of ions formed and c) electron impact studies (12).

#### 2.2.5. Instrumentation

#### 2.2.5.1. Ionization Techniques

The first step of the MS is to produce ions of the sample molecules. The different ionization techniques can be separated into "hard" and "soft" methods; the difference between the two is that in the hard methods, the sample molecule is fragmented in pieces at the same time the ions are generated, however in the soft techniques the degree of breakage is reduced and in some cases almost no fragmentation occurs. Hard methods impose a limitation to the size of the sample one can study whereas using soft methods one can have virtually no size limitation (33).

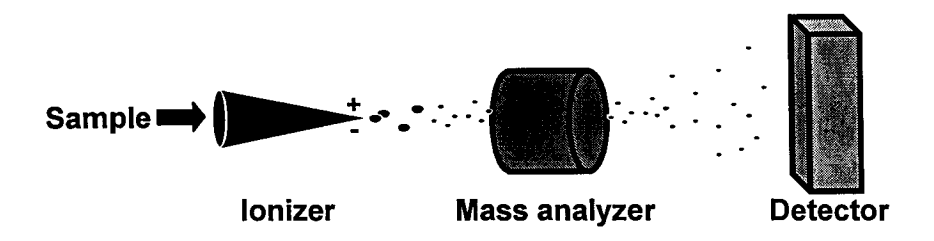


Figure 13. Schematic representation of a mass spectrometer. The sample is injected and ionized in either positive or negative ions which are then separated by mass and quantified.

#### **2.2.5.1.1.** Hard Methods

The following are only two examples of the different hard ionization techniques.

## **2.2.5.1.1.1.** Electron Impact (EI)

This is the first ionization method developed and is still used to study small species in the range of 1 to 1 000 Daltons. The procedure involves heating the sample until evaporation occurs and then bombard the gas phase with electrons emitted from a hot wire filament. The molecules are therefore shattered to fragments of different sizes, computer programs help to reconstruct the original molecule.

## 2.2.5.1.1.2. Fast Atom Bombardment (FAB)

Here a solid sample is bombarded with an accelerated neutral atom (i.e.: Argon); ions are produced with the impact, analyzed and quantified. This method is able to examine peptides up to 6 kDa.

#### **2.2.5.1.2.** Soft Methods

There are several different soft ionization techniques, this is only one example but two others are found under desorption methods.

Chemical Ionization (CI) creates the ions using a diversity of chemical reactions. It is not suitable for big molecules and requires time-consuming sample preparation.

#### 2.2.5.1.3. Desorption Techniques

Under this division are found the ionization methods that involve the "pulling out" or desorption of sample atoms or molecules from the sample surface.

## 2.2.5.1.1.1. Laser Desorption

This is an ionization method that uses a high-energy laser beam focused on to a small area of a solid sample. This exposes the sample to very high temperatures and is generally not suitable for biological samples.

# 2.2.5.1.1.2. Matrix Assisted Laser Desorption Ionization (MALDI)

This is a soft method which is able to study peptides, proteins or DNA up to 500 kDa. The sample is dissolved in a matrix solution in proportions of 1:1000 or 1:10000. A laser beam is focused to a dried aliquot; the laser energy is absorbed by the matrix molecules and transferred to the sample that undergoes phase transition and ionization. The Figure 14 show a diagram of the MALDI desorption using cyano-hydroxy cinnamic acid as the matrix and a laser with a frequency of 370 nm.

# 2.2.5.1.1.3. ElectroSpray Ionization (ESI)

This is another soft method useful to study peptides or proteins up to 200 kDa. A liquid solution of the sample is injected into the instrument; a high voltage is applied to the capillary tip and tiny droplets containing an excess of positively charged particles (can be also reversed to negatively charged) are dried and driven to the mass analyzer. The Figure 15 illustrate the general principle of ESI, the accumulation of positively charged molecules in the tip disturbs the solution meniscus and leads to the formation of a cone from which droplets are jet emitted. These droplets are split into smaller droplets which shrink by the evaporation produced from a stream of hot dry gas. Finally they become gas-phase positive ions.

There are different means to achieve the formation of the sample aerosol needed for ESI; Figure 16 show four different techniques to achieve this purpose fig. 16A shows the simple liquid flow; fig. 16B shows the liquid flow helped with a sheath flow; fig. 16C shows the liquid flow assisted with a nebulizing gas that runs around the sample; and fig. 16D shows the liquid flow facilitated with ultrasonic waves.

#### 2.2.6. ESI-MS and Protein Structure

As previously discussed, ESI-MS is a good candidate to study biological samples due to its capability to handle big molecules such as proteins; it contains relevant structural information that can serve a myriad of applications.

The other good technique that can serve this purpose is NMR but with a limitation on molecular size. ESI-MS has virtually no limitation pertinent to the size of the molecule of study.

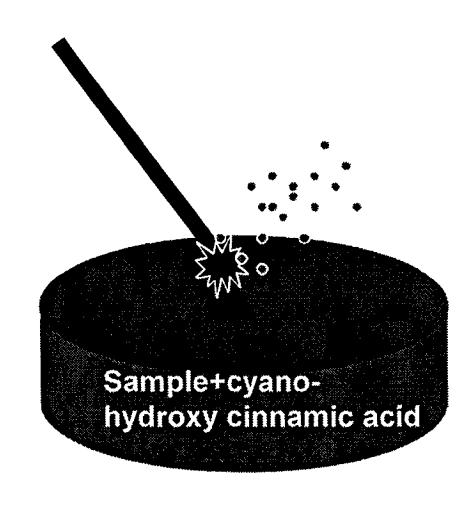
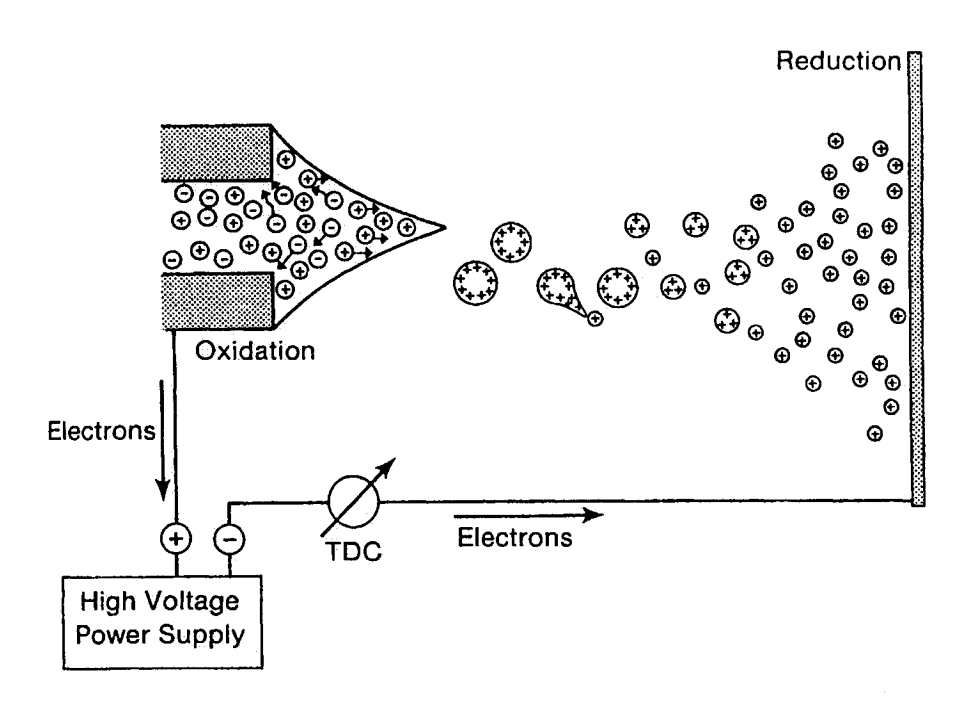


Figure 14. Schematic representation of the MALDI desorption technique using cyanohydroxy cinnamic acid as the matrix and a laser beam of 370 nm.



**Figure 15**. Schematic representation of the electrospray ionization technique. Positively charged ions are forced to concentrate in the tip of the capillary by a high voltage electric current; tiny droplets are jet emitted and dried to form gas-phase ions (from Ref. 12).

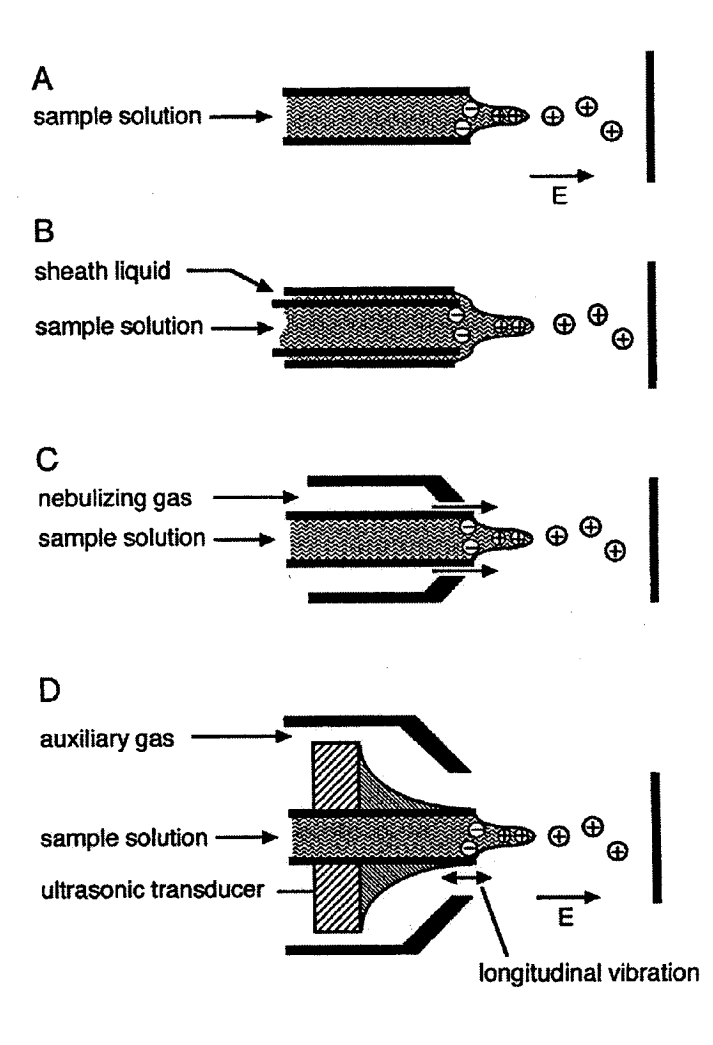


Figure 16. Different modes of creating the sample aerosol for ESI. (A) Simple liquid flow. (B) With sheath flow. (C) With pneumatic assistance. (D) With ultrasonic assistance (from Ref. 12).

Although some studies has been made combining the information obtained from the two techniques (ESI-MS and NMR) helping in the understanding of protein refolding (31).

ESI-MS has proved through the years it's usefulness in a variety of studies, such as: a) protein denaturation; b) protein-ligand interactions; c) protein characterization and d) protein conformation studies.

# 2.2.6.2. Application of ESI-MS in the Study of Protein structure

ESI-MS has been employed for the determination of the changes in the tertiary structure of protein. For example, changes in the structure of ferricytochrome c caused by increasing concentrations of hydrochloric acid in different concentrations of methanol were examined by Konermann and Douglas (1997). In 3% methanol the decrease in pH causes a cooperative unfolding at pH 2.6 with a loss of the native secondary and tertiary structure of the protein. At 50% methanol concentration the unfolding transition occurs at pH 4.0 with only a breakdown in the tertiary structure, with the secondary structure largely unaffected (24). Babu et al. (2001) studied the methanol-induced conformational changes under acidic conditions of  $\beta$ -Lactoglobulin, cytochrome c, and ubiquitin. They found partially unfolded intermediates with induced α-helix structures. These intermediates were formed at 35% methanol concentration. The authors contrasted their findings with previous results from optical methods like circular dichroism (4). Anderegg and Wagner (1995) studied the stability of a recombinant src homology 2 (SH-2) domain from pp60c-src protein kinase bound to a variety of synthetically produced ligands. They characterized the different effects of the ligands on the hydrogen-deuterium exchange of the complex (2). Slanger and Visser (1999) studied the nonglycosylated and glycosylated forms of α-lactalbumin; they identified the nonglycosylated fraction with a mass of 14178 Da and for the glycosylated fraction they found a variety of components (as much as 14 types) with mass values from 15840 to 16690 Da (40). Sanglier et al. (2003) compared the oligomeric state of hemocyanins (Hc) from crabs living at different sea depths. The results indicate that for Bythograea thermydron, a deep sea crab, its Hc was arranging in as many as 30 subunits. The oligomeric state of the Hc is then directly related to the amount of oxygen found in that particular biotope (38). Stevens et al.

(2002) isolated and analyzed various cytolysin proteins from the sea anemone *Stichodactyla helianthus*; they also studied peptides obtained by the trypsin digestion of the proteins (41). Nilsson *et al.* (2002) characterized the highly hydrophobic outer membrane component P13 from *Borrelia burgdorferi* and some mutant forms of this protein (35).

The different quaternary structures of concanavalin A were investigated by Light-Wahl *et al.* (1993). In a later publication the same group expanded their work investigating avidin and human haemoglobin (28, 27). The structural characterization of the synthetic peptide from the sequence 1-30 of *Par j* 1.0101 a major allergenic protein found in the pollen of *Parietaria judaica* was made by Cunsolo et al. (2001). They successfully identified and mapped the disulphide bonds present in the peptide (14). Hooke *et al.* (1995) studied the molecular folding of hen lysozyme using hydrogendeuterium exchange and <sup>15</sup>N isotopic labelling (18). The effect of trifluoroethanol on a synthetic myoglobin peptide and cytochrome *c* at low pH was investigated by Grandori et al. (2002). They found ESI-MS to be insensitive to changes in the secondary structure of the molecule, but capable to detect changes in the tertiary structural level (16). Mohimen et al. (2003) developed a chemometric protocol to analyze information from ESI-MS relative to multiple protein conformers in solution. The signals from the different states of a protein in the same sample often overlap yielding a confusing spectrum. The use of modern chemometrics helped to overcome this limitation (32).

In general terms MS study the weight of molecules, but with ESI one can also observe and quantify the population of charged species formed by the ionization process. In the traditional analysis the data is used to calculate, as accurate as possible, the mass of the sample molecule. But there is another analysis that is becoming popular and it include the study of the third dimensional structure of proteins interpreting in a new fashion the data from ESI-MS.

The principle of the analysis is that the more flexible (relaxed structure) the protein is, the easier will be to charge groups in the interior of the molecule at the ionization stage. In this sense, the more relaxed the protein a higher proportion of the

population of molecules will display higher charges (1). The chart displaying the different charged states of the molecule of study is called charged-state-distribution (CSD).

A protein in its native state will show a CSD inclined to the range of lower charges or a higher mass-over-charge (m/z) ratio. An unfolded protein will have a larger m/z ratio as previously buried groups in the structure get ionized by exposing them to an acidic solvent (1).

In this work FTIR and Raman spectroscopy and ESI-MS will be employed in the elucidation of the changes in the structure of individual whey proteins and whey protein isolates in solution, exposed to varying magnitudes of ultra high hydrostatic pressure that alter the viscoelastic properties of the proteins. Changes in the rheological properties of the proteins solution will also be examined by dynamic rheology techniques. The results obtained from this work will lay the foundation for understanding the molecular basis of viscoelastic properties of proteins.

#### 2.3. References

- 1. Alomirah H.F., Alli I., Konishi Y. 2000. Applications of Mass Spectrometry to Food Proteins and Peptides. Journal of Chromatography A. 893:1-21.
- 2. Anderegg R.J., Wagner D.S. 1995. Mass Spectrometric Characterization of a Protein-Ligand Interaction. J Am Chem Soc 117:1374-1377.
- 3. Andersen S.K., Hansen P.W., Andersen H.V. 2002. Vibrational Spectroscopy in the Analysis of Dairy Products and Wine. In: Chalmers J.M., Griffiths P.R., eds. Handbook of Vibrational Spectroscopy. New York: John Wiley & Sons, Vol 5, pp 1-10.
- 4. Babu K.R., Moradian A. Douglas D.J. 2000. The Methanol-Induced Conformational Transitions of β-Lactoglobulin, Cytochrome c, and Ubiquitin at Low pH: A Study by Electrospray Ionization Mass Spectrometry. Am Soc Mass Spectrom 12:317-328.
- 5. Boye J.I., Alli I., Ismail A.A. 1996. Interactions Involved in the Gelation of Bovine Serum Albumin. J Agric Food Chem 44:996-1004.
- 6. Boye J.I., Alli I., Ismail A.A. 1997. Use of Differential Scanning Calorimetry and Infrared Spectroscopy in the Study of Thermal and Structural Stability of α-Lactalbumin. J Agric Food Chem 45:1116-1125.
- 7. Boye J.I., Ismail A.A., Alli I. 1996. Effect of Physico-Chemical Factors on the Secondary Structure of β-Lactoglobulin. J Dairy Res **63**: 97-109.

- Boye J.I., Ma C.Y., Ismail A.A., Harwalkar V.R., Kalab M. 1997. Molecular and Microstructural Studies of Thermal Denaturation and Gelation of β-Lactoglobulins A and B. J Agric Food Chem 45:1608-1618.
- 9. Carey P.R. 1982. Biochemical Applications of Raman and Resonance Raman Spectroscopies. New York: Academic Press.
- Cocciardi R.A. 2003. Evaluation of Single-Bounce Attenuated Total Reflectance/Fourier Transform Infrared and Two-Dimensional Correlation Spectroscopy in Quantitative Analysis. PhD dissertation, McGill University, Montreal, Canada.
- 11. Cocciardi R.A., Ismail A.A., van de Voort F.R., Sedman J. 2002. A Rapid Fourier Transform Infrared Quality Control Method for the Determination of Lactose, Sucrose, Fat and Total Solids in Chocolate Milk. Milchwissenschaft 57(2):90-93.
- 12. Cole R.B. ed. 1997. Electrospray Ionization Mass Spectrometry. Fundamentals, Instrumentation, and Applications. New York: John Wiley & Sons. XXII+577pp.
- 13. Coleman P.B., ed. 2003. Practical Sampling Techniques for Infrared Analysis. Boca Raton, FL: CRC Press.
- 14. Cunsolo V., Foti S., Saletti R., Ceraulo L., Di Stefano V. 2001. Detection and Localization of Disulphide Bonds in a Synthetic Peptide Reproducing the Sequence 1-30 of Par *j* 1.0101 by Electrospray Ionisation Mass Spectrometry. Proteomics 1:1043-1048.
- 15. Fenn J.B., Mann M., Meng C.K., Wong S.F., Whitehouse C.M. 1989. Electrospray Ionization for Mass Spectrometry of Large Biomolecules. Science. **246**:64-71.
- 16. Grandori R., Matecko I., Müller N. 2002. Uncoupled Analysis of Secondary and Tertiary Protein Structure by Circular Dichroism and Electrospray Ionization Mass Spectrometry. J Mass Spectrom 37:191-196.
- 17. Hirschfeld T., Chase B. 1986. FT-Raman Spectroscopy: Development and Justification. Appl Spectrosc 40:133-137.
- Hooke S.D., Eyles, S.J. Miranker A., Radford S.E., Robinson C.V., Dobson C.M. 1995. Cooperative Elements in Protein Folding Monitored by Electrospray Ionization Mass Spectrometry. J Am Chem Soc 117:7548-7549.
- 19. Hosseini-Nia T., Ismail A.A., Kubow S. 1999. Pressure-Induced Conformational Changes of β-Lactoglobulin by Variable-Pressure Fourier Transform Infrared Spectroscopy. J Agric Food Chem 47:4537-4542.
- 20. Hosseini-Nia T., Ismail A.A., Kubow S. 2002. Effect of High Hydrostatic Pressure on the Secondary Structures of BSA and apo- and holo-α-Lactalbumin Employing Fourier Transform Infrared Spectroscopy. J Food Sci 67:1341-1347.
- 21. http://www.nobel.se/physics/laureates/1906/thomson-bio.html
- 22. Jolliffe I.T. 1986. Principal Component Analysis. New York: Springer.

- 23. Kemsley E.K., Appleton G.P., Wilson R.H. 1994. Quantitative Analysis of Emulsions Using Attenuated Total Reflectance (ATR). Spectrochem Acta A 50:1235-1242, 1994.
- 24. Konermann L., Douglas D.J. 1997. Acid-Induced Unfolding of Cytochrome c at Different Methanol Concentrations: Electrospray Ionization Mass Spectrometry Specifically Monitors Changes in the Tertiary Structure. Biochemistry 36:12296-12302.
- 25. Li-Chan E.C.Y. 1996. The Applications of Raman Spectroscopy in Food Science. Trends Food Sci Technol 7:361-370.
- 26. Li-Chan E.C.Y., Ismail A.A., Sedman J., van de Voort F.R. 2002. Vibrational Spectroscopy of Food and Food Products. In: Chalmers J.M., Griffiths P.R., eds. Handbook of Vibrational Spectroscopy. New York: John Wiley & Sons, New York, Vol 5, pp 3629–3662.
- Light-Wahl K.J., Schwartz B.L., Smith, R.D. 1994. Observation of the Noncovalent Quaternary Associations of Proteins by Electrospray Ionization Mass Spectrometry. J Am Chem Soc. 116:5271-5278.
- 28. Light-Wahl K.J., Winger B.E., Smith R.D. 1993. Observation of the Multimeric Forms of Concanavalin A by Electrospray Ionization Mass Spectrometry. J Am Chem. 115:5869-5870.
- 29. Martens H., Naes T. 1989. Multivariate Calibration, 2<sup>nd</sup> ed. Chichester, United Kingdom: John Wiley & Sons.
- 30. McQueen D.H., Wilson R.H., Kinnunen A., Jensen E.P. 1995. Comparison of Two Infrared Spectroscopic Methods for Cheese Analysis. Talanta 42:2007-2015.
- 31. Miranker A., Robinson C.V., Radford S.E., Aplin R.T., Dobson C.M. 1993. Detection of Transient Protein Folding Populations by Mass Spectrometry. Science. 262:896-900.
- 32. Mohimen A., Dobo A., Hoerner J.K. Kaltashov I.A. 2003. A Chemometric Approach to Detection and Characterization of Multiple Protein Conformers in Solution Using Electrospray Ionization Mass Spectrometry. Anal Chem 75:4139-4147.
- 33. Morris H.R. ed. 1980. Soft Ionization Biological Mass Spectrometry. Proceedings of the Chemical Society Symposium on Advantages in Mass Spectrometry Soft Ionization Methods. Heyden & Son Ltd. editorial. XII+156pp.
- 34. Nathier-Dufour N., Sedman J., van de Voort F.R. 1995. A Rapid ATR/FTIR Quality Control Method for the Determination of Fat and Solids in Sweetened Condensed Milk. Milchwissenschaft **50**:462-466.
- 35. Nilsson C.L., Cooper H.J., Håkansson K., Marshall A.G., Östberg Y., Lavrinovicha M., Bergström S. 2002. Characterization of the P13 Membrane Protein of *Borrelia burgdorferi* by Mass Spectrometry. J Am Soc Mass Spectrom. **13**:295-299.
- 36. Nonaka M., Li-Chan E.C.Y., Nakai S. 1993. Raman Spectroscopic Study of Thermally Induced Gelation of Whey Proteins. J Agric Food Chem 41:1176-1181.

- 37. Osborne B.G., Fearn T., Hindle P.H. 1993. Practical NIR Spectroscopy with Applications in Food and Beverage Analysis. Harlow, Essex: Longman.
- 38. Sanglier S., Leize E., van Dorsselaer, A. 2003. Comparative ESI-MS study of ~2.2 MDa Native Hemocyanins from Deep-Sea and Shore Crabs: from Protein Oligomeric State to Biotope. J Am Soc Mass Spectrom. 14:419-429.
- 39. Siamwiza M.N., Lord R.C., Chen M.C., Takamatsu T., Harada I., Matsuura H., Shimanouchi T. 1975. Interpretation of the Doublet at 850 and 830 cm<sup>-1</sup> in the Raman Spectra of Tyrosyl Residues in Proteins and Certain Model Compounds. Biochemistry 14:4870-4876.
- 40. Slangen, C., Visser, S. 1999. Use of Mass Spectrometry to Rapidly Characterize the Heterogeneity of Bovine α-Lactalbumin. J Agric Food Chem 47:4549-4556.
- 41. Stevens Jr S.M., Kem, W.R., Prokai, L. 2002. Investigation of Cytolysyn Variants by Peptide Mapping Enhanced Protein Characterization Using Complementary Ionization and Mass Spectrometric Techniques. Rapid Commun Mass Spectrom. 16:2094-2101.
- 42. Stuart B. 1997. Biological Applications of Infrared Spectroscopy. Chichester, United Kingdom: John Wiley & Sons.
- 43. Surewicz W.K., Mantsch H.H. 1988. New Insight into Protein Secondary Structure from Resolution-Enhanced Infrared Spectra. Biochim Biophys Acta 952:115-130.
- 44. Surewicz W.K., Mantsch H.H., Chapman D. 1993. Determination of Protein Secondary Structure by Fourier Transform Infrared Spectroscopy: A Critical Assessment. Biochemistry 32:389-394.
- 45. van de Voort F.R., Sedman J., Emo G. 1992. A rapid FTIR Quality Control Method for Fat and Moisture Determination in Butter. Food Res Int 25:193-198.
- 46. Williams P., Norris K. 2001 Near-Infrared Technology in the Agricultural and Food Industries, 2<sup>nd</sup> ed. St. Paul, MN: American Association of Cereal Chemists.

# Chapter 3

# Structure-Functionality Relationship of Ultra High Hydrostatic Pressure Processed Whey Proteins

#### 3.1. Abstract

Ultra high pressure (UHP) treatment is increasingly being employed as an alternative to heating for the reduction of microbial count, inactivation of spores and has the added benefit of retaining the vitamin potency and natural flavours of the food. More recently, UHP has been found to play a role in improving protein functionality and gel texture. The effects of instantaneous UHP exposure compared to 30-minutes holding time on the secondary and tertiary structure of whey proteins employing Fourier transform infrared (FTIR) spectroscopy was investigated. The rheological characteristics of pressureinduced gels were also investigated. UHP treatments exerted different effects on the whey protein isolates (WPI) and on the individual proteins found in WPI. Furthermore, the pressure effects were dependent on the source of WPI. The pressure required for causing on-set gelation of WPI solutions and the pressure holding time were found to be inversely proportional. Similar results were observed for  $\beta$ -lg. WPI and isolated  $\beta$ -lactoglobulin (β-lg) formed translucid gels after pressure treatment; whereas the viscosity and elasticity of α-lactalbumin and glycomacropeptides (GMP) solutions remained unchanged. In all cases changes in rheological properties of the pressure-treated protein solutions were accompanied by significant changes in the secondary and tertiary structure of the proteins.

**Key words**:  $\beta$ -lactoglobulin,  $\alpha$ -lactalbumin, whey protein isolates, ultra high pressure, UHP, infrared spectroscopy, FTIR, secondary structure, tertiary structure, rheology, structure-functionality.

# 3.2. Introduction

Ultra high pressure (UHP) processing methods are growing as an alternative to the classical thermal food processing techniques. Applying ultra high hydrostatic pressures ranging from 100 to 1000 MPa has been shown to make foods safer and extends their shelf life, while allowing the product to retain many of its organoleptic and nutritional attributes. This meets consumer demands for freshness without the disapproval related to other methods such as irradiation. UHP has been used on many products to: inactivate food-borne pathogens (19), inactivate bacterial spores (4), enhance (13) or inhibit selected enzymes (9), tenderize meat (25), shuck oysters (21), extend shelf life (16), promote ripening of cheeses (20), and minimize oxidative browning (10). Ultra high pressure in conjunction with elevated temperatures can also be employed for the sterilization of many food products (3, 22). Recent studies have also revealed that pressurization of a protein solution causes partial protein unfolding that can lead to the irreversible process of gelation. Pressure induced gels have superior texture and viscoelastic properties in comparison to temperature-induced gels. Pressure-induced gel formation is dependent on a multitude of parameters including the nature of the protein, protein concentration, level of the pressure applied and holding time, number of pressure cycles, temperature, pH, ionic strength (14, 15, 21, 26, 27). The relationship between pressure-induced structural changes that lead gelation is still under investigation. In this work the effect of UHP on the secondary and tertiary structure of  $\beta$ -lactoglobulin and  $\alpha$ lactalbumin is examined by Fourier transform infrared (FTIR) spectroscopy. Also the changes in viscoelastic properties of  $\alpha$ -lac,  $\beta$ -lg, glycomacropeptides (GMP) and whey protein isolates (WPI) prepared by different separation methods, as a function of varying UHP treatment is investigated to better understand the molecular basis of viscoelastic properties of proteins in solution and in gels.

# 3.3. Materials and Methods

The proteins used in this work were: 90% dry basis beta-lactoglobulin ( $\beta$ -lg) protein powder; 95% dry basis alpha-lactalbumin ( $\alpha$ -lac) protein powder; 90% dry basis glycomacropeptides (GMP) powder; and 90% dry basis whey protein isolate (WPI) Bipro®. These proteins were generously donated by Davisco Foods International (MN,

USA) and used without further purification. Deuterium oxide (D<sub>2</sub>O 99.9 % D) was purchased from Aldrich (St. Louis. MO, USA).

UHP treatment was achieved using an Alstom Co. (Nantes, France) ultra high pressure machine unit, with a chamber volume of 3 litres. The pressure medium used was water. The maximum operational pressure of 650 MPa is reached in approximately 4 minutes; the depressurization time was around 10 seconds. The sample was placed in the high pressure vessel at 4 °C and during pressurization the adiabatic increase in temperature reached a maximum 10 °C. This rise in temperature can be assumed to have no additional effect on the high pressure treatment.

The following notation is employed to designate the physicochemical parameters used: P/t/C where P is the pressure level in mega-Pascals (MPa); t is the holding time in minutes; and C is the number of cycles, i.e. how many times the pressure level and holding time is achieved, released and applied again. For example, 650/5/3 means a pressure treatment at 650 MPa, with 5 minutes of holding time, repeated 3 times.

#### 3.3.1. Series A

Solutions of 12.5% (w/v) protein in D<sub>2</sub>O were prepared and sealed in plastic bags for high pressure treatment. This concentration was selected to avoid the formation of pressure-induced hard gels which are difficult to analyze by FTIR spectroscopy. Samples bags were submerged in the water chamber and the subjected to 100, 200, 300 and 400 MPa treatment with 30 minutes of holding time. After the pressure treatment the FTIR spectrum of each sample was immediately recorded.

#### 3.3.2. Series B

Solutions of 12.5% (w/v) protein in  $D_2O$  were prepared and sealed in plastic bags for high pressure treatment. Samples bags were submerged in the water chamber and subjected to UHP treatment 450/0/1; 550/0/1; 650/0/1 and 650/5/3.

After the pressure treatment each sample was divided in two, one part used to record the rheological properties of the samples and the other part were immediately frozen, lyophilized and re-dissolved in  $D_2O$  to a concentration of 5% (w/v) for FTIR spectroscopic analysis.

# 3.3.3. Rheology

Samples of 12.5% (w/v) protein were pressurized as follows: 450/0/1, 550/0/1, 650/0/1, 450/0/3 and 650/5/3; and analyzed right after pressure treatment without further manipulation.

All measurements were recorded using an AR-2000 rheometer (TA Instruments. New Castle, DE, USA) employing a parallel plate geometry, constant angular frequency of 1Hz (0.6284 rad/sec) and temperature controlled at 10 °C. G' and G" parameters were recorded at 100 seconds operational time, which was considered to be the equilibration time.

# 3.3.4. FTIR spectroscopy

FTIR spectra were recorded using a Nicolet 8210E FTIR spectrometer (Nicolet. WI, USA) equipped with a deuterated triglycine sulphate (DTGS) detector. The spectrometer was continuously purged with dry air from a Balston dryer (Balston. MA, USA).

Approximately 8 μL of 5% (w/v) protein sample in D<sub>2</sub>O were placed between two CaF<sub>2</sub> windows separated by a 50μm thick Teflon <sup>TM</sup> spacer. The temperature of the cell was regulated by an Omega temperature controller (Omega Engineering. CT, USA). A total of 512 scans were co-added at 4 cm<sup>-1</sup> resolution. The absorbance spectra were subjected to band narrowing techniques using Fourier self deconvolution (FSD) employing a bandwidth of 20 cm<sup>-1</sup> (w) and enhancement factor of 2.4 (k) followed by a two-point baseline correction starting at 1710 and ending at 1590 cm<sup>-1</sup> using Omnic 6.0 software (Nicolet. WI, USA).

## 3.4. Results and Discussion

#### 3.4.1. Series A

The amide I' absorption region (1700-1600 cm<sup>-1</sup>) in the infrared spectrum of a protein is one of the most useful for secondary structure elucidation (24). The amide band assignments of whey proteins are summarized in Table 4 and are based on previous works (1, 2, 5, 11, 12, 17, 18, 23, 24). The irreversible changes in the secondary structure of  $\beta$ -lg

Table 4. Band assignment of the amide I' spectral region of  $\beta\text{-lg}.$ 

Band position (cm <sup>-1</sup> )	Assignment	Band position (cm <sup>-1</sup> )	Assignment
1692	Hidden antiparallel β-sheet	1633	Antiparallel β-sheet
1684	Antiparallel β-sheet (aggregation)	1629	Parallel β-sheet
1680-1676	β-structure	1622	Parallel β-sheet II
1645	α-helix and unordered	1614	Intermolecular β-sheet (aggregation band)

subjected to different pressure levels with a holding time of 30 minutes are shown in Figure 17. The modification of secondary structure is evident from the changes in the relative intensity of the amide I' band in the infrared spectra at 200 MPa. At 400 MPa the amide I' bands become broader indicating appreciable loss of structural integrity. Also noticeable is the loss of the intensity of 1692 cm<sup>-1</sup> band assigned to the H-bond amide groups of a  $\beta$ -sheet buried in the interior of the protein, inaccessible to the solvent (2). The loss in the band intensity of the 1692 cm<sup>-1</sup> peak is attributed to a change in tertiary structure causing the protein to become more flexible, or less tightly folded, which in turn allows the buried  $\beta$ -sheet to become accessible to  $D_2O$ . The exchange of hydrogen by deuterium (H/D exchange) of this  $\beta$ -sheet shifts the 1692 cm<sup>-1</sup> band to a lower wavenumber (2). A plot of the difference spectra shows the decline in the intensity of the 1692 cm<sup>-1</sup> band as a function of pressure treatment (Figure 18) and indicates that the change in the tertiary structure of  $\beta$ -lg is observable above 100 MPa.

An increase in  $\alpha$ -helix and unordered-structure content with increasing pressure is inferred from the increase in the intensity of the 1645 cm<sup>-1</sup> band. A significant reduction in the intensity of the band at 1622 cm<sup>-1</sup> is indicative of a reduction in parallel  $\beta$ -sheet structure with increasing pressure. This is accompanied by an increase in antiparallel  $\beta$ -sheet based on the increase in the intensity of the 1633 cm<sup>-1</sup> band. Accordingly, some of the parallel  $\beta$ -sheets may associate to form antiparallel  $\beta$ -sheet structures or form unordered/ $\alpha$ -helical structures. These changes are associated with the formation of soft gels of the pressure treated  $\beta$ -lg samples. Also disulphide bonds formation has been proposed as the mechanism that leads to the gelation of globular proteins (7, 8, 11, 14, 15, 18).

#### **3.4.2.** Series B

FTIR spectra (shown in Figure 19) of  $\beta$ -lg samples exposed to UHP (450-650 MPa) without a holding time, were comparable to spectra recorded from pressure treated samples at lower pressure (with a 30-min holding time). The specific structural changes of  $\beta$ -lg using instantaneous UHP can be derived from the difference spectra (Figure 20).

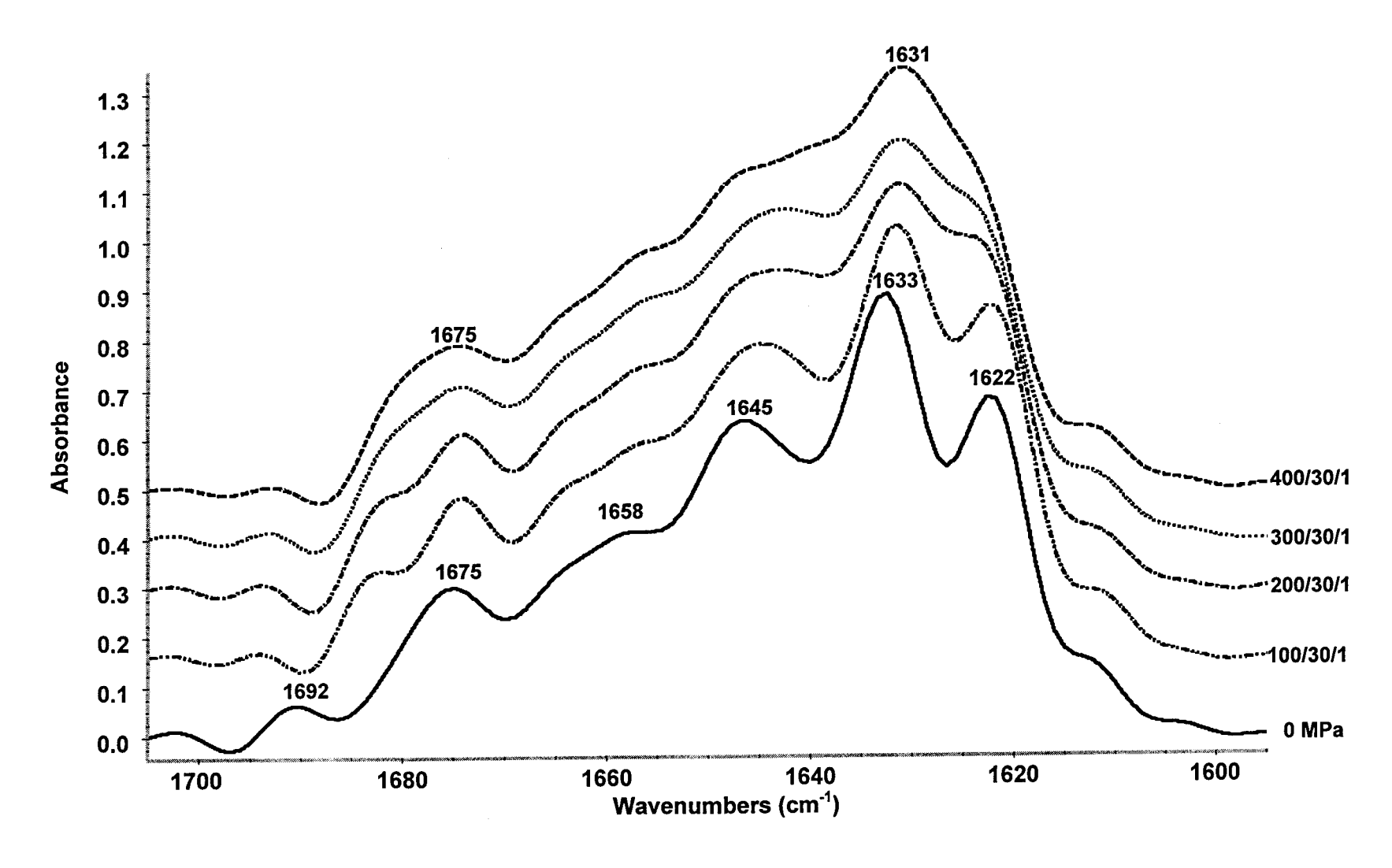


Figure 17. Series A: Non-reversible effect of pressure on the amide I' region of the FSD-FTIR spectra of  $\beta$ -lg (w = 20.0, k = 2.4). The pressure level was held for 30 minutes. The loss in general secondary structure is noticeable from 200 MPa of pressure.

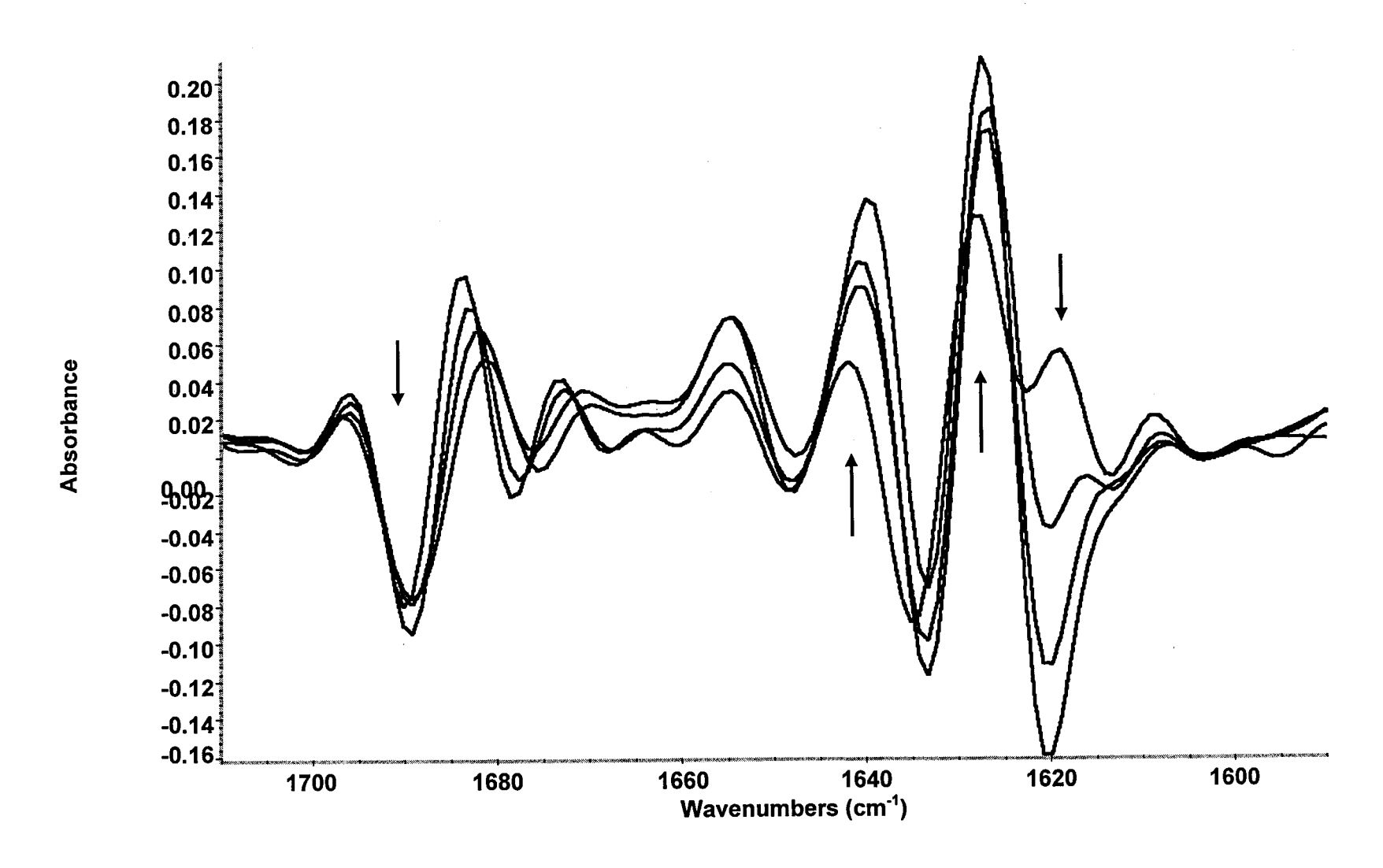


Figure 18. Series A: Difference spectra from figure 17, β-lg subjected to pressures from 0 to 400 MPa for 30 minutes.

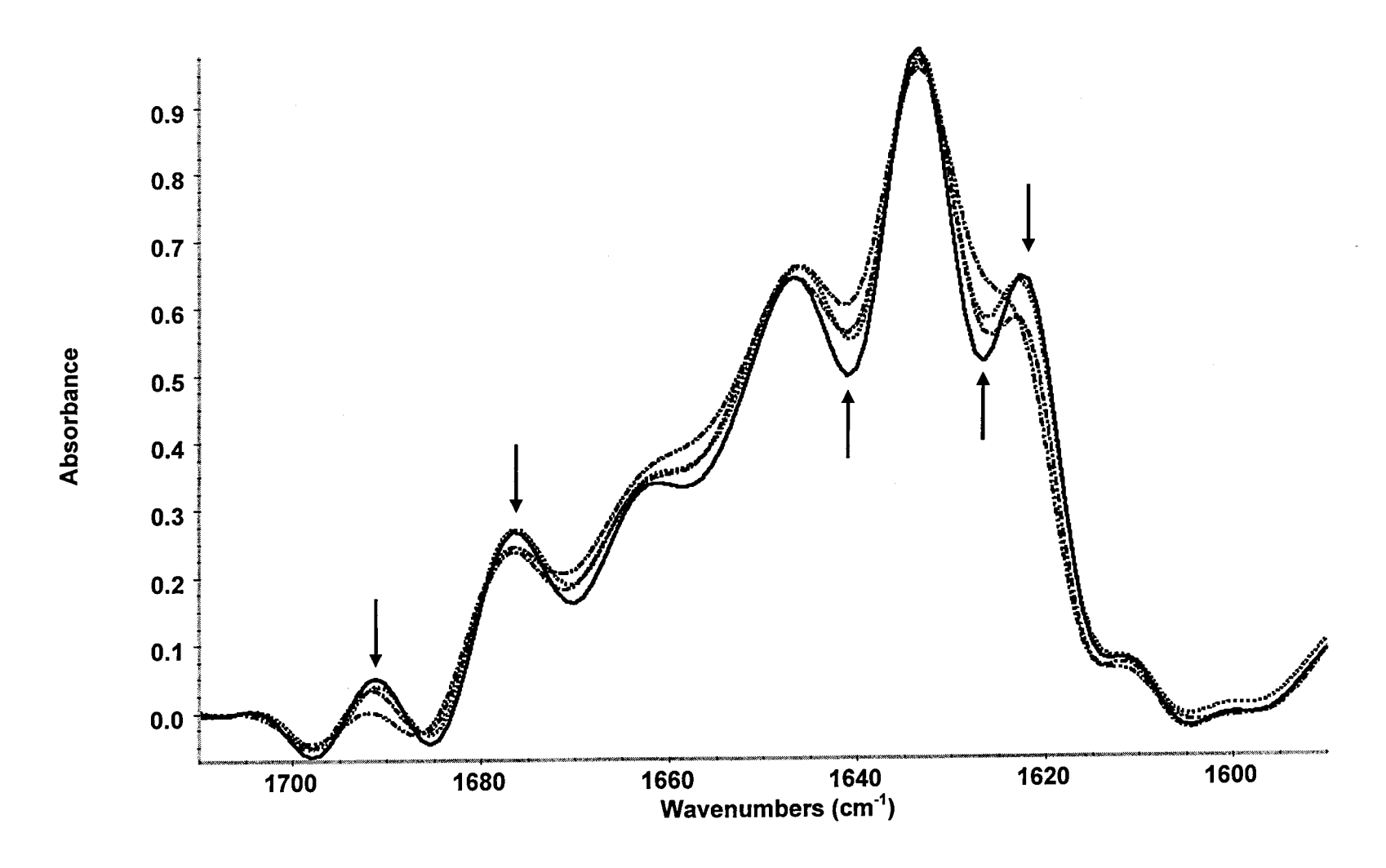


Figure 19. Series B: Non-reversible effect of pressure on the amide I' region of the FSD-FTIR spectra of  $\beta$ -lg (w = 20.0, k = 2.4). Samples were subjected to instant pressure, 1 cycle; lyophilized and re-dissolved in D<sub>2</sub>O. Changes are comparable to the ones achieved in Series A.

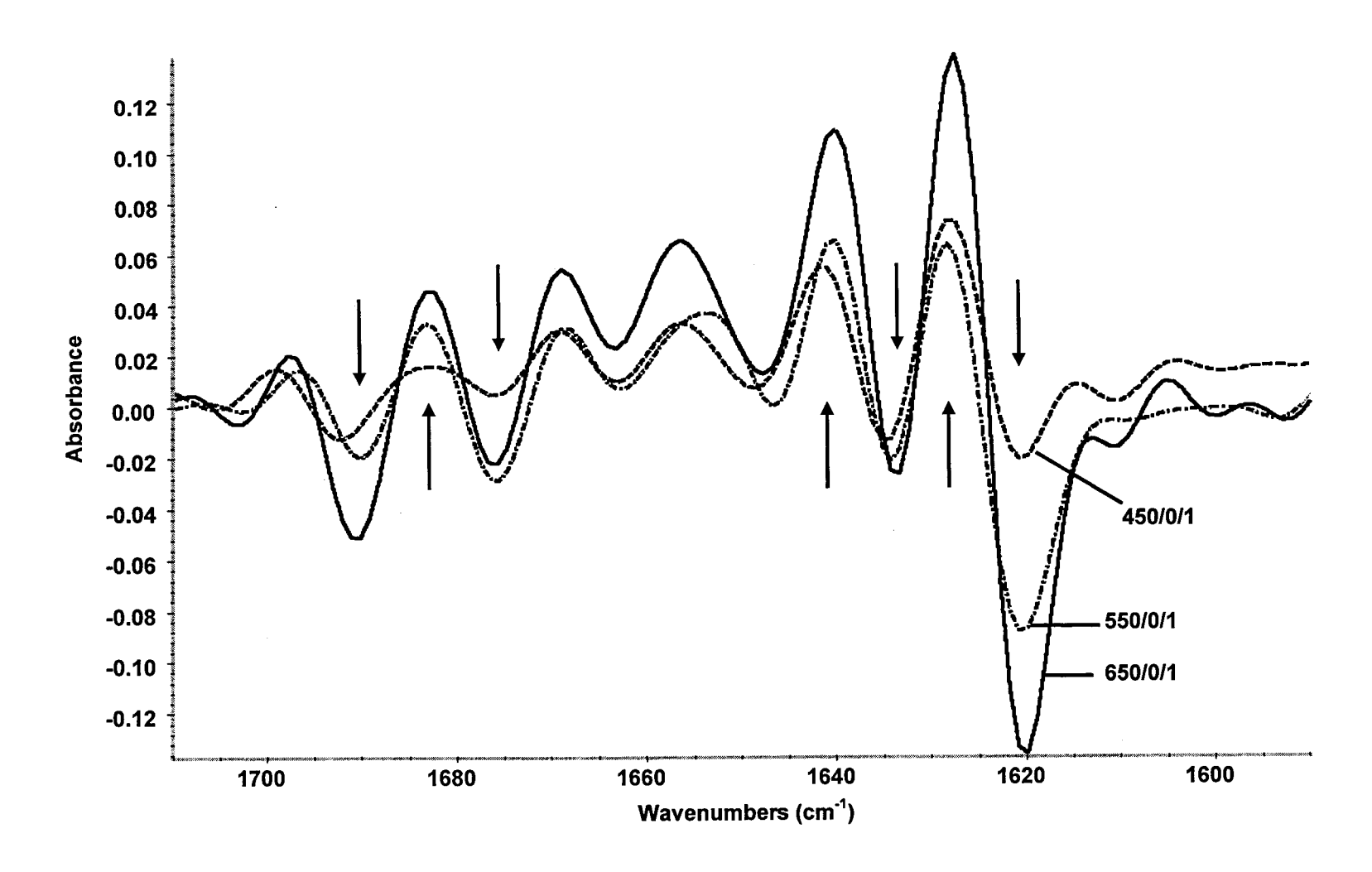


Figure 20. Series B: Difference spectra from figure 19,  $\beta$ -lg subjected to instant pressures of 450, 550 and 650 MPa.

In this case the pressure-treated solutions of  $\beta$ -lg in H<sub>2</sub>O were freeze-dried and redissolved in D<sub>2</sub>O, therefore the drop in absorbance of the peak at 1692 cm<sup>-1</sup> which is indicative of some conformational change of the buried  $\beta$ -sheet. The band at 1645 cm<sup>-1</sup> assigned to  $\alpha$ -helix or unordered structure increases with pressure, whereas the band at 1622 cm<sup>-1</sup> assigned to parallel  $\beta$ -sheet, and the bands at 1633 and 1676 cm<sup>-1</sup> assigned to antiparallel  $\beta$ -sheets decrease with increasing pressure. The minor change in the intensity of the 1692 cm<sup>-1</sup> band indicates that the pressure-induced unfolding of the protein is partially reversible. The decrease in the 1622 cm<sup>-1</sup> band along with the 1633 cm<sup>-1</sup> band may indicate that the pressure induces an increase in unordered or a-helical structure (reflected in the increase in the 1645 cm<sup>-1</sup> band).

## 3.4.3. Rheology

The pressurization of  $\beta$ -lg and WPI samples lead to an increase in both viscosity and elasticity of the solutions (Figures 21B, 21D); the formation of a true gel where the elasticity (G') is greater than the viscosity (G'') is only achieved when a holding time and higher number of pressure cycles are applied. For example, 3 pressure cycles at 650 MPa with a holding time of 5 minutes for each cycle produced strong  $\beta$ -lg gels. This observation is in agreement with the findings from Fertsch et al. (2003) (7). To achieve the same gel strengths for WPI required higher holding times.

Samples of  $\alpha$ -lac or GMP (Figures 21A, 21C) are insensitive to pressure regardless of the treatment; only a minor decrease in viscosity is observed when the GMP sample is pressurized compared to the control (non pressure-treated samples). The relative insensitivity of  $\alpha$ -lac to pressure treatment may be as a result of the re-folding of the protein when the pressure is released (6). In the case of GMP, these changes, if any, are also fully reversible; possible as a result of the shorter peptide lengths of GMP.

The  $\beta$ -lg concentration selected for this work result in changes in the protein tertiary and secondary structure after relatively low pressure (100 to 400 MPa) with a 30-minute holding time and at higher pressures (450 to 650 MPa) without a holding time.

In an attempt to assess the changes in viscoelastic characteristics of the  $\beta$ -lg solutions exposed to UHP treatment, an exponential model was developed to predict the

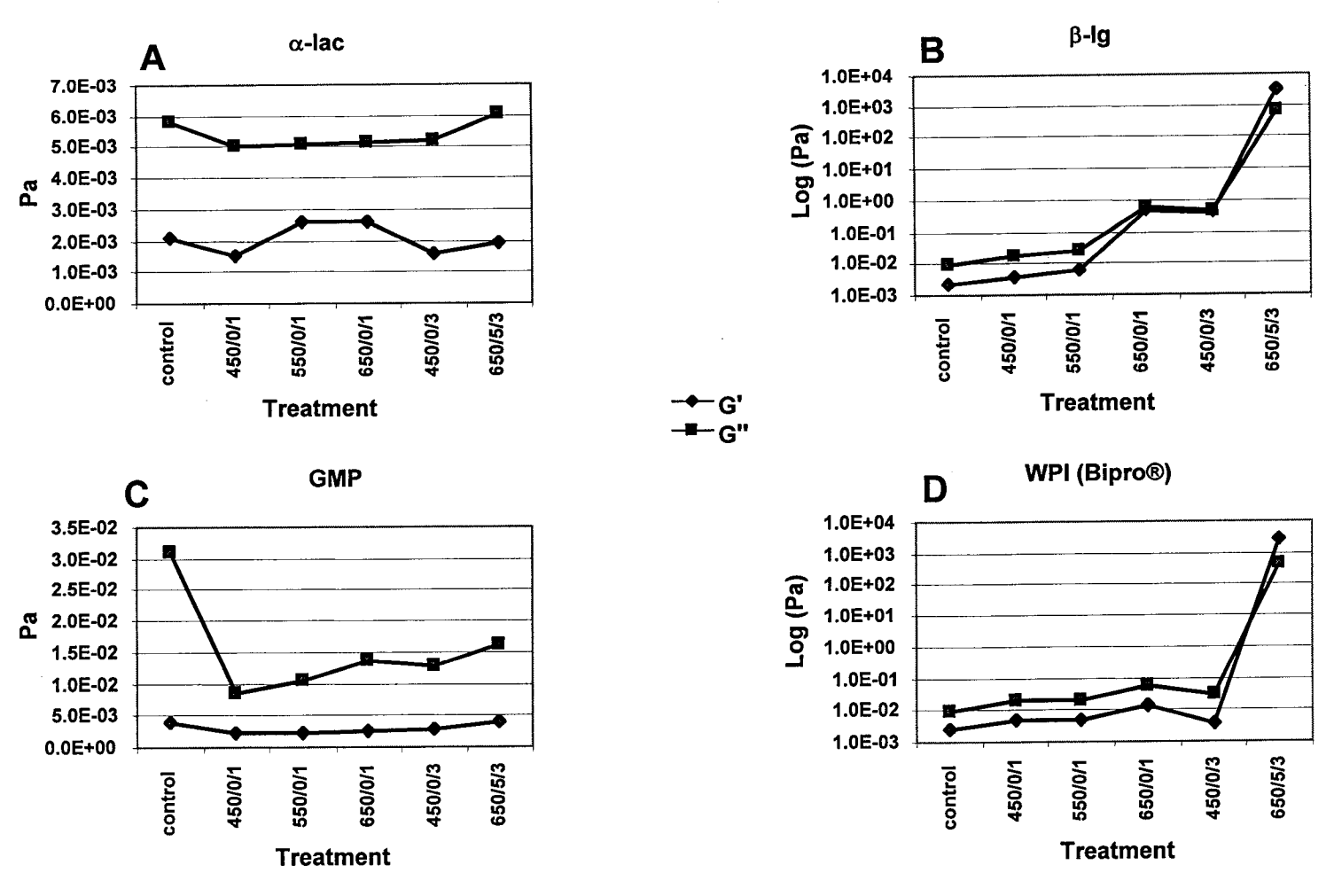


Figure 21. Rheological data for whey proteins with different pressure treatments. (A and B)  $\alpha$ -lac and GMP shows no significant change in viscosity or elasticity. (B and D) The formation of a "true gel" is only achieved when  $\beta$ -lg or WPI samples are subjected to an extreme HPP treatment; however, both viscosity and elasticity increase when pressure and/or number of cycles is increased.

G' value of the  $\beta$ -lg protein solution in terms of G' =  $0.0021e^{0.0017x}$  ( $R^2 = 0.91$ ) where G' is in Pascals and "x" is the pressure treatment applied in MPa (between 0 and 550 MPa) and G" =  $0.0093e^{0.0017x}$  ( $R^2 = 0.90$ ).

In the case of WPI (Bipro®) a single cycle of pressure (between 0 and 550 MPa) with no holding time yield  $G' = 0.0026e^{0.0013x}$  ( $R^2 = 0.98$ ), and  $G'' = 0.0094e^{0.0015x}$  ( $R^2 = 0.91$ ). Is important to note that these correlations are only true for the specific conditions detailed in the materials and methods section of this work, evermore importantly, in the case of WPI, these models are only valid for Bipro® due to the many differences in production methods among manufacturers can result in different protein ratios within the whey protein isolates, differences in mineral content and differences in pH.

#### 3.5. Conclusion

High pressure treatments exert an influence over both tertiary and secondary structures of the protein molecule; these changes can be reversible or irreversible depending on such factors as the protein nature, its concentration, pH, pressure level, number of cycles and holding time between each cycle. These structural changes can be measured by FTIR spectroscopy. In this work, the holding time and the magnitude of the pressure were found to be inversely proportional. Thus, one can achieve the same results, from the structural point of view, by using lower pressure treatment with longer holding time or by using higher pressure levels with shorter (or without any) holding time. For example, the higher pressures employed in Series B appear to compensate for the longer holding time employed in Series A. From the manufacturing point of view, having to wait 30 minutes for a single batch of product is not cost effective, thus the use of ultra high pressure can result in a faster turnaround time. The relationship between the viscoelastic characteristics of protein solutions subjected to high pressure treatment levels (and holding time) and the changes in the protein structure as elucidated by FTIR spectroscopy provides the means for understanding the molecular basis of functionality and facilitates the development of new products.

#### 3.6. References

- 1. Allain A.-F., Paquin P., Subirade M. 1999. Relationships between conformation of β-lactoglobulin in solution and gel states as revealed by attenuated total reflection Fourier transform infrared spectroscopy. International Journal of Biological Macromolecules. 26:337-344.
- 2. Boye J.I., Ismail A.A., Alli I. 1996. Effects of physicochemical factors on the secondary structure of β-Lactoglobulin. Journal of Dairy Research. 63: 97-109.
- 3. Clery-Barraud C., Gaubert A., Masson P., Vidal D. 2004. Combined effects of high hydrostatic pressure and temperature for inactivation of Bacillus anthracis spores. Applied and Environmental Microbiology. **70**:635-637.
- 4. Delacour H., Clery C., Masson P., Vidal D.R. 2002. Inactivation of bacterial spores by high hydrostatic pressure. Annales Pharmaceutiques Françaises. 60:38-43.
- 5. Dong A., Matsuura J., Manning M.C., Carpenter J.F. 1998. Intermolecular β-sheet results from Trifluroethanol-induced nonnative α-helical structure in β-sheet predominant proteins: infrared and circular dichroism spectroscopic study. Archives of Biochemistry and Biophysics. 275-281.
- 6. Dzwolak W., Kato M., Shimizu A., Taniguchi Y. 2000. FTIR study on heat-induced and pressure-assisted cold induced changes in structure of bovine α-lactalbumin: stabilizing role of calcium ion. Biopolymers. **62**: 29-39.
- 7. Fertsch B., Muller M., Hinrichs J. 2003. Firmness of pressure-induced casein and whey protein gels modulated by holding time and rate of pressure release. Innovative Food Science & Emerging Technologies. 4:143-150.
- 8. Funtenberger S., Dumay E., Cheftel J.C. 1997. High pressure promotes β-lactoglobulin aggregation through SH/S-S interchange reactions. Journal of Agricultural Food Chemistry. 45: 912-921.
- 9. Garcia-Palazon A., Suthanthangjai W., Kajda P., Zabetakis I. 2004. The effects of high hydrostatic pressure on β-glucosidase, peroxidase and polyphenoloxidase in red raspberry (Rubus idaeus) and strawberry (Fragaria × ananassa). Food Chemistry. 88:7-10.
- 10. Hong S.-I., Kim D.-M. 2001. Storage quality of chopped garlic as influenced by organic acids and high-pressure treatment. Journal of the Science of Food and Agriculture. **81**:397-403.
- 11. Hong Y-H., Creamer L.K. 2002. Changed protein structures of bovine β-lactoglobulin B and α-lactalbumin as a consequence of heat treatment. International Dairy Journal. 345-359.
- 12. Hosseini-Nia T., Ismail A.A., Kubow S. 1999. Pressure-induced conformational changes of β-lactoglobulin by variable-pressure Fourier transform infrared spectroscopy. Journal of Agricultural Food Chemistry. 47: 4537-4542.

- 13. Jung S., de Lamballerie-Anton M., Taylor R.G., Ghoul M. 2000. High-Pressure Effects on Lysosome Integrity and Lysosomal Enzyme Activity in Bovine Muscle. Journal of Agricultural and Food Chemistry. 48:2467-2471.
- 14. Kanno C., Mu T.-H., Hagiwara T., Ametani M., Azuma N. 1998. Gel Formation from Industrial Milk Whey Proteins under Hydrostatic Pressure: Effect of Hydrostatic Pressure and Protein Concentration. Journal of Agricultural and Food Chemistry. 46:417-424.
- 15. Keim S., Hinrichs J. 2004. Influence of stabilizing bonds on the texture properties of high-pressure-induced whey protein gels. International Dairy Journal. 14:355-363.
- 16. Lee J.W., Cha D.S., Hwang K.T., Park H.J. 2003. Effects of CO<sub>2</sub> absorbent and high-pressure treatment on the shelf-life of packaged kimchi products. International Journal of Food Science and Technology. **38**:519-524.
- 17. Lefevre T., Subirade M. 2000. Molecular differences in the formation and structure of Fine-Stranded and Particulate β-lactoglobulin gels. Biopolymers. **54**: 578-586.
- 18. Panick G., Malessa R., Winter R. 1999. Differences between the pressure and temperature-induced denaturation and aggregation of β-lactoglobulin A, B, and AB monitored by FT-IR spectroscopy and small-angle X-ray scattering. Biochemistry. 38: 6512-6519.
- 19. Ritz M., Tholozan J.L., Federighi M., Pilet M.F. 2002. Physiological damages of Listeria monocytogenes treated by high hydrostatic pressure. International Journal of Food Microbiology. **79**:47-53.
- 20. Saldo J., Sendra E., Guamis B. 2000. High hydrostatic pressure for accelerating ripening of goat's milk cheese: proteolysis and texture. Journal of Food Science. 65:636-640.
- 21. San Martin M.F., Barbosa-Canovas G.V., Swanson B.G. 2002. Food processing by high hydrostatic pressure. Critical reviews in food science and nutrition. **42**:627-45.
- 22. Spilimbergo S., Elvassore N., Bertucco A. 2002. Microbial inactivation by high-pressure. Journal of Supercritical Fluids. 22:55-63.
- 23. Subirade M., Loupil F., Allain A.-F., Paquin P. 1998. Effect of dynamic high pressure on the secondary structure of β-lactoglobulin and on its conformational properties as determined by Fourier transform infrared spectroscopy. International Dairy Journal. 8:135-140.
- 24. Susi H., Byler D.M. 1988. Fourier transform infrared spectroscopy in protein conformation studies. In Methods for Protein Analysis. Cherry, J. P., Barford, R. A., Eds. American Oil Chemists Society. Champaign, IL. pp 235-250.
- 25. Suzuki A., Kim K., Honma N., Ikeuchi Y., Saito M. 1992. Acceleration of meat conditioning by high pressure treatment. Colloque INSERM. 224:219-27.
- Van Camp J., Feys G., Huyghebaert A. 1996. High pressure-induced gel formation of haemoglobin and whey proteins at elevated temperatures. Food Science & Technology. 29:49-57.

27. Van Camp J., Huyghebaert A. 1995. High pressure-induced gel formation of a whey protein and Haemoglobin protein concentrate. Lebensm.-Wiss. u.-Technol. 28:111-117.

# Chapter 4

# Effect of Ultra High Hydrostatic Pressure on the Electrospray Ionization Mass Spectroscopy (ESI-MS) Profile of Whey Proteins

#### 4.1. Abstract

Milk whey is composed of many proteins among them  $\beta$ -lactoglobulin ( $\beta$ -lg),  $\alpha$ lactalbumin (α-lac), bovine serum albumin (BSA) and glycomacro peptides (GMP). High pressure processing (HPP) is an alternative to the conventional temperature process of food products. It offers the possibility of reduction of the microbial count and inactivation of spores without the loss of vitamin content, chemical reactions or changes in the organoleptic characteristics of the product. This paper studies the effects of different ultra HPP (UHP) treatments on the tertiary structure of  $\beta$ -lg and  $\alpha$ -lac using electrospray ionization mass spectroscopy (ESI-MS). Protein-protein interactions after UHP in two brand names of whey protein isolates (WPI) were studied using ESI-MS. UHP exerts an influence on the tertiary structure of the protein molecules, revealed as differences in the charge-state-distribution (CSD) of whey protein solutions. Structural changes can be reversible or irreversible depending on the nature of the protein, its concentration, the presence or absence of other proteins, pressure level and holding time as well as the number of pressure cycles. The effect of holding time the magnitude of the applied hydrostatic pressure on the protein structure was found to be inversely proportional. The protein-protein interactions in WPI after subjected to UHP were different from one WPI brand to another; these differences are due mainly to discrepancies in production methodologies that generate variations in the concentration of GMP and the final pH of the WPI solutions.

Key words:  $\beta$ -lactoglobulin,  $\alpha$ -lactalbumin, WPI, Bipro®, Inpro®, ultra high pressure, ESI-MS, tertiary structure, protein-protein interactions.

#### 4.2. Introduction

Electrospray ionization is a desorption soft-ionization technique that generates ions with different charge distribution of intact molecules (6, 13). The output of the instrument is a graph of different peaks corresponding to the different charged species generated in the desorption process; in the x-axis one finds the mass-over-charge (m/z) ratio of each specie and in the y-axis the relative abundance of that particular specie in the overall population of molecules. This representation is called charged-state-distribution or CSD (see Figure 22).

In a protein sample in its native conformation it is understood that the solvent can not reach all the ionizable groups of the protein and therefore a relatively low and narrow CSD is observed. On the other hand, if the native more compact folding of the protein is changed by any means and the structure becomes partially unfolded or relaxed, the solvent will be able to ionize more groups within the interior of the protein previously buried and therefore a broader CSD is observed (10). Thus ESI-MS provides an effective means of measuring changes in the tertiary structure that takes place in response to physicochemical changes or protein-protein interactions.

The pressurization of a protein solution causes partial protein unfolding that can lead to the irreversible process of gelation depending on many factors including: the nature of the protein, concentration, level of the pressure applied and holding time, number of pressure cycles, temperature, pH, ionic strength (2, 3).

This paper studies the effects of different ultra high hydrostatic pressure treatments (up to 650 MPa) on the tertiary structure of  $\beta$ -lactoglobulin and  $\alpha$ -lactalbumin using electrospray ionization mass spectroscopy (ESI-MS). Also the protein-protein interactions after pressure treatment in of whey protein isolates (WPI), obtained from two different isolation methods, were studied using ESI-MS.

## 4.3. Materials and Methods

The proteins used in this research were: 90% dry basis beta-lactoglobulin ( $\beta$ -lg) protein powder; 95% dry basis alpha-lactalbumin ( $\alpha$ -lac) protein powder; 90% dry basis whey protein isolate (WPI) Bipro®. These samples were donated by Davisco Foods International (MN, USA) and used without further purification. WPI Inpro® (90% dry

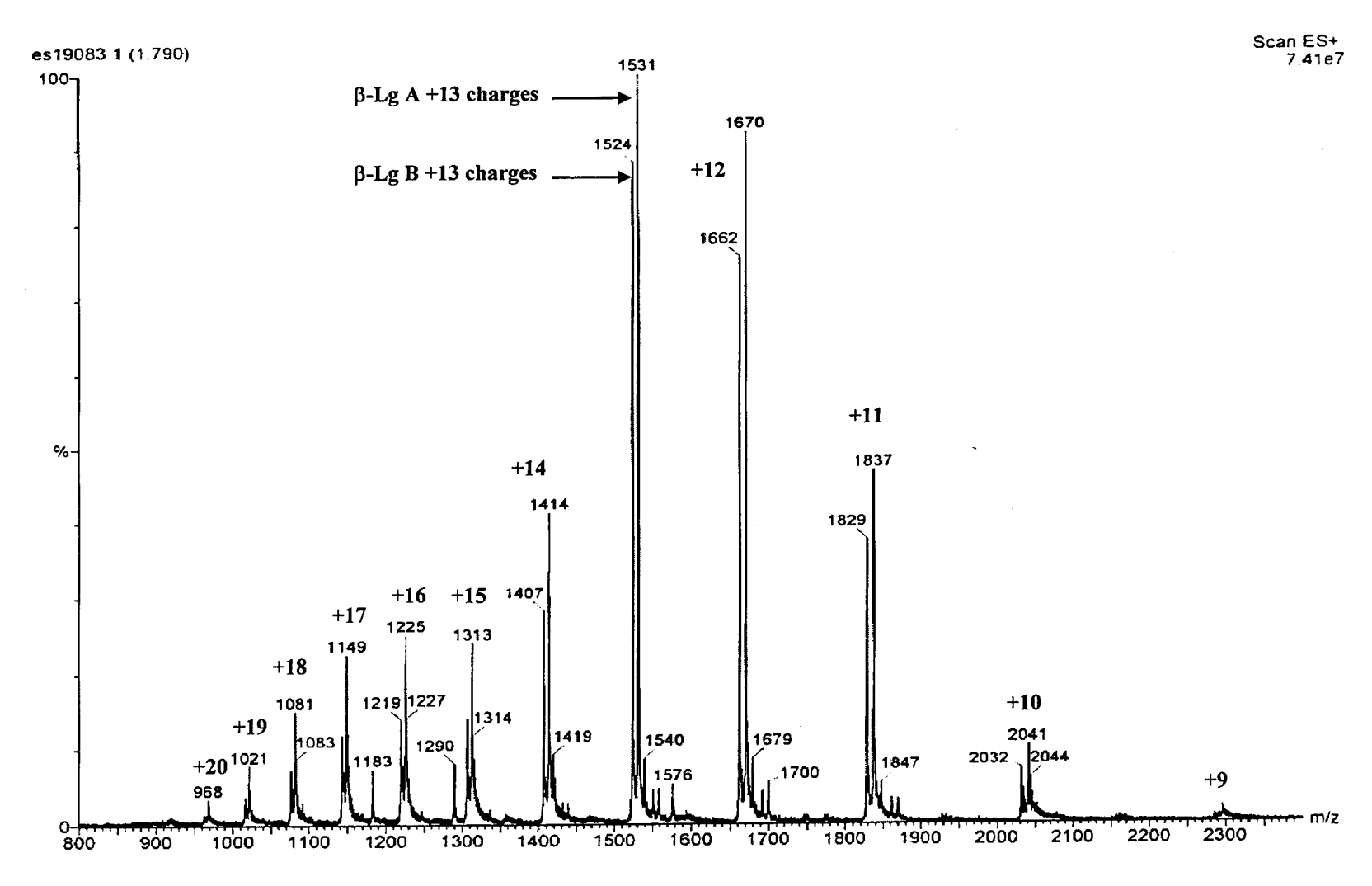


Figure 22. Electrospray ionization mass spectrometry (ESI-MS) relative charge-state-distribution (CSD) of  $\beta$ -lg A and B genetic variants without pressure treatment. The charged states of both  $\beta$ -lg variants are shown and they are relative to  $\beta$ -lg A +13 which is considered to be 100 %.

basis) was supplied by Inovatech (Abbotsford, BC. Canada) and used as received. Deuterium oxide (D<sub>2</sub>O 99.9 % D) was purchased from Aldrich (St. Louis. MO, USA).

The high pressure treatment was achieved using an Alstom Co. (Nantes, France) ultra high pressure machine unit, with a chamber volume of 3 Litres. The pressure medium used was water. The maximum operational pressure of 650 MPa is reached in approximately 4 minutes; the depressurization time was around 10 seconds. The sample was introduced in the high pressure machine at 4 °C and during pressurization the adiabatic increase in temperature reached a maximum 10 °C. This rise in temperature can be assumed to have no additional effect over the high pressure treatment.

The following notation was employed to designate the physicochemical parameters used: P/t/C where P is the pressure level in mega-Pascals (MPa); t is the holding time in minutes,; and C is the number of cycles, i.e. how many times the pressure level and holding time is achieved, released and applied again. For example, 650/5/3 means a pressure treatment at 650 MPa, with 5 minutes of holding time, repeated 3 times.

A special 3 cycles treatment (3C) was also tried. This treatment can be described as: bringing up the pressure to 400 MPa and holding it for 10 minutes, then releasing the pressure and subjecting the sample to two addition pressure cycles of 400 MPa pressure without a holding time (8, 9).

## 4.3.1. Experiment A

Solutions of 15% (w/v) of each of the major components found in whey:  $\beta$ -lg,  $\alpha$ -lac and GMP were prepared in H<sub>2</sub>O, and sealed in plastic bags for high pressure treatment. This concentration was selected to avoid the formation of hard  $\beta$ -lg gels which after lyophilization can be difficult to re-dissolve. Samples bags were submerged in the water chamber and the ultra-high pressure treatments applied were 450/0/1, 550/0/1, 650/0/1 and 3C. After the pressure treatment the samples were immediately frozen, subsequently lyophilized and re-dissolved to 0.5 mg/mL in 1% aqueous acetic acid (pH 3) for ESI-MS examination.

## 4.3.2. Experiment B

Solutions of 15% (w/v) Bipro® and Inpro® WPI in H<sub>2</sub>O were prepared, and sealed in plastic bags for high pressure treatment. This concentration was selected to avoid the formation of hard gels which are difficult to handle for ESI-MS analysis.

Samples bags were submerged in the water chamber and the ultra-high pressure treatments applied were 550/0/1 and 3C. After the pressure treatment the samples were immediately frozen, subsequently lyophilized and re-dissolved to 0.5 mg/mL in 1% aqueous acetic acid (pH 3) for ESI-MS examination.

## 4.3.3. ESI Mass Spectrometer

ESI-MS analysis was carried out using a Micromass Quattro II Triple Quadrupole mass spectrometer (Waters. Manchester, UK) equipped with an electrospray source. Data acquisition and analyses were carried out using MassLynx version 3.5 software (Waters. Manchester, UK). Nitrogen was used as curtain gas (400 l/h, 100 °C) and nebulising gas (20 l/h). The ESI capillary was set at 1.94 kV while the MS analysis was carried out at a cone voltage of 80 V with an inter-scan delay of 0.1 s and a scan range of 800–2400 Da. The analytes were assayed in the positive mode with a flow rate of 300 mL/h.

ESI-MS measures the different charged species formed from a specific molecule of certain molecular weight. Based on this, the interpretation of ESI-MS results from GMP is a real challenge because GMP comprises a multitude of molecules with a range of molecular weight; each of these molecules will produce a number of different charged species that appears in the CSD as many peaks. Also the presence of the sugar unit in GMP can block the injectors and the high temperatures involved can create Millard byproducts not present in the original sample; accordingly, the analysis of GMP samples was not performed.

#### 4.4. Results and Discussion

The pressurization of a  $\beta$ -lg solution causes an irreversible process of gelation, the structural and rheological characteristics of the treated solution, now gel, depends on many factors including the protein concentration and the pressure level applied (12). Gels from pure  $\beta$ -lg protein and WPI (Bipro®) from Davisco were translucid in appearance

and had very good water-holding capacity. WPI (Inpro®) from Inovatech formed a turbid gel with poor water-holding capacity.  $\alpha$ -lac solutions did not form gels (see Chapter 3).

Figure 22 shows CSD of the  $\beta$ -lg genetic variants A and B. The peak corresponding to  $\beta$ -lg A (charged with 13 positive charges) is the most abundant of the species; all the other peaks are in relative proportion to this peak. Based on the absolute number of molecules that hit the detector with a given mass and charge, the absolute CSD can be estimated (Figures 23-25). The absolute CSD can be calculated as follows: knowing the molecular mass of the specie in question, the total number of molecules generated for all the charged states can be measured. For example, assuming that  $\beta$ -lg A can be ionized to generate ten different charged states going from +10 to +19 charges, one can calculate the total number of  $\beta$ -lg A molecules by adding up intensity of the signal reaching the detector having a charge of +10 thru +19; then the absolute proportions are created by dividing the intensity of the signal of each charged species by the total intensity. It is important to note that each different ESI-MS run can have a different total number of molecules that reach the detector thus different total intensities can be observed, however the relative intensity of each species will be dependent on the changes in the protein conformation (1).

In the relative CSD (Figure 22) the x axis is represented by the mass over charge (m/z) of each charged species; but when the absolute CSD is generated the x axis is transformed to merely charge (by dividing the mass by the m/z ratio) to facilitate interpretation.

## 4.4.1. Effect of UHP on the conformation of $\beta$ -lg and $\alpha$ -lac

Pure protein components of whey were exposed to different pressure treatments and absolute CSD were generated. In the case of  $\beta$ -lg only the mix of A and B genetic variants was available and was pressurized as the mix; afterwards the absolute CSD of each genetic variant was obtained by separating the data in two sets and taking into account only the relevant peaks corresponding to each genetic variant.

The changes in the CSD attributed to changes in the tertiary structure of  $\alpha$ -lac and  $\beta$ -lg after different pressure treatments are presented in Figure 23. Pure  $\alpha$ -lac solutions are largely insensitive to pressure treatment (Figure 23A); the  $\alpha$ -lac tertiary structure

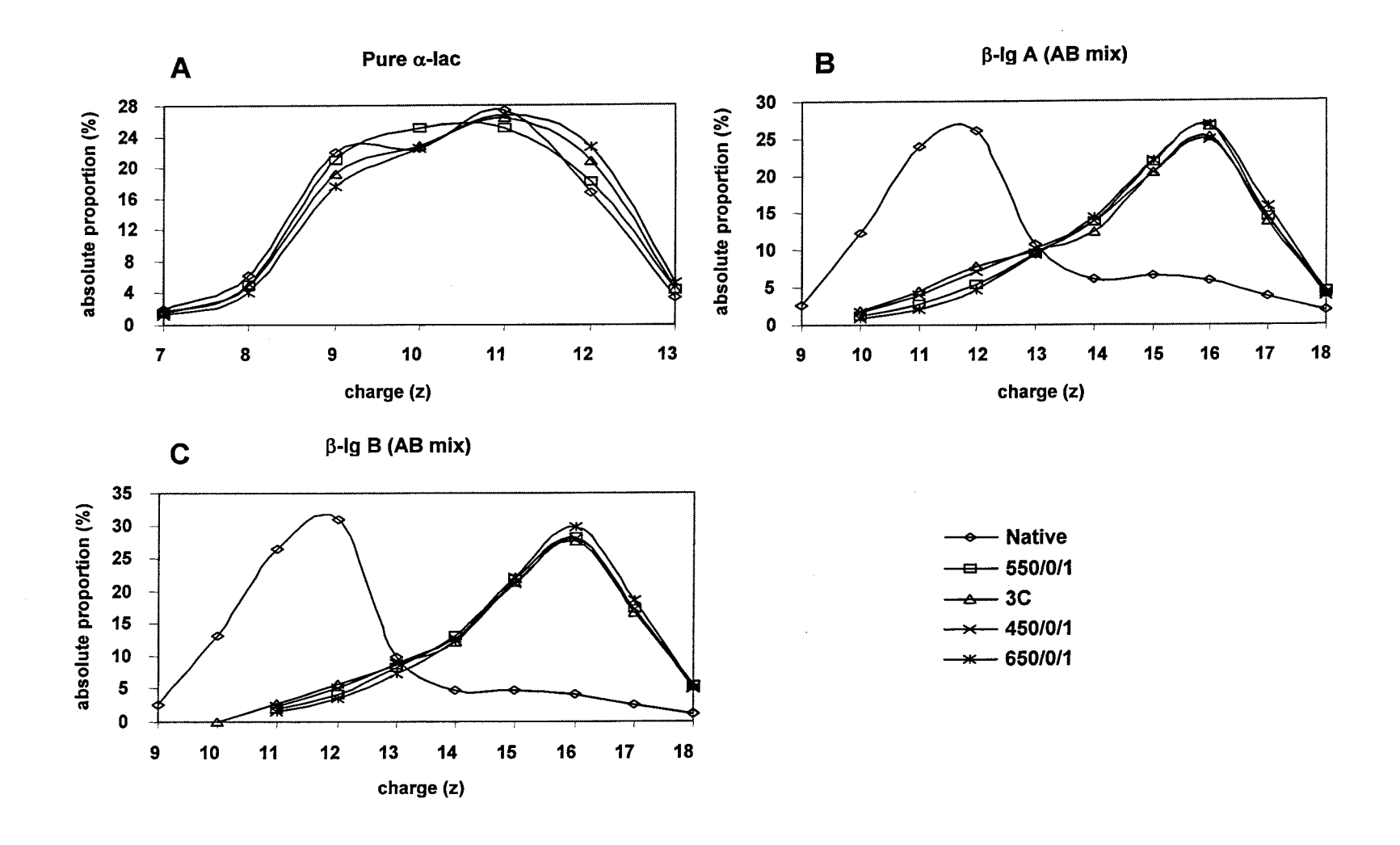


Figure 23. Series A: ESI-MS absolute CSD of the pure whey proteins solutions after pressure. (A) pure  $\alpha$ -lac solution show no considerable change in the amount of charges. (B and C)  $\beta$ -lg A and  $\beta$ -lg B in the AB mix; both proteins show an important change towards higher charges of the species after pressure.

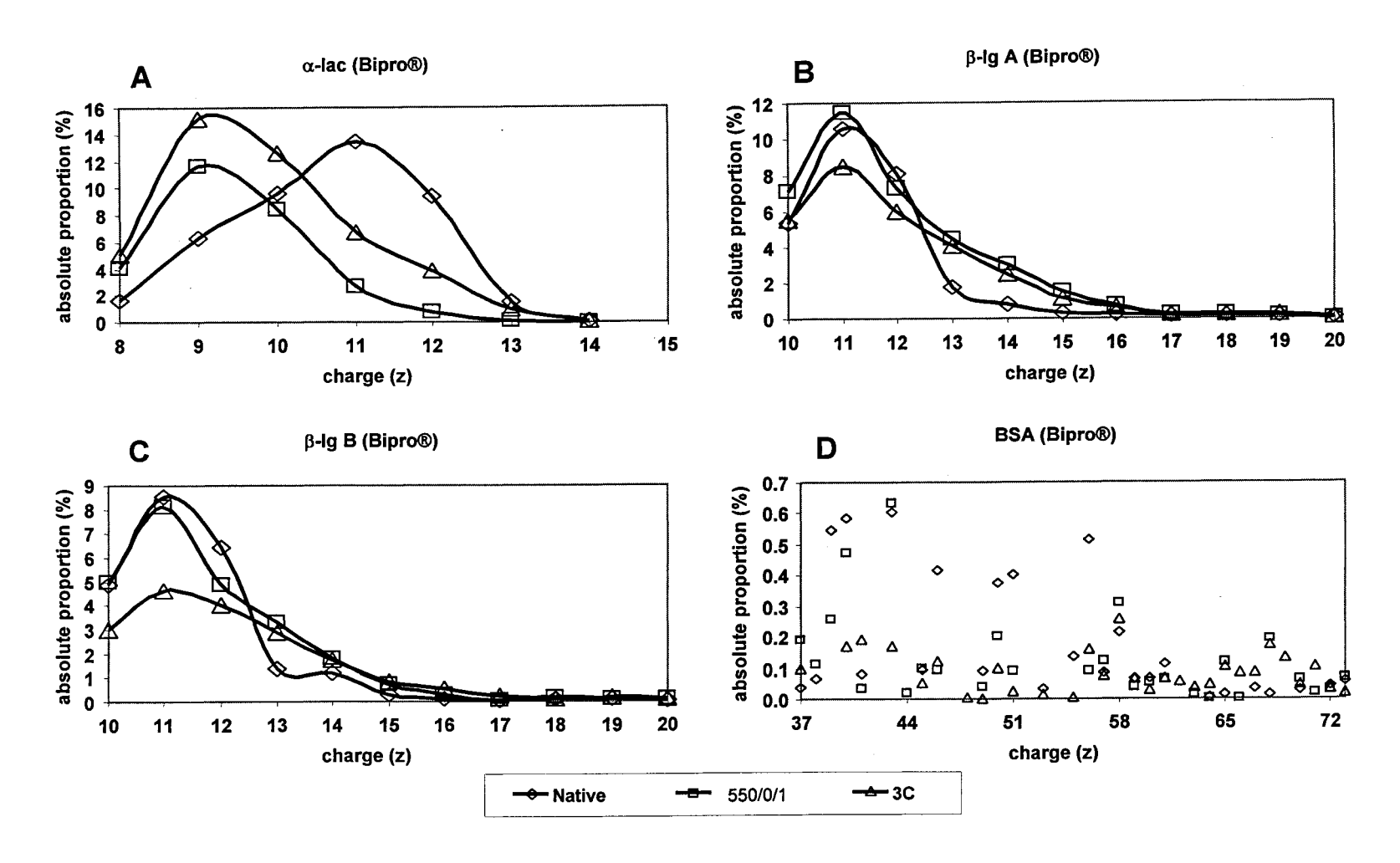


Figure 24. Series B: ESI-MS absolute CSD of the protein components in WPI Bipro® after pressure. (A)  $\alpha$ -lac in the mix shows a considerable change in the amount of charges from a maximum at +11 to +9 charges after pressure. (B and C)  $\beta$ -lg A and  $\beta$ -lg B in the mix; both proteins show a small change towards higher charges after pressure (broadening of the line contour). (D) BSA in the mix shows no explainable pattern.

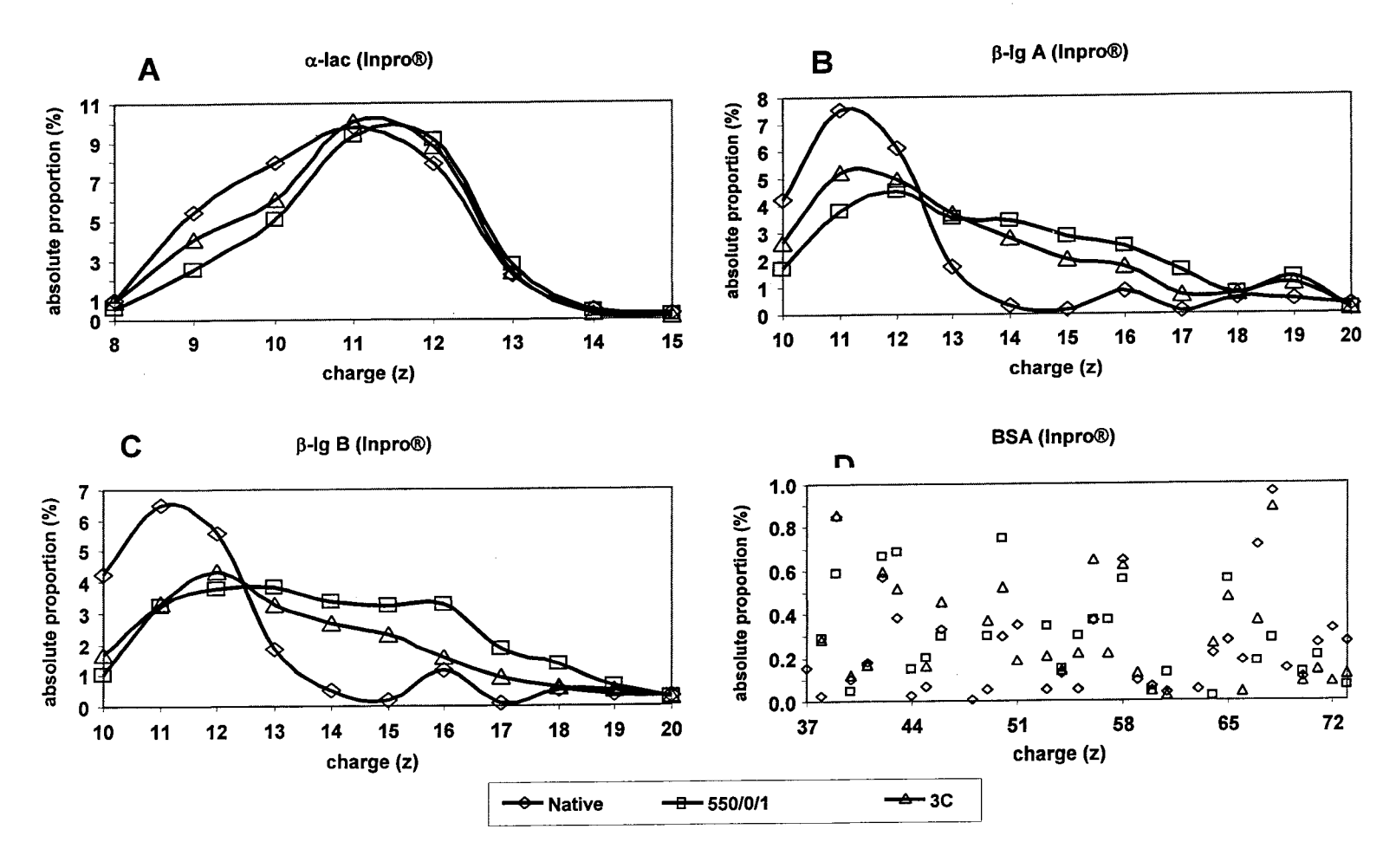


Figure 25. Series B: ESI-MS absolute CSD of the protein components in WPI Inpro® after pressure. (A)  $\alpha$ -lac in the mix shows a very small change towards higher charges after pressure. (B and C)  $\beta$ -lg A and  $\beta$ -lg B in the mix; both proteins show a change to higher charges after pressure (broadening of the line contour). (D) BSA in the mix shows no explainable pattern.

remains unchanged for the most extent, and remains as a compact and tightly packed.  $\beta$ -lg A and B variants behave similarly when exposed to the pressure treatments (Figures 23B and 23C). Both native  $\beta$ -lg shows a CSD centred around +12 charges; after pressure is applied in all the cases the CSD shifts to higher charges and is now centred at +16. Exposure to high hydrostatic pressure results in changes in the tertiary structure permitting some groups buried in the hydrophobic core of the molecule (4) and previously inaccessible to the solvent to get charged thereby increasing the CSD. It is of interest to note that the changes in the tertiary structure also results in an increase in the viscoelastic properties of the  $\beta$ -lg solution and ultimately leads to gel formation. In the absence of any change in the tertiary structure, as in the case of  $\alpha$ -lac, no change in the rheological properties is observed (see Chapter 3).

#### 4.4.2. Effect of UHP on the conformation of $\beta$ -lg and $\alpha$ -lac in WPI

For this part of the study, solutions of two different brand names of whey protein isolate (WPI), Bipro® and Inpro® were subjected to different pressure treatment and holding time. The absolute CSD of each different protein component in the WPI mix, before and after pressure treatment was calculated. Knowing the molecular mass of each of the protein components one can separate the data corresponding to  $\beta$ -lg A,  $\beta$ -lg B,  $\alpha$ -lac and BSA from the relative CSD of the WPI; and with that information one can create different absolute CSD corresponding to each protein.

### 4.4.2.1. Bipro®

Figure 24 shows the absolute CSD of the different components of Bipro® WPI. For  $\alpha$ -lac in Bipro® (Figure 24A) we noticed a dramatic shift in charge after pressure treatment, from +11 to +9 charges; this suggests that the  $\alpha$ -lac fraction of Bipro® is becoming even more compact after pressure treatment. UHP treatment of the two  $\beta$ -lg genetic variants in Bipro® (Figures 24B and 24C) caused the charges to be widespread to charges > +11.

Figure 3D shows the absolute CSD of BSA a minor component of WPI. BSA is known to form gels when exposed to high hydrostatic pressure (7). There was no

recognizable pattern assignable to the absolute CSD of BSA, probably attributable to the low concentration of this protein in the WPI.

# 4.4.2.2. Inpro®

The absolute CSD of each individual protein component in Inpro® was generated from the relative CSD of the whole WPI (Figure 25). The changes in the CSD of  $\alpha$ -lac in WPI subjected to different pressure treatments are shown in Figure 25A. There are minimal changes in charge after pressurization towards higher charges which implies that the protein remains intact. This is in contrast to  $\alpha$ -lac in Bipro® which is sensitive to pressure treatment, this can be due to the differences in pH of the two WPI solutions; Bipro® had an unadjusted pH of 6.9 whereas Inpro® had an unadjusted pH of 5.9. Also differences in production methodologies can result in different relative protein components in WPI. Bipro® WPI is produced using an ion exchange resin to concentrate the liquid whey and Inpro® is produced by cross-flow microfiltration. Bipro® has a much lower content of glycomacro peptides (GMP) than the amount found in Inpro®. Even more importantly Bipro® has 1200 ppm of calcium whereas Inpro® has 5293 ppm of calcium; since  $\alpha$ -lac binds Ca, the 4 fold increase in Ca content may result in structural stability of  $\alpha$ -lac in Inpro® over Bipro® (5).

Both pressure treatments applied to the Inpro® samples; 550 MPa without a holding time and three pressure cycles; generated similar responses from the two  $\beta$ -lg genetic variants, exhibiting a high CSD (Figures 25B and 25C). Before pressure treatment the charge is centred at +11 and after pressure treatment the charge is widespread with a higher proportions having charges > +11. This demonstrates that pressure causes partial unfolding of the protein making more groups within the interior of the protein susceptible to salvation. Overall, the changes in the CSD distribution after pressure treatment observed in Inpro® were greater than those observed in Bipro®'s for  $\beta$ -lg. This may imply that the native structure of  $\beta$ -lg in Inpro® is less stable and may result in producing gels with different rheological properties than those of Bipro®.

#### 4.5. Conclusion

The changes in tertiary structure of whey protein isolates and pure protein components of the whey were investigated. ESI-MS proved to be a good tool for examining the changes in the global tertiary structure of proteins based on the differences in the CSD of whey protein solutions.

Holding time and pressure levels can be modified to achieve comparable results, lower pressures require higher holding time or multiple cycles. Holding time can be virtually eliminated if pressures in excess of 500 MPa are applied. In this study, the 3C and the single cycle 500/0/1 treatments produced similar CSD of WPI. High hydrostatic pressure induces changes in the tertiary structure of whey proteins. These changes in some cases involve a relaxation of the native structure of the molecule. Once the protein has been ingested, gastro-intestinal enzymes will have the opportunity to attack some groups previously buried in the structure of the protein and unreachable by these enzymes due to the tight packing of the protein (11, 14, 15).

## 4.6. References

- 1. Alomirah, H. F., I. Alli and Y. Konishi. 2000. Applications of Mass Spectrometry to Food Proteins and Peptides. Journal of Chromatography A. 893: 1-21.
- 2. Boye J.I., Alli I., Ismail A.A., Gibbs B.F., Konishi Y. 1995. Factors affecting molecular characteristics of whey protein gelation. Int. Dairy Journal. 5:337-353.
- 3. Boye J.I., Ismail A.A., Alli I. 1996. Effects of physicochemical factors on the secondary structure of β-lactoglobulin. Journal of Dairy Research. 63:97-109.
- 4. Brownlow S., Morais J.H., Cooper R., Flower D. R., Yewdall S. J., Polikarpov I., North A.C.T., Sawyer L. 1997. Bovine β-lactoglobulin at 1.8Å resolution-still an enigmatic lipocalin. Structure. 5: 481-495.
- 5. Dzwolak W., Kato M., Shimizu A., Taniguchi Y. 2000. FTIR study on heat-induced and pressure-assisted cold induced changes in structure of bovine β-lactoglobulin: stabilizing role of calcium ion. Biopolymers. **62**: 29-39.
- 6. Fenn J.B., Mann M., Meng C.K., Wong S.F., Whitehouse C.M. 1989. Electrospray Ionization for Mass Spectrometry of Large Biomolecules. Science. **246**:64-71.
- 7. Galazka V.B., Ledward D.A., Sumner I.G., Dickinson E. 1997. Influence of High Pressure on Bovine Serum Albumin and its Complex with Dextran Sulfate. J. Agric. Food Chem. 45:3465-3471.

- 8. Hosseini-Nia T. 2000. Structural and nutritional properties of whey proteins as affected by hyperbaric pressure. PhD dissertation, McGill University, Montreal, Canada.
- 9. Hosseini-Nia T., Kubow S., Ismail A. 2001. Hyperbaric pressurization of proteins and therapeutical uses of pressurized proteins thereof. PCT Int. Appl.
- 10. Konermann L., Douglas D.J. 1997. Acid-Induced Unfolding of Cytochrome c at Different Methanol Concentrations: Electrospray Ionization Mass Spectrometry Specifically Monitors Changes in the Tertiary Structure. Biochemistry **36**:12296-12302.
- 11. Korhonen H., Pihlanto-Leppala A., Rantamaki P., Tupasela T. 1998. Impact of processing on bioactive proteins and peptides. Trends in Food Science & Technology. 9: 307-319.
- 12. Lefevre T., Subirade M. 2000. Molecular differences in the formation and structure of Fine-Stranded and Particulate β-Lactoglobulin gels. Biopolymers. **54**: 578-586.
- 13. Miranker A., Robinson C.V., Radford S.E., Aplin R.T., Dobson C.M. 1993. Detection of Transient Protein Folding Populations by Mass Spectrometry. Science. **262**:896-900.
- 14. Nakamura T., Sado H., Syukunobe Y. 1993. Production of low antigenic whey protein hydrolysates by enzymatic hydrolysis and denaturation with high pressure. Milchwissenschaft. 48:141-145.
- 15. Smacchi E., Gobbetti M. 2000. Bioactive peptides in dairy products: synthesis and interaction with proteolytic enzymes. Food Microbiology. 17: 129-141.

# Chapter 5

# Tertiary Structure Changes of Whey Proteins after Ultra High Hydrostatic Pressure Process

#### 5.1. Abstract

Ultra high pressure (UHP) treatment is increasingly being employed as an alternative to thermal process to reduce bacterial count and inactivation of spores without the loss in appearance, vitamins or nutritional value of the food. More recently, UHP has been found to play a role in improving protein functionality and gel texture. The effects of different UHP treatments on the tertiary structure of whey proteins employing near-ultraviolet circular dichroism (near-UV CD), fluorescence and Fourier transform Raman (FT-Raman) spectroscopy, was investigated. Results suggest that the native β-lg tertiary structure changes with increasing pressure to a more relaxed, flexible conformation. Also, the proteins in Bipro® WPI are relaxing its structure from the more compact native state. On the other hand, Inpro® WPI proteins appear to be resistant to pressure treatment compared to Bipro® WPI. Results indicate that higher instant pressure treatments can be compensated for with longer holding times and multiple cycle treatments. One can achieve the same results, from the structural point of view, with lower pressure and longer time or higher pressure and shorter time.

Key words:  $\beta$ -lactoglobulin, WPI, ultra high pressure, FT-Raman, fluorescence, ANS, CD, tertiary structure.

## 5.2. Introduction

Ultra high pressure (UHP) treatments exert an influence over both tertiary and secondary structures of the protein molecule. These changes can be reversible or irreversible and can also lead to gelation, depending on such factors as the protein nature, its concentration, pH, pressure level, number of cycles and holding time between each cycle (2). The relationship between pressure-induced structural changes that lead gelation is still under investigation.

This paper studies the effects of different ultra high hydrostatic pressure treatments (up to 650 MPa) on the tertiary structure of β-lactoglobulin and whey protein isolates (WPI) obtained from two different isolation methods; using near-ultraviolet circular dichroism (near-UV CD), FT-Raman and fluorescence spectroscopy.

#### 5.3. Materials and Methods

The proteins used in this research were: β-lactoglobulin (90% dry basis) protein powder; α-lactalbumin (95% dry basis); Bipro® whey protein isolate (90% dry basis). These samples were donated by Davisco Foods International (MN, USA) and used without further purification. Inpro® WPI (90% dry basis) was supplied by Inovatech (Abbotsford, BC. Canada) and used as received. Deuterium oxide (D<sub>2</sub>O 99.99 % D) was purchased from Aldrich.

The high pressure treatment was achieved using an Alstom Co. (Nantes, France) ultra high pressure machine unit, with a chamber volume of 3-L. The pressure medium used was water. The maximum operational pressure of 650 MPa is reached in approximately 4 minutes and the depressurization time was around 10 seconds. The sample was introduced in the high pressure machine at 4 °C and during pressurization the adiabatic increase in temperature reached a maximum 10 °C. This rise in temperature can be assumed to have no additional effect over the high pressure treatment.

The following notation to designate the physicochemical parameters was used: P/t/C where P is the pressure level in mega-Pascals (MPa); t is the holding time in minutes and C is the number of cycles, i.e., how many times the pressure level and holding time is achieved, released and applied again. For example, 650/5/3 means a pressure treatment at 650 MPa, with 5 minutes of holding time is repeated 3 times.

A different 3-cycle treatment (3C) required an increase in the pressure to 400 MPa and holding it for 10 minutes, then releasing the pressure and subjecting the sample to two additional pressure cycles of 400 MPa pressure without a holding time (i,e., 400/10/1 followed by 400/0/2) (4, 5).

#### **5.3.1.** Series A

Solutions of 15% (w/v)  $\beta$ -lg were prepared in H<sub>2</sub>O and sealed in plastic bags for high pressure treatment. This concentration was selected to avoid the formation of hard  $\beta$ -lg gels which after lyophilization can be difficult to re-dissolve for study and can cause artifacts in the fluorescence.

The bags were submerged in the water chamber and subjected to ultra-high pressure treatments at 100/0/1, 250/0/1, 300/0/1, 400/0/1, 450/0/1, 500/0/1, 550/0/1, 600/0/1, 650/0/1 and 3C. After the pressure treatment the samples were immediately frozen, subsequently lyophilized and manipulated accordingly to the method of analysis.

#### **5.3.2.** Series B

WPI Bipro® and Inpro® were subjected to 550/0/1 and 3C pressure treatments and the fluorescence of the hydrophobic probe ANS was recorded.

## 5.3.3. Fluorescence spectroscopy using ANS as probe

The emission spectra of ANS bounded to  $\beta$ -lg or WPI (5 mM protein solution containing 50 mM ANS in  $H_2O$ ) was placed in a 10 mm pathlength quartz cuvette. An excitation wavelength of 486 nm and 2 nm slit was employed and the spectra were recorded from 400 to 600 nm using an Aminco-Bowman AB 2 spectrofluorimeter (Spectronics Instruments. Rochester, NY).

## 5.3.4. Near UV circular dichroism spectroscopy

A Jasco 710 spectropolarimeter (Easton, MD. USA) was used to acquire the CD spectra of 3.33 mg/ml of  $\beta$ -Lg in H<sub>2</sub>O placed in a 10-mm pathlength rectangular quartz cell. The spectral region from 320 to 250 nm was scanned at a rate of 20 nm/min with a 2

sec response, a 1-nm bandwidth, a 0.2 nm step resolution, a sensitivity setting of 30 and 5 accumulations.

## 5.3.5. FT-Raman spectroscopy

The FT-Raman spectra were recorded using a Raman module coupled to a Nexus 670 FTIR spectrometer (Thermo-Nicolet. Madison, WI). Lyophilized protein powder was placed in a 1-mm glass capillary. A maximum laser power of 500 mW from a near-IR with a 1064 nm excitation laser was focused to a 100 µm diameter. A total 512 co-added scans at 8 cm<sup>-1</sup> spectral resolution were recorded for each sample. Spectra were normalized using the intensity of the 1005 cm<sup>-1</sup> band which is insensitive to changes in structure (8).

#### 5.4. Results and Discussion

#### **5.4.1.** Series A

# 5.4.1.1. Fluorescence spectroscopy using ANS as probe

The extrinsic probe 8-anilino-1-naphthalene sulfonic acid (ANS) is a small molecule that has a relatively weak fluorescence by itself, but when it binds to hydrophobic sites or pockets in a molecule its fluorescence increases dramatically accompanied by a blue shift of some 40 nm (11). This effect is also noticeable when ANS is dissolved in a non-polar solvent. This property is useful for the study of the changes in tertiary structure of protein molecules that leads to exposure of hydrophobic sites previously unreachable to ANS (6, 7, 10, 11).

Powder  $\beta$ -lg samples previously exposed to increasing ultra high pressure treatments were dissolved in water containing a determined concentration of the probe ANS. Figure 26A shows the increasing fluorescence intensity obtained from samples exposed to increasing pressure treatments. The fluorescence intensity at  $\lambda_{max}$  of 486 nm was plotted against the pressure (Figure 26B). The graph shows a clear positive relationship between pressure and fluorescence intensity. These results are similar to the ones from Ikeuchi *et al.* (2001), Yang *et al.* (2001) and Yang et al. (2003) (6, 10, 11).

These results indicate that  $\beta$ -lg structure is changing becoming more loose thereby allowing ANS molecules to enter to the hydrophobic core of the protein. Another

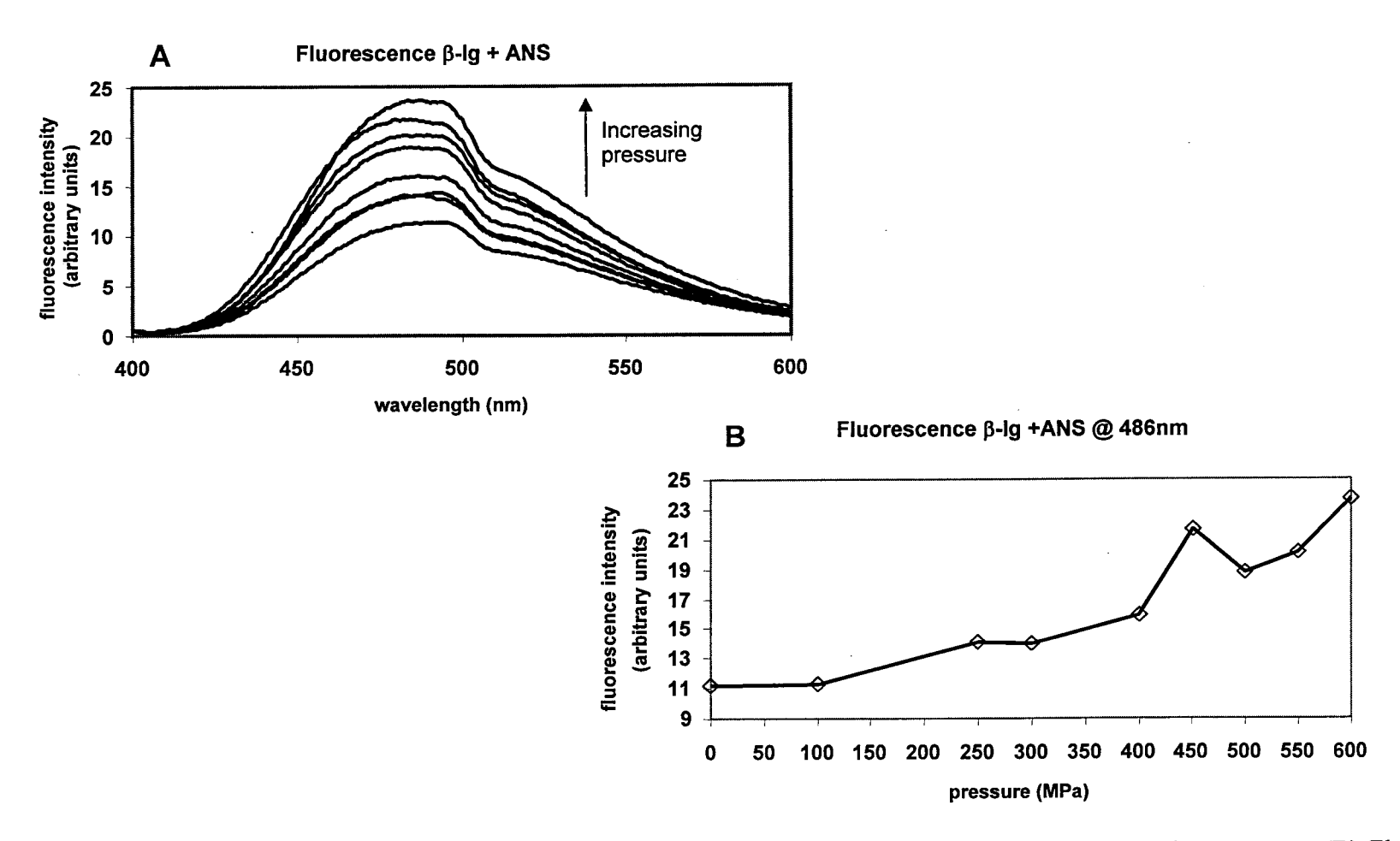


Figure 26. Series A: (A) Fluorescence spectra of ANS bind to pure  $\beta$ -lg protein subjected to increasing pressure. (B) Fluorescence intensity at  $\lambda_{max}$  from A, 486 nm of the complex ANS-β-lg as function of pressure pre-treatment applied. When increasing the pressure pre-treatment applied, the protein molecule lets more ANS to bind to its hydrophobic pockets by relaxing its structure. After 450 MPa the molecule relaxes more than after 500 or 550 MPa.

possibility is that the protein is changing its three-dimensional structure so as to expose small hydrophobic pockets previously inaccessible to solvent or ANS.

An interesting result is obtained from β-lg exposed to 450 MPa of pressure. This sample stand out of the trend by exhibiting a higher fluorescence compared to 500 and 550 MPa pressure treated samples. A maximum relaxation of the protein molecule is achieved at 450 MPa. It may be possible that above such a pressured intermolecular interaction between the exposed hydrophobic groups may limit the biding of ANS.

## 5.4.1.2. Near UV circular dichroism spectroscopy

The same set of samples used in the fluorescence experiments was analyzed by near-UV CD spectroscopy. Selected near-UV CD spectra of pressure-treated samples are shown in Figure 27. The signals from Phe and Tyr residues do not follow any explainable pattern, but the Trp intensity at 293 nm decreases with increasing pressure. The later may be attributed to a change in the spatial rearrangement of residues where the tryptophan amino acids are moving towards a more polar (or hydrophilic) environment. These findings are in agreement with the studies from Aouzelleg *et al.* (2004), Ikeuchi *et al.* (2001) and Yang *et al.* (2001) (1, 6, 10). Is of interest to note that at 450 MPa of pressure the decrease in the Trp intensity is at its maximum. This is analogous to the florescence results obtained above.

#### 5.4.1.3. FT-Raman spectroscopy

The FT-Raman spectra of β-lg exposed to different pressure treatments was recorded from the protein powder after lyophilization. Figure 28 shows the FT-Raman spectrum of the native β-lg. The band at 505 cm<sup>-1</sup> is indicative of the presence of disulphide bonds (S-S). In contrast with infrared spectroscopy, where C-S, disulphide and thiol bands are almost invisible, one can detect S-S, C-S and S-H modes and their varying conformations in a Raman spectrum (3, 8). The peaks at 830 and 850 cm<sup>-1</sup> are attributed to tyrosine residues present in the protein; the band at 1340 cm<sup>-1</sup> and the shoulder at 1360 cm<sup>-1</sup> are produced by the tryptophan residues. The sharp line at 1005 cm<sup>-1</sup> is caused by the vibration of the phenylalanine rings, also known as "ring breathing"; this vibration is insensitive to changes in conformation of the protein structure, and is useful as an internal

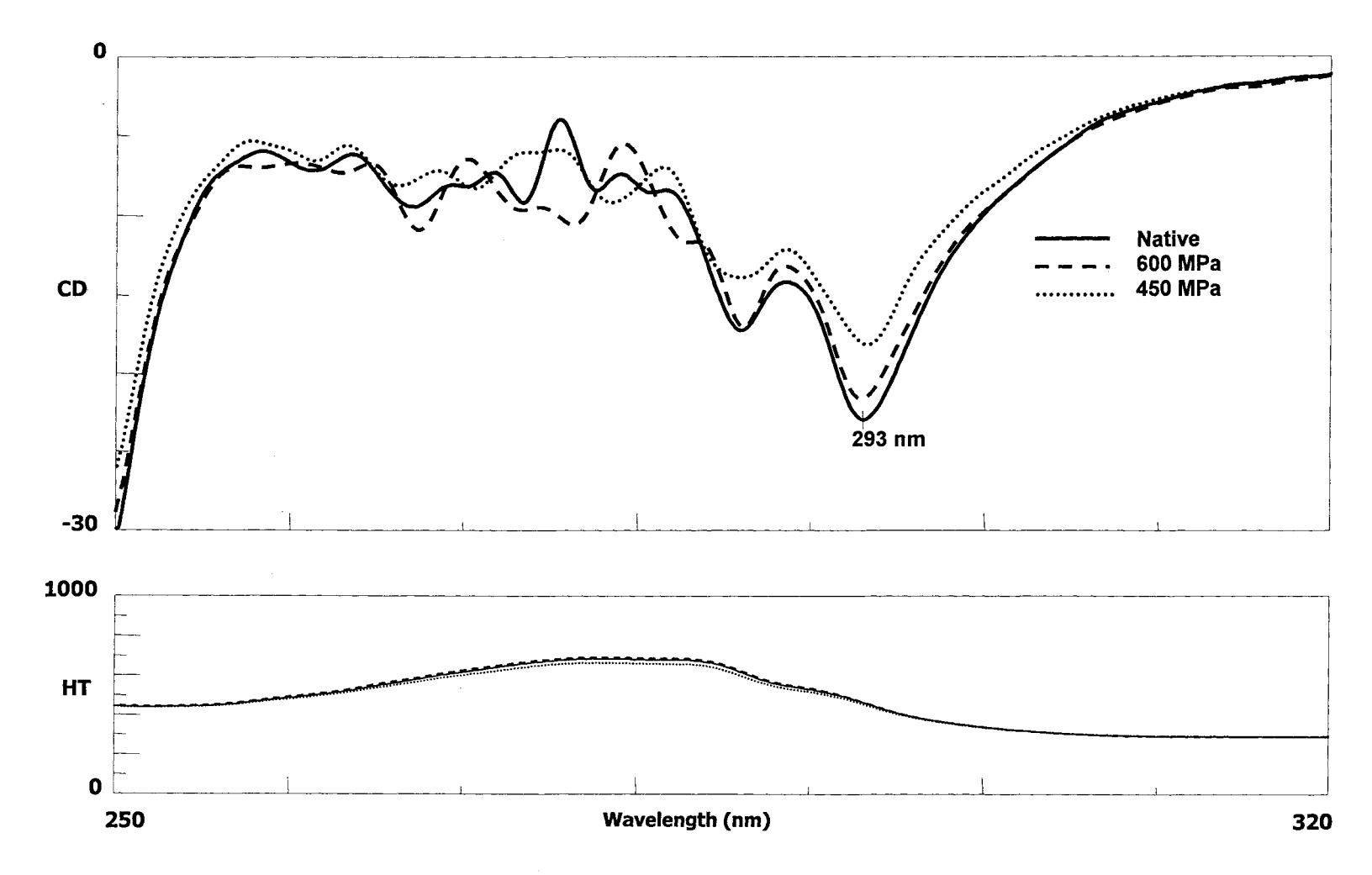


Figure 27. Series A: Near-UV CD spectra of pure β-lg protein subjected to different pressure treatments. The peak at 293 nm corresponds to the absorbance of tryptophan residues; the amino acid is migrating to a more polar environment (surface exposed) when increasing the pressure treatment. The biggest change is achieved after 450 MPa of pressure.

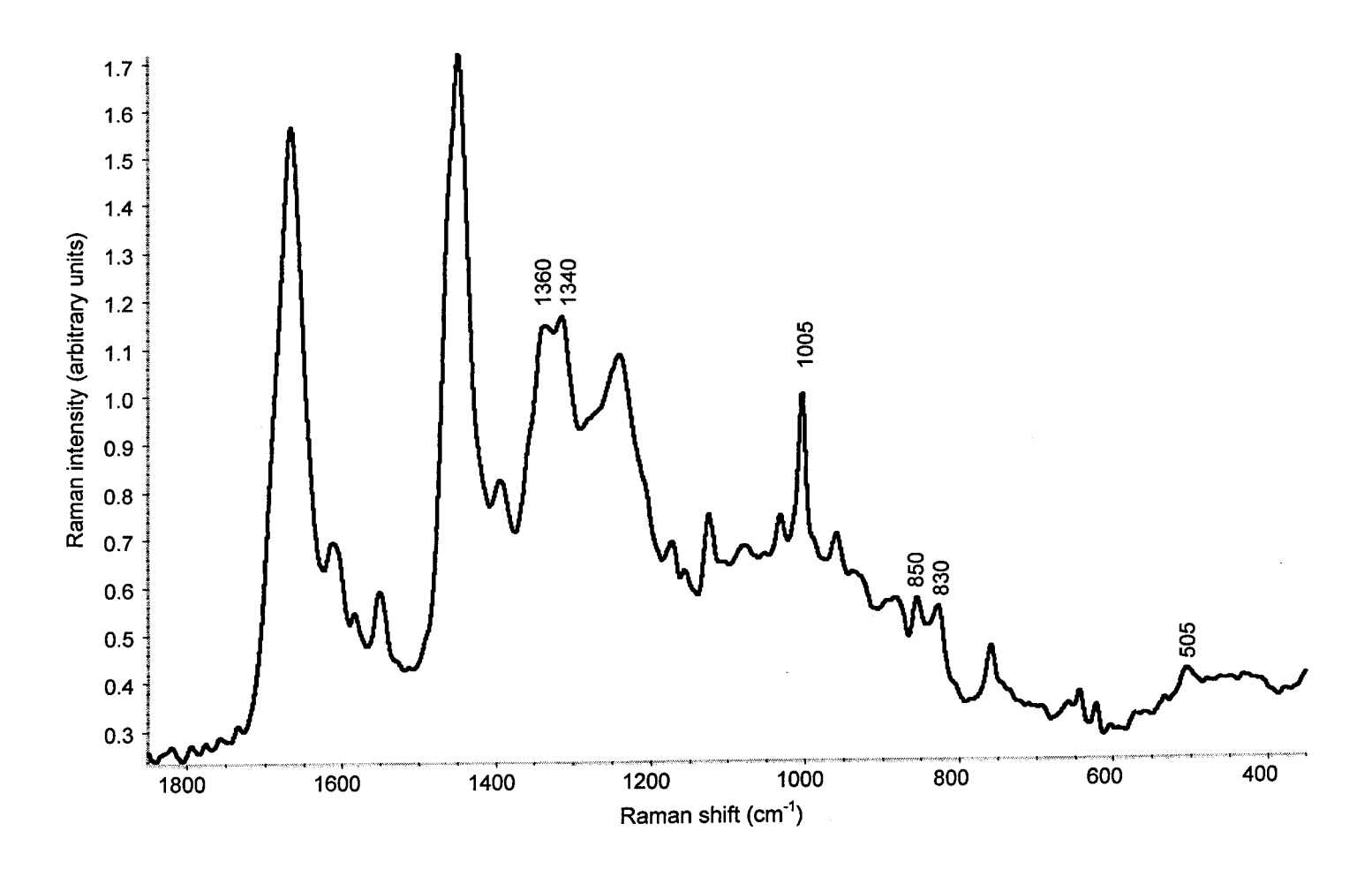


Figure 28. Series A: FT-Raman spectrum of  $\beta$ -lg powder not pressure treated, in a capillary tube; 512 scans; 8 cm<sup>-1</sup> resolution; 1064 nm excitation (near-IR) laser; laser power 500 mW. Fine structure information is present even before any data enhancement manipulations. The band at 505 cm<sup>-1</sup> is indicative of disulphide bonds present in the structure of the protein.

intensity standard; samples are normalized against this band to correct the smallest variation in concentration between samples (8).

Table 5 summarizes some ratios of band intensities belonging to tryptophan and tyrosine residues that are useful for elucidating the tertiary structure of protein samples. Following these "rules", the β-lg samples spectra in Figure 29 were analyzed. The position of the tryptophan residues in β-lg exposed to different pressure treatments is shown in Figure 29A. The ratio of the intensity at 1360 cm<sup>-1</sup> over the intensity at 1340 cm<sup>-1</sup> is lower than 1.0 in all cases, therefore tryptophan is in a hydrophilic environment. The I<sub>1360</sub>/I<sub>1340</sub> ratio also decreases with increasing pressure, indicating that the tertiary structure is affected by ultra high hydrostatic pressure treatment. These results are consistent with the ESI-MS (Chapter 4). Similar observations were found with thermally induced gels (9). The  $I_{850}/I_{830}$  ratio of the tyrosine bands is  $\sim 1$ ; this indicates that the tyrosine residues are exposed to a polar environment in all cases. Also, this ratio is decreasing with increasing pressure which indicates that the tyrosine residues are getting buried in the molecule with increasing pressure exposure. No dramatic change in the FT-Raman spectrum is observed for samples exposed to 450 MPa pressure. This may be due to the fact that the protein sample in this case lyophilized, as opposed to the other two techniques; the differences of state can have a profound effect on the tertiary structure of the samples.

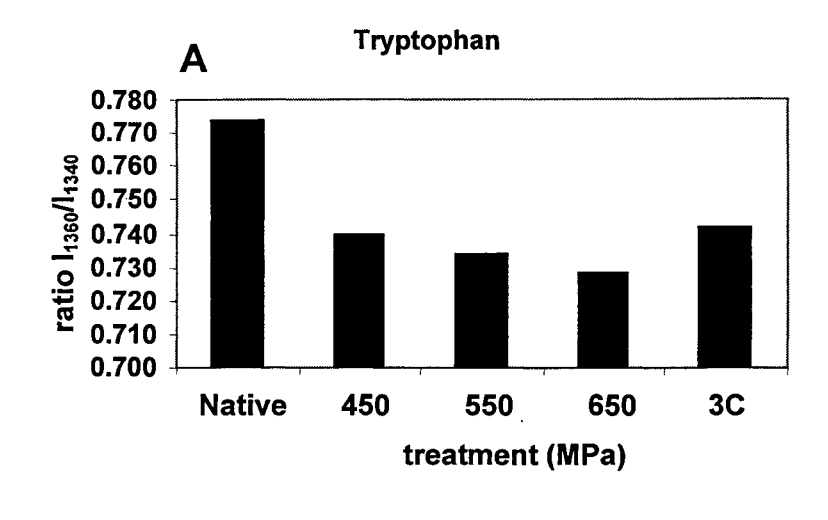
An attempt was made to measure the cystine (S-S) content of the  $\beta$ -lg samples exposed to different pressure treatments (Figure 29C). But the results were inconclusive, no discernable pattern was found. This may be attributed to the week signal of the bands.

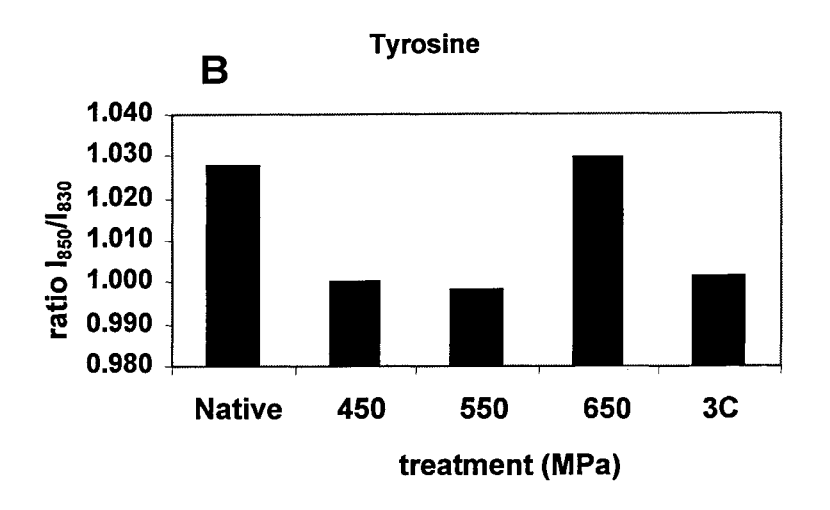
#### **5.4.2.** Series B

Figure 30A shows the fluorescence of ANS bound to non-pressure treated Bipro® and Bipro® WPI exposed to 550 MPa of pressure; and Bipro® exposed to 3C treatment. The fluorescence intensity of ANS increases with increasing pressure cycles. This indicates that ANS is binding to additional hydrophobic regions exposed to ANS with increasing pressure treatment. The effect of a lower pressure used in 3C (400 MPa) is compensated for by a 10 minutes holding time in the first cycle in addition to the two

**Table 5**. Information about the third dimensional orientation of the amino acids Tyrosine and Tryptophan in protein is achieved by some specific ratios of bands intensities after the FT-Raman spectra have been normalized.

Side Chain	Bands ratio	Scenarios
Tyrosine	I <sub>850</sub> /I <sub>830</sub>	Ratio around 1 Tyr exposed to a polar environment Ratio higher than 2.5 Tyr acts as H-bond acceptor Ratio lower than 0.5 Tyr acts as H-bond donor
Tryptophan	I <sub>1360</sub> /I <sub>1340</sub>	Ratio higher than 1 Trp H-bonding in a hydrophobic environment Ratio lower than 1 Trp H-bonding in a hydrophilic environment





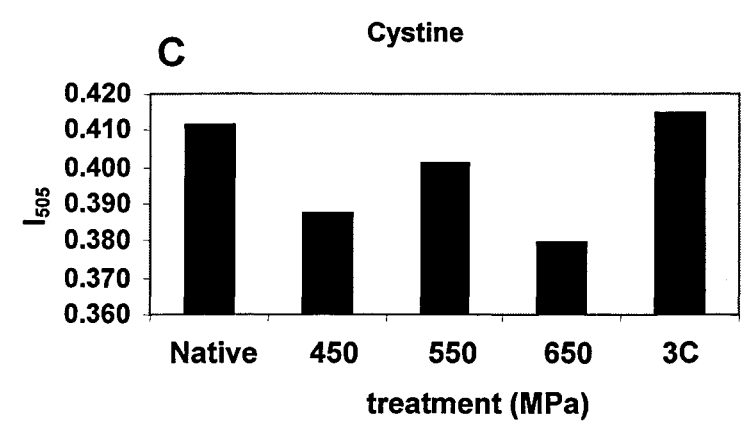


Figure 29. Series A: The third dimensional orientation of some amino acids groups in  $\beta$ -lg solutions after different pressure treatments, obtained from its FT-Raman spectrum. (A) Tryptophan residues are hydrogen-bonding in a hydrophilic environment increasingly with pressure. (B) Tyrosine residues are exposed to a polar environment increasingly with pressure which indicates that the protein molecule is rearranging. (C) The amount of disulphide bonds in  $\beta$ -lg after pressure could not be precisely determined due to some methodological challenges; therefore this analysis is inconclusive.

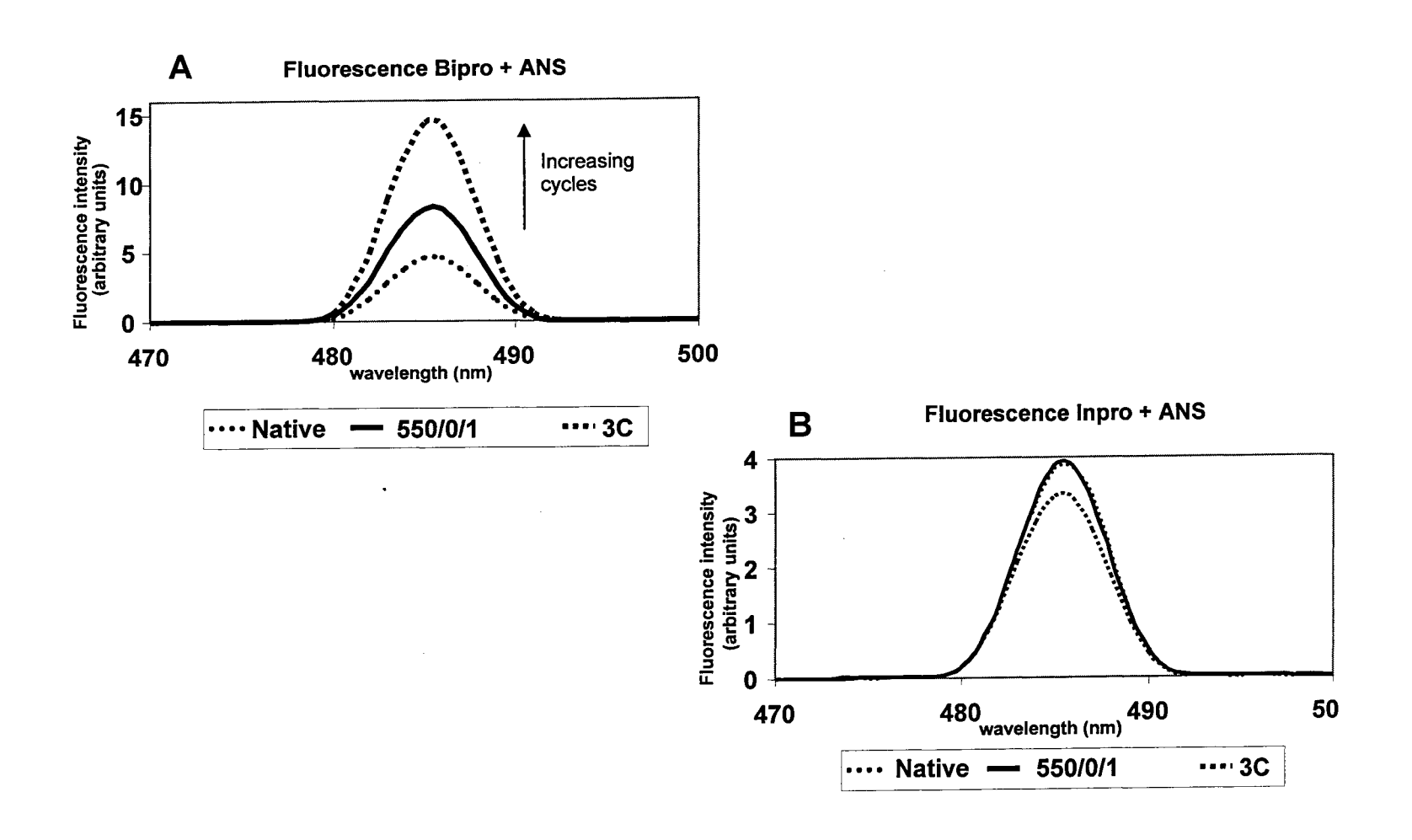


Figure 30. Series B: Fluorescence of ANS bind to two brand-names of WPI exposed to different pressure treatments. (A) Hydrophobic sites in Bipro® are increasingly exposed with increasing pressure; this means that the proteins in Bipro® became less compact. (B) In the other hand, Inpro® is not affected by pressure in the same way Bipro® is. The smaller intensity observed for 3C is due to a loss in protein concentration, related to some precipitation of the sample after pressure treatment.

additional cycles. At 550 MPa single cycle (with no holding time) pressure a smaller effect is observed.

Figure 30B shows the fluorescence intensity of ANS bound to non-pressure treated Inpro® WPI and Inpro® exposed to 550 MPa or to 3C treatment at 400 MPa. The fluorescence intensity of ANS remains unchanged after the pressure treatments; which suggest that the proteins in Inpro® are less responsive to pressure treatment. The fluorescence intensity of the Inpro® samples are comparable to that of the non-pressure treated Bipro® but not of the pressure treated Bipro®. The lower differences in the ANS intensity of the pressure-treated 3C sample maybe attributed to some precipitation of the protein as a result of pressurization. Alternatively, the higher Ca<sup>+2</sup> content of Inpro® may stabilize the protein against pressure-induced conformational changes. This is consistent with the ESI-MS results reported in Chapter 4.

## 5.5. Summary

The changes in tertiary structure of  $\beta$ -lg after different pressure treatments were investigated using diverse spectroscopic techniques. Also the changes in tertiary structure of two brand-names of WPI subjected to different pressure treatments were investigated using the fluorescence of the hydrophobic probe ANS.

Results from the fluorescence experiments showed that hydrophobic sites in β-lg and Bipro® WPI are increasingly exposed to solvent with increasing pressure; this can be interpreted as the molecule is relaxing its structure from the more compact native state. On the other hand, Inpro® WPI proteins appear to be resistant to pressure treatment compared to Bipro® WPI. From the fluorescence experiments with Bipro® exposed to different pressure treatments; one can conclude that higher instant pressure treatments can be compensated for with longer holding times and multiple cycle treatments. One can achieve the same results, from the structural point of view, with lower pressure and longer time or higher pressure and shorter time. Indeed, in this case the 3C treatment showed a higher effect over the proteins in Bipro® than at 550 MPa of instant pressure.

Results from CD and FT-Raman spectroscopic techniques showed that the tryptophan residues in  $\beta$ -lg are increasingly exposed to the surface of the protein with increasing pressure. Also FT-Raman spectroscopy results indicate that the tyrosine

residues in  $\beta$ -lg are exposed to a polar environment and that increasing pressure cause the groups to be buried.

#### 5.6. References

- 1. Aouzelleg A., Bull L.-A., Price N.C., Kelly S.M. 2004. Molecular studies of pressure/temperature-induced structural changes in bovine β-lactoglobulin. Journal of the Science of Food and Agriculture. 84:398-404.
- 2. Boye J.I., Ismail A.A., Alli I. 1996. Effects of physicochemical factors on the secondary structure of β-lactoglobulin. Journal of Dairy Research. 63: 97-109.
- 3. Carey P. 1983. Raman spectroscopy for the analysis of biomolecules. Trends in analytical chemistry. 2:275-277.
- 4. Hosseini-Nia T. 2000. Structural and nutritional properties of whey proteins as affected by hyperbaric pressure. PhD dissertation, McGill University, Montreal, Canada.
- 5. Hosseini-Nia T., Kubow S., Ismail A. 2001. Hyperbaric pressurization of proteins and therapeutical uses of pressurized proteins thereof. PCT Int. Appl.
- 6. Ikeuchi Y., Nakagawa K., Endo T., Suzuki A., Hayashi T., Ito T. 2001. Pressure-induced denaturation of monomer β-lactoglobulin is partially irreversible: comparison of monomer form (highly acidic pH) with dimer form (neutral pH). J. Agric. Food Chem. 49:4052-4059.
- 7. Laligant A., Dumay E., Casas-Valencia C., Cuq J.L., Cheftel J.C. 1991. Surface hydrophobicity and aggregation of β-lactoglobulin heated near neutral pH. Journal of Agricultural and Food Chemistry. 39:2147-2155.
- 8. Li-Chan E.C.Y. 1996. The Applications of Raman Spectroscopy in Food Science. Trends Food Sci Technol 7:361-370.
- 9. Nonaka M., Li-Chan E., Nakai S. 1993. Raman spectroscopic study of thermally induced gelation of whey proteins. Journal of Agricultural and Food Chemistry. 41:1176-81.
- 10. Yang J., Dunker A.K., Powers J.R., Clark S., Swanson B.G. 2001. β-lactoglobulin molten globule induced by high pressure. J. Agric. Food Chem. 49:3236-3243.
- 11. Yang J., Powers J.R., Clark S., Dunker A.K., Swanson B.G. 2003. Ligand and flavor binding functional properties of β-lactoglobulin in the molten globule state induced by high pressure. Journal of Food Science. **68**:444-452.

# Chapter 6

## **General Conclusion**

High pressure treatments exert an influence over both tertiary and secondary structures of the protein molecule; these changes can be reversible or irreversible depending on such factors as the nature of the protein, its concentration, pH, temperature, pressure level, number of cycles and holding time between each cycle. The changes in the secondary structure of whey proteins were investigated using FTIR spectroscopy, while the changes in the tertiary structure were investigated by ESI-MS based on the differences in the CSD of whey protein solutions. The changes in tertiary structure of βlactoglobulin ( $\beta$ -lg) and  $\alpha$ -lactalbumin ( $\alpha$ -lac) after different pressure treatments were also investigated using CD, fluorescence and FT-Raman spectroscopy. For the fluorescence studies, the changes in tertiary structure were examined using ANS as a probe. The changes in viscoelastic properties of the protein solutions were monitored by dynamic rheology techniques. The results of the above studies show that the magnitude of the applied pressure and holding time on protein conformation are inversely proportional. Thus, one can achieve the same results, from the structural point of view, by using lower pressure treatment with longer holding time or by using higher pressure levels with shorter (or without any) holding time. From the manufacturing point of view, having to wait longer for a single batch of product is not cost effective, thus the use of ultra high pressure can result in a faster turnaround time.

Results from the fluorescence experiments showed that hydrophobic sites in  $\beta$ -lg are increasingly being exposed to solvent with increasing pressure. Results from CD and FT-Raman spectroscopic techniques showed that some of the tryptophan residues in  $\beta$ -lg are increasingly exposed to the surface of the protein with increasing pressure. Also, FT-Raman spectroscopy results indicate that the tyrosine residues in  $\beta$ -lg are exposed to a polar environment and that increasing pressure causes the groups to be buried. This can be interpreted in terms of the molecule relaxing its structure, going from a more compact native state to an open structure or the protein undergoes a dramatic inversion where the core of the protein is exposed to solvent. The latter appears to be unlikely since the secondary structure changes would be expected to change dramatically, which is not

supported by the FTIR spectroscopic data. Accordingly, high hydrostatic pressure induces changes in the tertiary structure of whey proteins resulting in a relaxation of the native structure of the molecule. The relaxed or opened structures may be more easily digested by gastro-intestinal enzymes and may lead to different hydrolyzed peptide profiles. This is currently under investigation by a number of groups.

Finally, the relationship between the viscoelastic characteristics of protein solutions subjected to high pressure treatment levels and the changes in the protein structure as elucidated by the spectroscopic studies in this work provides the means for understanding the molecular basis of functionality. Where no structural changes in the protein occurs (as in the case of GMP and  $\alpha$ -lac), no change in viscosity is observed with increasing pressure. An increase in the viscosity of the proteins solution with increasing hydrostatic pressure is always accompanied by specific changes in the molecular structure of the protein.